Module level analysis of low breakdown voltage solar cells in urban landscapes

Simulation and Experimental Studies

Viswambher Kambhampati

Technische Universiteit Delft

TU Delft Delft University of Technology

Challenge the future

MODULE LEVEL ANALYSIS OF LOW BREAKDOWN VOLTAGE SOLAR CELLS IN URBAN LANDSCAPES

SIMULATION AND EXPERIMENTAL STUDIES

by

Viswambher Kambhampati

in partial fulfillment of the requirements for the degree of

Master of Science
in Sustainable Energy Technology

at the Delft University of Technology,

Student number:	4832582	
Supervisor:	Prof. dr. Olindo Isabella,	Delft University of Technology
Thesis committee:	Prof. dr. Olindo Isabella,	Delft University of Technology
	Dr. Patrizio Manganiello	Delft University of Technology
	Dr. Zian Qin	Delft University of Technology
	Ir. Andres Calcabrini	Delft University of Technology

An electronic version of this thesis is available at `http://repository.tudelft.nl/`.

TU Delft Delft University of Technology

ACKNOWLEDGEMENT

The basis for this research stems from my passion for contributing to a more sustainable world. Global climate change, population growth and a rapid increase in the primary energy consumption demand a transition towards renewable energy systems. Solar energy will play a crucial role in this transition as it is widely abundant and can be harvested by decentralized photovoltaic (PV) systems. Enhancing the shading tolerability of PV modules leads to a huge potential for increasing the deployment of PV systems in urban landscapes.

This graduation project is part of my master Sustainable Energy Technology at Delft University of Technology. The research was done in a nine-month project during the academic year 2019-2020 and was under the direct supervision of professor Dr. Olindo Isabella and assistant professor Dr. Patrizio Manganiello. Andres Calcabrini was my daily supervisor. Hereby, I would like to express my special gratitude to all the supervisors for their support, advice and guidance throughout the research process and for proofreading my report.

I am also thankful to my fellow students, my roommates and to my colleagues at the department of Photovoltaic Material and Devices for the positive, motivating and supportive working environment. Finally, I want to thank my parents and my brother for their love and support throughout my life. Your commitment and encouragement gave me the motivation to achieve things that I never imagined to be possible. I hope that you will enjoy reading this report.

Viswambher Kambhampati
Delft, September 2, 2020

ABSTRACT

In urban environments, more and more building added and building integrated photovoltaic (PV) systems are found. These systems use conventional solar modules which have a poor performance under non-uniform illumination conditions. When the module is partially shaded, either at least one subgroup is bypassed or the module current is limited by the current of the worst performing cell. This leads to significant and disproportionate power losses. One way to address this issue is to implement a solar module made of low reverse breakdown voltage (BDV) solar cells.

A thermo-electric simulation framework was developed in MATLAB to replicate two types of commercially available low BDV solar cells: Sunpower Maxeon gen2 and gen 3 cells. Using the above model the potential and performance of solar modules in urban landscapes has been evaluated. A comparative study of solar module models built with these cells and placed on three different locations on a single rooftop having completely different irradiance profiles has been assessed. A solar module with 3 bypass diodes made of gen 3 solar cells has a better performance than module made of gen 2 cells. This accounts not only for better forward parameters of gen 3 cells but also its improved mismatch losses owing to lower reverse breakdown voltage and better temperature coefficients.

The usage of low reverse breakdown solar cells is beneficial in conditions where partial shading is predominant. Other advantages of using these solar module over other technologies is there is that there is no need of any additional electronic components.

Viswambher Kambhampati
Delft, September 2, 2020

CONTENTS

LIST OF FIGURES

LIST OF TABLES

1

INTRODUCTION

1.1. GLOBAL ENERGY DEMAND

During the last century, there has been a huge increase in global energy consumption. In the last 40 years, global primary energy consumption has doubled and reached a value of 164×10^{12} kWh in 2018 and is expected to grow in the upcoming years. Figure 1.1 shows that the major share of the primary energy is generated from fossil fuels such as coal, crude oil and natural gas. It is clear that during the past 50 years the pace of burning fossil fuels has increased drastically. This has resulted in more pollution and raised CO_2 concentration to over 400 ppm [17]. This high CO_2 concentration has caused the global mean temperature to increase, resulting in various problems such as sea level rise and extreme weather conditions such as intense cyclones and hurricanes.

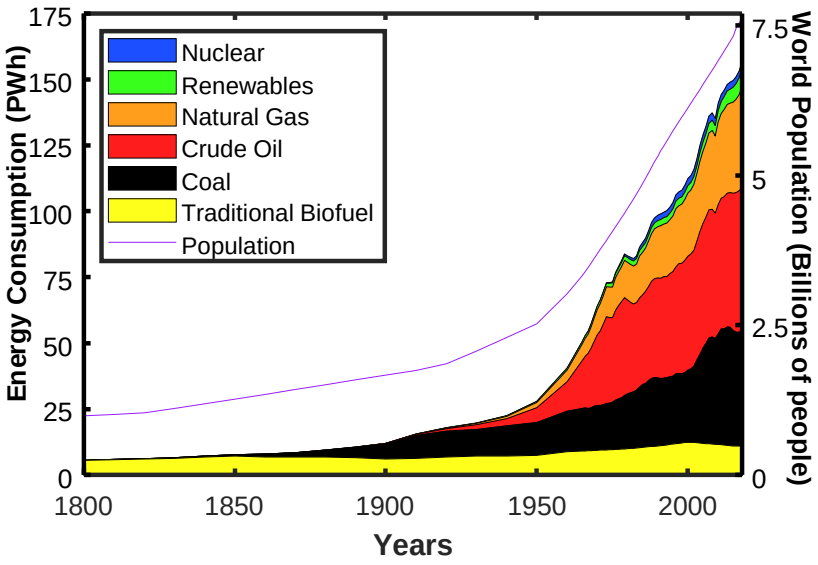

Figure 1.1: Annual global primary energy consumption from 1800 to 2018 and world population. Data adapted from [[56],[9],[68], [30]] (population data were interpolated where necessary).

Figure 1.1 might be slightly misleading as it appears that the world population and energy consumption follow the same trend. But when energy consumption is expressed in terms of per-capita as shown in Figure 1.2, it is clear that energy use per inhabitant has also increased. From this figure

it is also visible that the CO_2 concentration has increased enormously. In the event that these patterns proceed, the world will come up short on fossil fuels in the upcoming decades and the impact of greenhouse effect could be irreparable [47]. Not only to meet the fast-growing energy demand but also to reduce atmospheric pollution, clean and widely abundant renewable energy sources are essential.

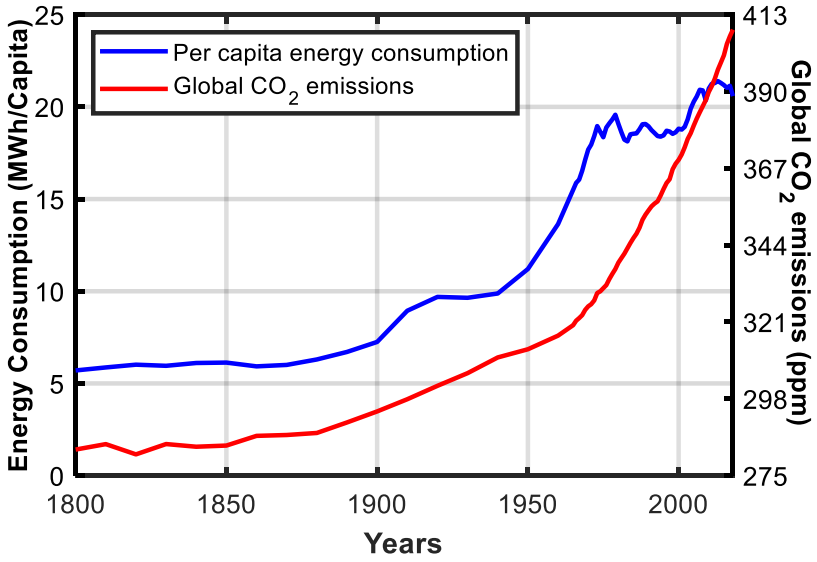

Figure 1.2: Annual global energy consumption per capita and CO_2 emissions from 1800 to 2018 and world population. Data adapted from [[56],[9],[68], [30], [39]] (CO_2 emissions data were interpolated where necessary).

As seen in Figure 1.1, the share of renewable energy sources is relatively small compared to the global energy mix. However, solar energy has a significant development potential and by far has the largest prospects in terms of capacity. Solar energy is converted into electricity using "indirect" thermoelectric generation (heat exchange) and "direct" generation (using photovoltaics (PV) devices) conversion methods [70]. Moreover, solar energy can be harvested by decentralised systems and requires minimal maintenance due to the absence of dynamic parts [55].

Like any other technology, photovoltaic technologies also face significant challenges namely: low conversion efficiency, fluctuations in energy yield on a daily and seasonal basis, and electrical mismatch losses due to irregular working conditions. Nonetheless, over the past few decades, a lot of research has been done on increasing the conversion efficiency and also on storage technologies to mitigate the intermittent nature of solar energy. Research is also being done on reducing production costs of PV systems. As a result, PV technologies are becoming much more economically feasible source of electricity on different parts of the globe [10].

1.2. STATUS OF PV INSTALLATIONS

Growing awareness about climate change leads to rapid developments in the energy sector. In 2018, more than 512 GW of PV was deployed worldwide [28]. This is an increase of around 100 GW from previous year. A considerable share of this new capacity is installed in residential PV systems especially on commercial rooftops. Plummetting installation prices accompanied with incentives for renewables, is allowing building owners to invest in urban PV systems even at non-ideal locations where partial shading is inevitable. In urban landscapes, partial shading of solar modules is a common phenomenon as shown in Figure 1.3. [23]. When a part of the solar module is shaded, it can be said that the solar module is partially shaded. It occurs due to nearby objects, like trees, chimneys

or neighbouring buildings.

Figure 1.3: Partial shading caused by chimneys, dormers,trees, the shape of the building itself, etc. [5]

1.3. PROBLEM STATEMENT

When a solar module is shaded, the module current is limited by the current of the worst performing (i.e. most shaded) solar cell since the cells are connected in series. This results in power loss. Sometimes the unshaded solar cells, force the shaded solar cells to operate in the reverse bias A conventional solar module consists of multiple solar cells connected in series. The solar module generally has three solar cell arrays connected in series, each with a bypass diode connected in parallel. The purpose of bypass diodes is to reduce power dissipation and prevent hot-spot formation which can permanently damage the module. Ideally, the reduction in the output power should vary proportionally to the reduction in the incident irradiation on the module, and is known as shading linearity. In partial shading conditions, the irradiation incident on a solar module is non uniformly distributed. Due to the series connection of solar cells and the limited number of bypass diodes in a conventional solar module, current mismatch leads to significant and disproportionate power losses. By shading one half of a cell of any conventional front-back contacted multi or mono c-Si solar module which has 3 bypass diodes, a whole subgroup of the module could be bypassed potentially reducing the power output by a third of its maximum output.

Improving the shading resilience of modules increases the electrical performance of PV systems especially in urban landscapes where partial shading is very common. Additionally, the potential of indoor, façade and other novel PV concepts can be explored. These applications help buildings to meet their energy demand and can be divided into building added photovoltaic (BAPV) and building integrated photovoltaic (BIPV) systems. It is a widely known fact that shading in urban landscapes has a huge impact on the electrical performance of these systems. Most research is currently focused on improving the forward bias characteristics of solar cell and reducing the costs of solar modules [37]. Innovative research looks into reverse bias characteristics of a solar cell and reducing the losses. Improving these reverse characteristics would come in handy especially for urban photovoltaics where operation of solar cell in reverse bias is common due to partial shading.

1.4. PARTIAL SHADING IN A SOLAR MODULE

Partial shading has significant impact on the output power of the solar module. This can be understood with the help of the following example: When a conventional solar module is partially shaded, the incident irradiation drastically reduces followed by a decrease in photo-generated current. Solar cells in conventional modules are usually connected in series, hence, the shaded cell limits the current flowing through the module which leads to an overall decrease in power output. The affects of partial shading could be as bad as losing one third of power output by shading less than 1 % of the entire solar module.

In many (if not most) cases, a shaded solar cell is enforced to operate in reverse bias by the unshaded cells, which enforces the voltage across the shaded cell to be higher in magnitude than the reverse breakdown voltage. The reverse breakdown voltage is defined in different ways in the literature. But, one of the most common ways, defines the breakdown voltage as the voltage across a dark solar cell when 2 A of current is forced through it. In conventional solar modules, bypass diodes are incorporated to prevent the cells to reach the breakdown voltage, i.e., even before a shaded cell begins to operate at the breakdown voltage, the corresponding bypass diode starts conducting, protecting the solar cell and hence the solar module.

In partial shading conditions, the shaded module rather than generating, dissipates power and heats up the solar module. As the temperature of the solar module increases, its output current increases exponentially, while the voltage output is reduced linearly ultimately reducing the power output. The rise in module temperature not only reduces the efficiency of the solar cell but it could also lead to cracks in encapsulation material, or other materials wearing out and consequently formation of hotspots [35]. Hence, partial shading leads to variable illuminations and temperatures on a solar module.

1.5. RESEARCH GOAL AND OUTLINE

The aim of this report is to study the impact of the reverse characteristics of c-Si solar cells in the annual energy yield of partially shaded PV systems. This objective can be divided into the following sub questions:

1. What is the ultimate electrical potential of solar modules made of low breakdown voltage solar cells in urban landscapes?
2. Which thermo-electrical model accurately represents commercially available solar cells with low reverse breakdown voltage.
3. How does the performance of the solar modules made of the two types of commercially available solar cells compare with each other?

These questions will be answered by creating an equivalent electrical model of the solar module which are assumed to be made with low reverse BDV solar cells. With the help of measurements of the available low reverse BDV solar cells a thermo-electrical model would be characterised. Finally accurate simulations are run for a typical PV system in an urban landscape to determine the potential and electrical performance of the solar module.

Chapter 2 gives a brief introduction on operating principles of photovoltaic technologies. This chapter also introduces an equivalent mathematical model to simulate the electrical behaviour of solar cells. Chapter 3 addresses the architecture of the proposed solar module and its potential in a typical urban landscape. A comparative performance study between conventional and low BDV solar

cells. In chapter 4 a thermo-electric model of commercially available low BDV solar cells has been generated with which an accurate performance study has been made in Chapter 5. Finally, chapter 6 provides conclusions and recommendations for further research to substantially improve the potential of solar modules in the urban environment.

2

LITERATURE REVIEW

2.1. BASIC OPERATION OF SOLAR CELLS

Solar cells are the most basic components of a solar module. A solar cell converts light into electricity, using the photovoltaic effect: the generation of a potential difference between two different materials upon exposure to light. The production of electricity happens in four phases: absorption, generation, separation and collection of charge carriers. When a semiconductor material is exposed to sunlight it absorbs light of a particular wavelength. If the energy of the incident photon is larger than the bandgap of the semiconductor, an electron-hole pair can be formed. If this electron-hole pair is not separated, it recombines to release energy as a photon. Therefore, a combination of p-type and n-type doped material is used to separate these free charge carriers[55]. To put the energy contained by charge carriers to use, the electrical contacts of the solar cell should be connected to a load. Spectral mismatch, recombination and other losses should be as low as possible to achieve high efficiencies.

The current density of a single junction solar cell is in the range of 25-45 $\mathrm{mA\,cm^{-2}}$ which roughly translates to 10 A for a 6-inch squared cell. The voltage of the solar cell is dependant on the band gap energy of the semiconductor material and is in the range of 0.6-0.7 V. The voltages are too low for most applications, hence solar cells in a module are connected in series. Therefore, the solar modules electrical behaviour is similar to that of solar cells. Alike all semiconductor devices, a solar cell can operate in both forward and reverse bias. In special situations such as partial shading, the shaded solar cell is sometimes forced to operate in reverse bias. Other than that, a solar cell usually operates in forward bias to generate power. Hence, most of the research in this field has been focused on improving the forward characteristics.

2.2. SOLAR CELL TECHNOLOGIES

During the last century a huge number of solar cell technologies have been developed for various applications. PV technologies are broadly classified into three generations.

2.2.1. WAFER-BASED SOLAR CELLS

Silicon wafer technology is the fundamental technology used for first-generation solar cells. With over 90 % market share of solar cell production, crystalline silicon (c-Si) wafer-based solar cells are currently the most dominant technology [21]. These cells have a single junction structure. Theoretically an efficiency upto 33 % can be achieved with these cells [63]. First-gen solar cell is the most mature technology and hence, they last longer and have higher efficiency compared to other solar cells. These cells when compared to other cell technologies, not only have higher production costs

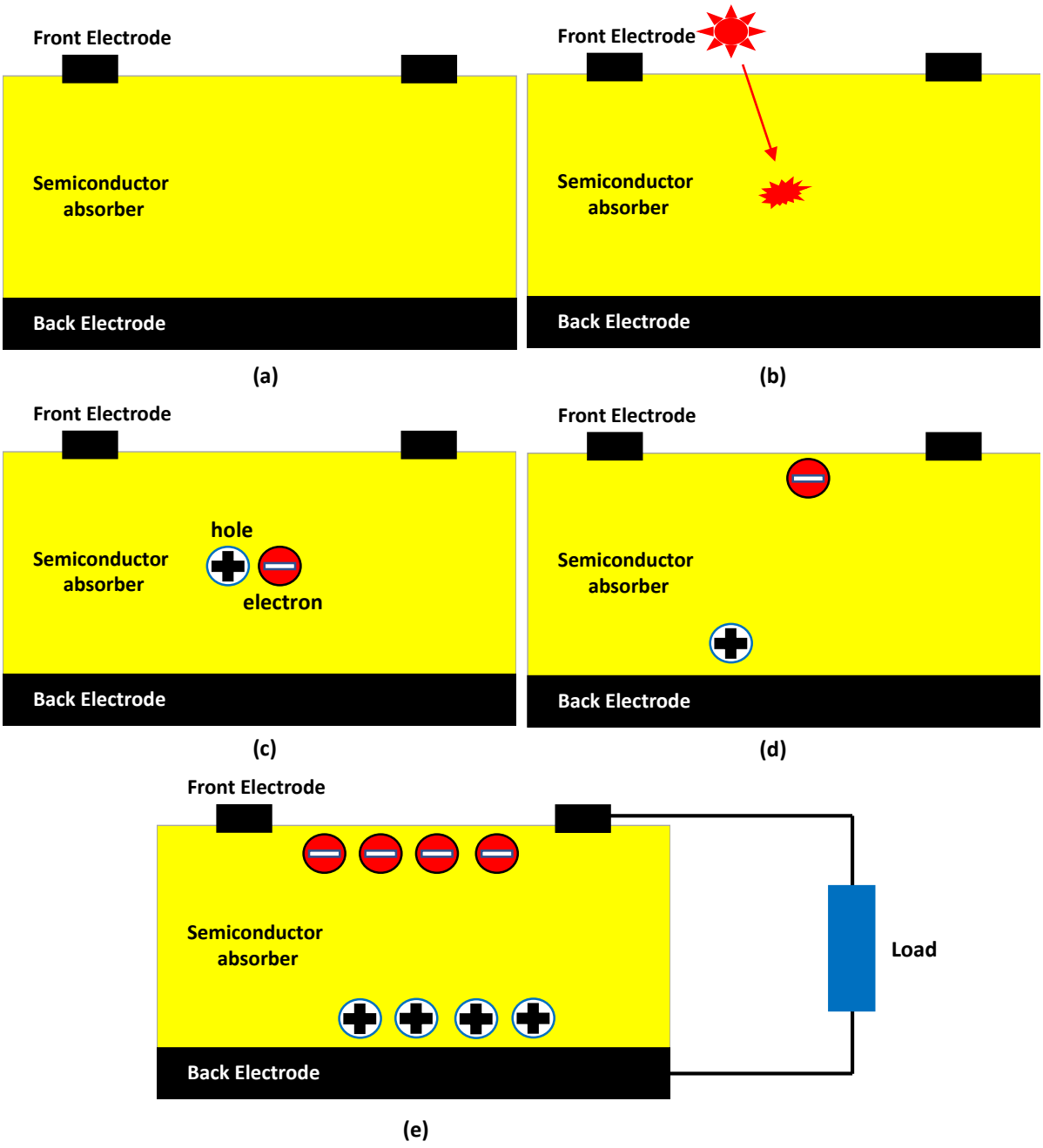

Figure 2.1: (a) Simplified structure of a typical front-back contacted solar cell (b) Absorption of light by solar cell (c) Generation of electron hole pair (d) Separation of electron hole pair (e) Collection of excess charge carriers

but also degrade easily at high temperatures [73].

2.2.2. THIN FILM SOLAR CELLS

Second-generation solar cells are a lower cost version of single-junction devices. Amorphous silicon, CdTe and CIGS are the three most common types of thin film cells and occupy around 6.6 % of the cumulative PV production[21]. Second-generation solar cells are usually manufactured by thin-film PV technology. These cells are usually made of very thin layers of semiconductors when compared to the first generation cells and hence, their manufacturing cost in terms of semiconduc-

tor material is drastically reduced. These thin layers cells help in making the cells flexible and also allows the solar modules to be printed. The efficiencies of these cells are usually lower compared to first-generation cells since, lesser amount of semiconductor material is used [73]. The efficiency of these cells varies proportionately with their manufacturing costs. CdTe solar cells have the least costs among thin film cells and it's efficiency varies from 9.4 % to 13.8 %. CIS and CIGS technologies efficiency typically ranges from 11 %-19 % [74]

2.2.3. THIRD-GENERATION SOLAR CELLS

The main aim of these solar cells is to generate high-efficiency and low cost devices by continuing the use of thin-film technology. A variety of new materials such as solar inks, nanotubes, organic dyes, conductive plastics, etc., are used to achieve this target. A lot of research and development on the third-generation PV technology is being conducted by research groups in universities or companies laboratories and are still at the niche market level such as aerospace applications [73]. The current world record efficiency for a multi-junction cell (GaInP/GaAs; GaInAsP/GaInAs) under an intensity of 508 Suns is 46 % [22].

2.3. CURRENT-VOLTAGE (I-V) CURVES AND EXTERNAL SOLAR CELL PARAMETERS

The IV curve shows all possible operating points of a PV cell. They are achieved by measuring the voltage across and current through the solar cell while changing the value of a resistive load connected between the cell's electrical contacts. The current-voltage relation can be used to derive a number of important external parameters which are used to describe and compare the electrical performance of different solar cells. Figure 2.2 shows a typical IV curve in the first and second quadrants along with the external parameters of a solar cell. In the first quadrant the solar cell operates in the forward bias and works as a generator. The solar cell sometimes operates in the second quadrant during partial shading conditions. From this quadrant, it can be said it is a conventional solar cell with a breakdown of around -14 V. The scales of the two quadrants are different so as to obtain proportionate curves for better readability.

The main parameters which reflect the electrical performance of a solar cell are the peak power (P_{mpp}), the open circuit voltage (V_{oc}), the short circuit current density (J_{sc}), fill factor (FF) and efficiency (η). The J_{sc} and V_{oc} are the maximum current density through and maximum voltage across a solar cell when the solar cell works as a generator i.e in the first quadrant. The generated power at these operating points is zero since they are operating either in short-circuit (zero voltage) or in open-circuit conditions (zero current).

The point where the product of current and voltage reaches a maximum is known as the maximum power point (MPP) and the corresponding voltage and current values are (V_{mpp}) and (I_{mpp}) as indicated in Figure 2.2. The mathematical expression to find the maximum power point uses the derivative with respect to the voltage and is given by

$$\frac{dP}{dV} = \frac{d(JV)}{dV} = 0 \tag{2.1}$$

Power is only generated when both the current and voltage are positive. The solar cell dissipates power when either the current or voltage is negative. The fill factor (FF) is defined as the ratio between the maximum power of the PV cell and the product of J_{sc} and V_{oc}.

$$FF = \frac{P_{mpp}}{J_{sc}V_{oc}} = \frac{J_{mpp}V_{mpp}}{J_{sc}V_{oc}} \tag{2.2}$$

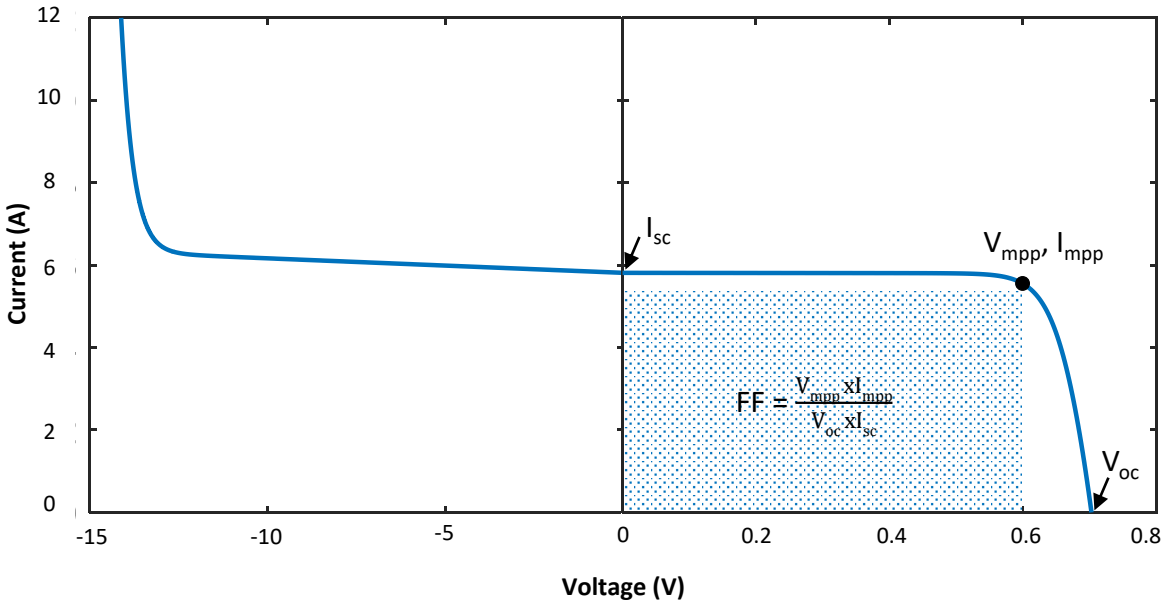

Figure 2.2: Typical IV curve with its external parameters

where P_{mpp}, J_{mpp} and V_{mpp} are respectively the power, current and voltage at maximum power point. The conversion efficiency in terms of the solar cell parameters and incident irradiance on solar cell (P_{in}) is given by

$$\eta = \frac{P_{mpp}}{P_{in}} = \frac{J_{sc} V_{oc} FF}{P_{in}} \tag{2.3}$$

Since the electrical performance of a cell is dependent on both irradiance and temperature, tests are usually performed at standard test conditions (STC). These conditions require an irradiance of $1000\,W\,m^{-2}$ using the AM 1.5 spectrum and a cell temperature of 25 °C.

2.4. EQUIVALENT SOLAR CELL CIRCUIT

The electrical performance of a solar cell can be simply determined by tracing its IV curve. However, changes in measurement conditions such as fluctuations in irradiance and cell temperature affect the experiments. Therefore, an electrically equivalent model of a solar cell built with basic electronic components is often simulated to understand it's electrical behaviour at desired conditions.

There are many equivalent solar cell models out of which the two most common models (a) Five parameter single diode model (b) 7 parameter double diode model are shown in 2.3. The common parameters in both the models are the photogenerated current (I_{ph}), shunt resistance (R_{sh}) and series resistance (R_s). The other parameters being diode(s) and ideality factor(s) whose numbers change with the model used.

The single diode equivalent circuit of a solar cell is a current source in parallel with a single diode considering two lumped resistances which are the shunt (or parallel) resistance and the series resistance. Similarly, the double diode equivalent circuit of a PV cell is a current source in parallel with two diodes considering two lumped resistances which are the shunt and the series resistance. The configuration of the equivalent electrical circuit is shown in Figure 2.3

Electron-hole pairs will be generated in the solar cell provided that the incident photon has an energy greater than that of the band gap. The current produced by these electron-hole pairs is known as the photogenerated current and is represented by the current source. The losses due to leakage in a solar cell are represented with shunt (R_{sh}) and series resistances (R_s). The losses due to the recombination in the p-n junction is represented using diodes. The ideality factor is a fitting parameter used to compare the diode's behaviour with that predicted by theory. It is usually assigned with a constant value but in reality it is a function of voltage across the device.

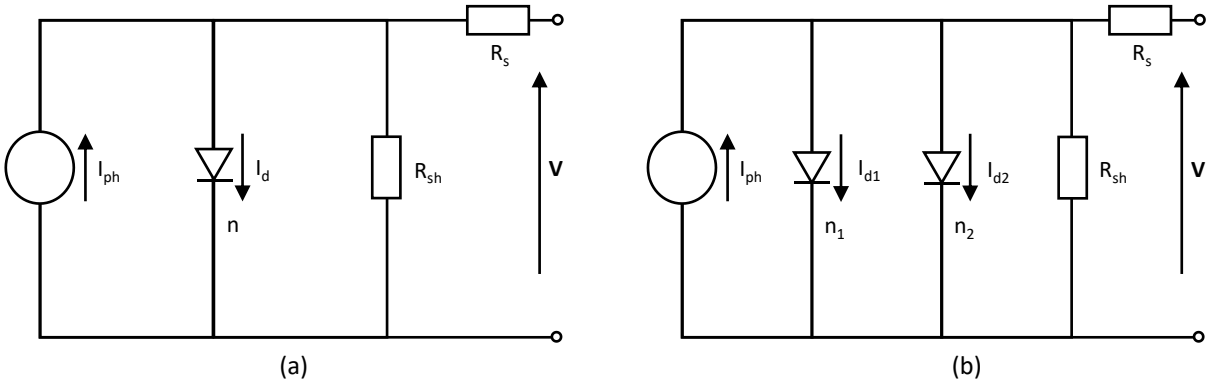

Figure 2.3: (a)One-diode & (b) two diode equivalent circuit of a solar cell

The shunt resistance is caused by manufacturing defects and provides an alternative path for current between both two terminals of the solar cell. The series resistance is due to the bulk resistance in the p-n junction, the contact resistance between the junction and electrodes and the resistance of the electrodes [5]. Ideally, the shunt resistance should be infinite and the series resistance should be zero.

From figure 2.3(b) the current generated in a two diode model of the solar cell can be derived using Kirchhoff's law and is given by:

$$I = I_{ph} - I_{d1} - I_{d2} - I_{sh} \tag{2.4}$$

where I is the output current of the solar cell, I_{ph} is the photogenerated current, the currents through the diodes I_{d1} and I_{d2} represent the dark current of solar cell and I_{sh} is the current through the shunt resistance. The voltage across both the diodes and shunt resistance is the sum of the output voltage of the solar cell and the voltage across the series resistance and equals $V + IR_s$. Substituting this in the Shockley diode equation gives:

$$I_d = I_0\left(\exp\left[\frac{q(V+IR_s)}{nkT}\right] - 1\right) \tag{2.5}$$

where I_0 is the reverse saturation current governed by diffusion and recombination of electrons and holes in the solar cell, q is the charge of an electron, k is the Boltzmann constant, T is the temperature and n is the diode ideality factor of the solar cell. The ideality factor (n) is 1 if the dark current is determined only by diffusion, and n > 1 if recombination in depletion region also contributes to the dark current [43]. The ultimate equation for the double diode solar cell model is given by

$$I = I_{ph} - I_{o1}\left(exp\left[\frac{q(V+IR_s)}{n_1kT}\right] - 1\right) - I_{o2}\left(exp\left[\frac{q(V+IR_s)}{n_2kT}\right] - 1\right) - \frac{V+IR_s}{R_{sh}} \tag{2.6}$$

By neglecting the recombination current i.e by equating $I_{d2} = 0$ in equation 2.4, the current equation for single diode model can be obtained. To find representative values for parameters such as saturation current and ideality factors is the biggest challenge of modelling a solar cell. This is discussed in detail in chapter 4.

2.4.1. EFFECTS OF VARIABLE IRRADIATION AND TEMPERATURE ON SOLAR CELL PARAMETERS

The principle solar cell parameters used to characterise their performance are the peak power P_{max}, the short-circuit current density J_{sc}, the open circuit voltage V_{oc}, and the fill factor FF, out of which J_{sc} and V_{oc} are critical. The open circuit voltage V_{oc}, as the name indicates is the voltage at which the external circuit of a solar cell is not connected to any load i.e. there is no current flow; the short circuit current J_{sc} is the current that flows when the external voltage is zero i.e. the solar cell terminals are short circuited. The V_{oc} and J_{sc} are the maximum voltage and current values a solar cell can achieve[55].

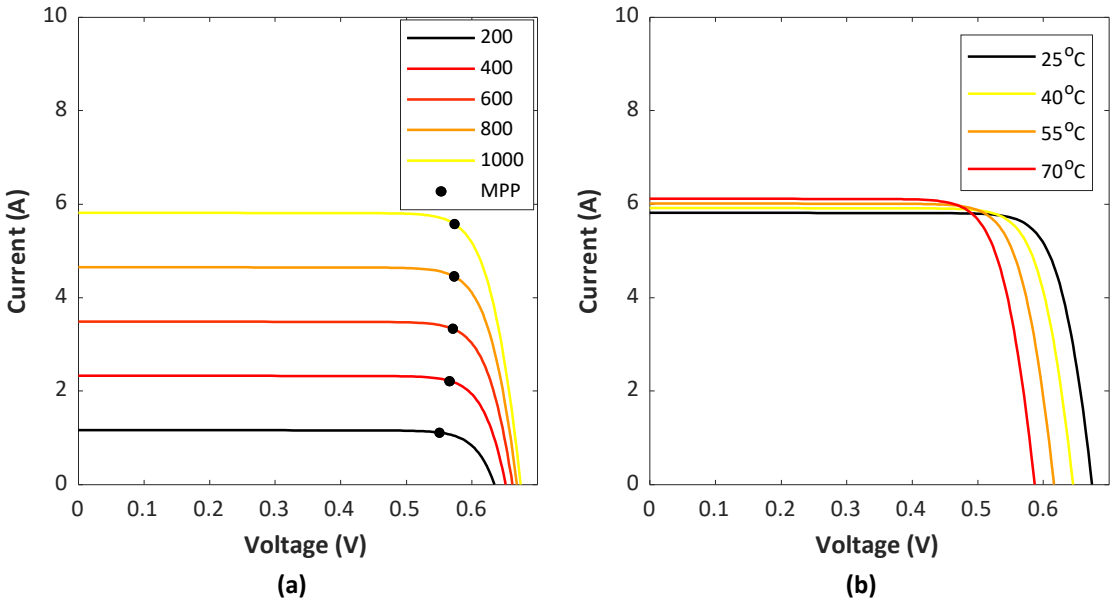

Figure 2.4: IV curves for (a) different irradiance values (b) different temperature values

The external parameters V_{oc} and J_{sc} of a solar cell are dependent on both irradiance and temperature. The photogenerated current depends linearly on the irradiance. It is assumed that the spectral distribution of the solar radiation is maintained and the short circuit current is equal to the photogenerated current I_{ph}. The short-circuit current can be approximated as

$$J_{sc}(G, T_{STC}) \approx \frac{G}{G_{STC}} J_{SC,STC} \tag{2.7}$$

where G is the irradiance, G_{STC} is irradiance at standard test conditions which is $1000\,W m^{-2}$ and $J_{SC,STC}$ is the short-circuit current at standard test conditions. The open-circuit voltage on the other hand depends logarithmically on the solar irradiation and is given by

$$V_{oc}(G, T_{STC}) = V_{oc,STC} + \frac{nkT}{q} \ln\left(\frac{I_{ph}}{I_0} + 1\right) \approx V_{oc,STC} + \frac{nkT}{q} \ln\left(\frac{G}{G_{STC}}\right) \tag{2.8}$$

where $V_{OC,STC}$ is the open-circuit voltage at standard test conditions. From equations 2.7 and 2.8 it is clear that the current varies proportional to irradiance whereas the voltage varies logarithmically. The IV curves for a range of irradiation intensities are shown in Figure 2.4(a) .

$$n_i{}^2 = N_c \cdot N_v \cdot \exp\left(\frac{-E_g}{kT}\right) \tag{2.9}$$

Equation 2.10 is the formula for the intrinsic carrier concentration represented in terms of effective density of states in conduction and valence band (N_c and N_v), band gap (E_g), boltzmann constant (k) and temperature (T).

$$I_0 = C \cdot T^3 \cdot \exp\left(\frac{-E_g}{kT}\right) \tag{2.10}$$

Equation 2.10 represents the saturation current as a function of temperature. C is a constant derived from a combination of doping and material parameters of solar cell. From equations 2.9 and 2.10 it can be deduced that I_0 is strongly dependant on the exponential term and hence on the intrinsic carrier concentration[44].

The bandgap of the semiconductor decreases with increase in temperature. This increases the photogenerated current because more photons have enough energy to create electron-hole pairs. The overall effect of temperature on the short-circuit current can be approximated by

$$J_{sc}(G_{STC,T}) \approx J_{sc}(G_{STC}, T_0)\Big(1 + \alpha_{Jsc}\Big(T - T_0\Big)\Big) \tag{2.11}$$

where $\alpha_{J_{sc}}$ is the temperature coefficient of J_{sc} and is positive and T_0 is the reference cell temperature and often equals 25°C [27]. Equation 2.8 suggests that the open-circuit voltage should increase with temperature. However, the saturation current drastically increases with the cell temperature as shown in equation 2.10, therefore the overall effect on the open-circuit voltage is given by

$$V_{oc}(G_{STC}, T) \approx V_{oc}(G_{STC}, T_0)\Big(1 + \beta_{Voc}\Big(T - T_0\Big)\Big) \tag{2.12}$$

where $\beta_{V_{oc}}$ is the temperature coefficient of V_{oc} and is negative. Since the relative temperature coefficient of V_{oc} has the largest magnitude, the maximum power point drops with increase in temperature. The IV curves for a range of cell temperatures are shown in Figure 2.4(b) .

Decrease in irradiance has minute effect on the open circuit voltage (V_{oc}) but the short circuit current density J_{sc} of the solar cell varies proportionally with the irradiance. The (V_{oc}) is the most affected parameter due to increase in temperature, whereas the J_{sc} slightly increases with temperature. Partial shading of solar modules causes change in temperature and irradiance leading to disproportional impacts on external electrical parameters.

2.4.2. BREAKDOWN VOLTAGE

The reverse voltage applied across a p-n junction, at which a sudden current flow begins, is called the breakdown voltage. In this report the breakdown voltage for a solar cell is defined as voltage across a dark solar cell when 2 A of current are forced through it. Linear behaviour at low bias and superlinear behaviour at a relatively higher bias are considered as the (characteristics of) general breakdown behaviour of a solar cell[11]. There are two classes of breakdowns namely: (a) Soft breakdown and (b) Hard breakdown. The main difference between these two breakdowns is: the soft breakdown is characterised by a small change of voltage or current while hard breakdown is detected by a much higher change of voltage or current during stress and a post-breakdown I-V characteristics [1] as shown in Figure 2.6(a).

The different types of breakdown voltages can be seen in the Figure 2.6(b) out of which the two most common types of breakdowns are avalanche breakdown and zener breakdown. Multiple free charge carriers move into high field region and accumulate into an avalanche resulting into high currents. The large increase in current even with small terminal voltages due to internal field emission, where an electron jumps over the forbidden gap because of the quantum mechanical tunnel effect is known as zener breakdown [40].

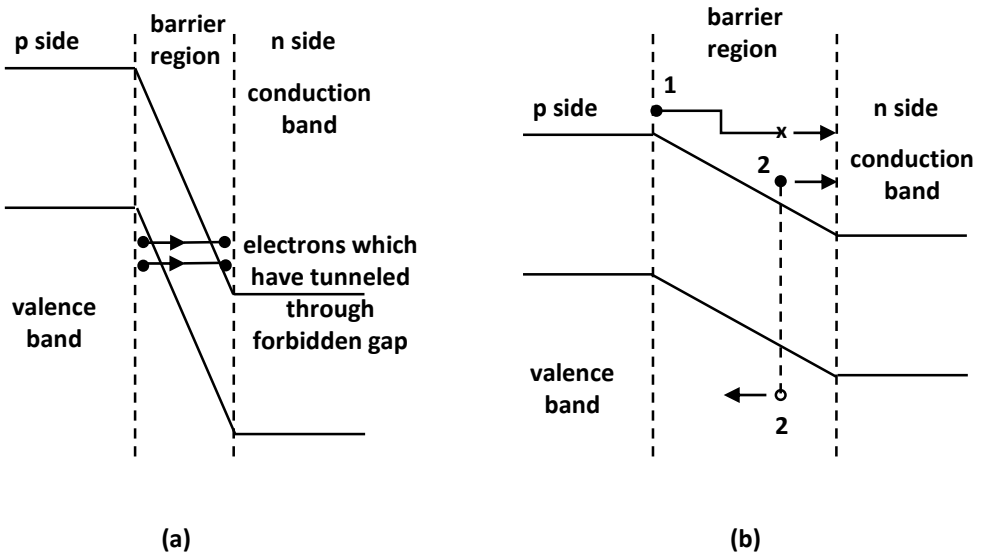

Figure 2.5: (a) Internal field emission : thin junction resulting in a high field across the junction (b) Avalanche breakdown: x represents the place at which the initial electron 1 is capable of producing an electron-hole pair which undergoes further multi- plication. Short vertical lines represent energy loss [40]

Introduction of dislocation-free Si crystals led to a halt of research on crystalline silicon breakdown mechanisms. However, the arrival of multi crystalline Si solar cells into the market brought back the breakdown problems. Breakdown in solar cells is complex and different breakdown types may exist intermixed side-by-side. However, in favorable cases and in certain regions one breakdown mechanism dominates. In the experiments performed by researcher Otwin Breitenstein three different types of breakdown appeared in different reverse bias range.

In a multi crystalline solar cells, the early breakdown is associated with the presence of Al particles on the surface even before the deposition of the antireflection layer and is observed before $-5\,V$. Al is a p-dopant which may overcompensate the n^+-emitter if the cell is heated up. Depending on size of the particle and Al doping a highly doped p-n junction may be formed. A highly doped p-n junction may break down already at a few volts reverse bias by internal field emission (Zener effect). Therefore it can be said that zener breakdown dominates the type I breakdown[11].

The type-2 breakdown sites is connected with recombination-active crystal defects. These defects are likely formed due to Fe contamination. The secondary breakdown ranges from $-9\,V$ to $-13\,V$ [11]. A few structural defects, intensify local electric field resulting in localized current flow and consequently cause premature breakdowns. The localized breakdown is referred to as secondary breakdown and the regions at which this happens is referred to as microplasmas [53].

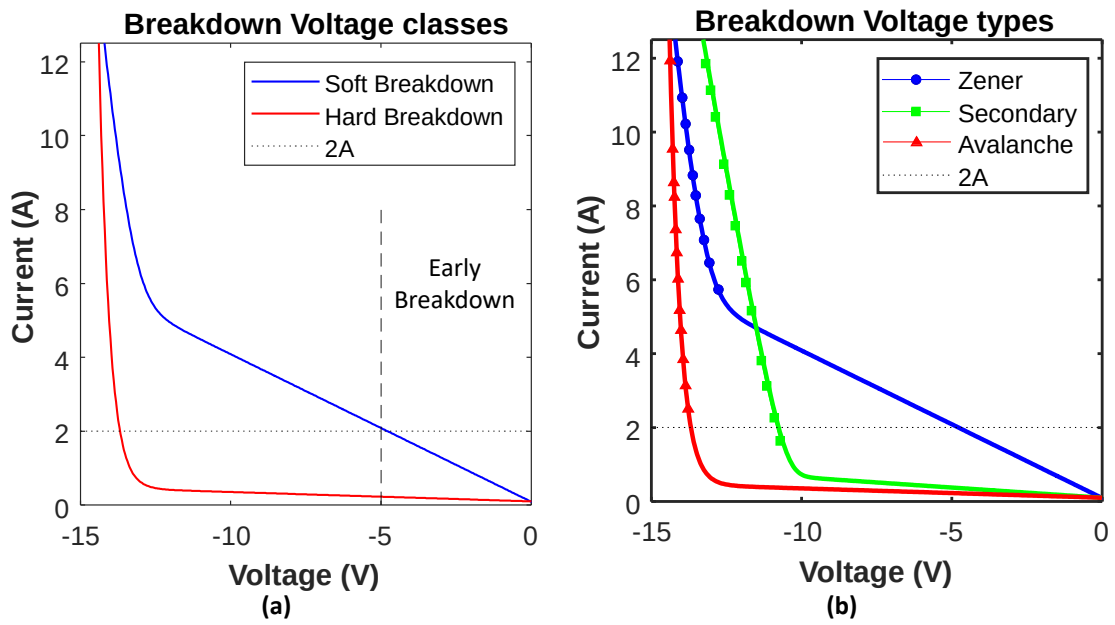

Figure 2.6: (a) Class and (b) types of breakdown

The etch pits formed during texturization using an acid solution leads to the last type of breakdown. It has been found that these etch pits lead to avalanche type of breakdown [6]. Hence, any breakdown appearing beyond −13 V is dominated by avalanche breakdown. [11]. The effect of the radius of curvature of the metallurgical junction of the tip of the etch pit and p-n junction reduces the breakdown voltage from -60V to -13 V which is exactly equal to the avalanche breakdown voltage further supporting our argument[61].

In case of CIGS solar cells, the reverse breakdown voltage reduces significantly under blue illumination compared to dark conditions. The breakdown under blue illumination usually occurs in the range of −3 V and −1.5 V. High quality CIGS withstand high current densities, indicating that bypass diodes can be avoided which improves reliability of the module.Hence, the design of CIGS deposition processes need to be done carefully[59].

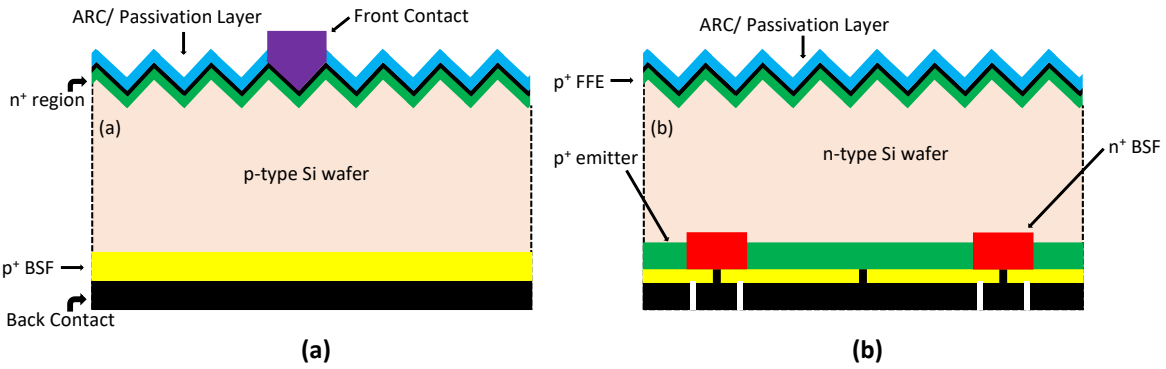

Figure 2.7: Cross sections of (a) Conventional crystalline silicon solar cell (b) inter digitated back contact cell (adapted from [51] and [18])

Unlike the conventional solar cells shown in Figure 2.7 (a), the interdigitated-back-contact solar cells (IBC cells) as shown in Figure 2.7 (b) have back contact energy conversion i.e both the electrons and holes are collected at the back contact.The breakdown of IBC cells is low, soft, uniform over the entire cell, hence it is harmless and enhances the system yield. The IBC cells have a typical p^+n^+ junction, whose doping profiles can be changed to produce an even lower breakdown voltage [16]. Research also demonstrated that breakdown in these cells is caused by the tunnelling effect rather than avalanche multiplication and results in a more uniform thermal breakdown [60]. Consequently, the power dissipation in reverse bias is considerably lower and will be distributed more uniformly across the shaded cell. Temperature rise will be limited and therefore hot-spot formation will most likely not occur in a series connection. This theory can be applied to produce an earlier breakdown in cells featuring the p^+n^+ junction; the metal wrap through (MWT) and emitter wrap through (EWT) solar cells[16] [31]. The solar cell cross sections of both these types of solar cells can be found in Figure 2.8

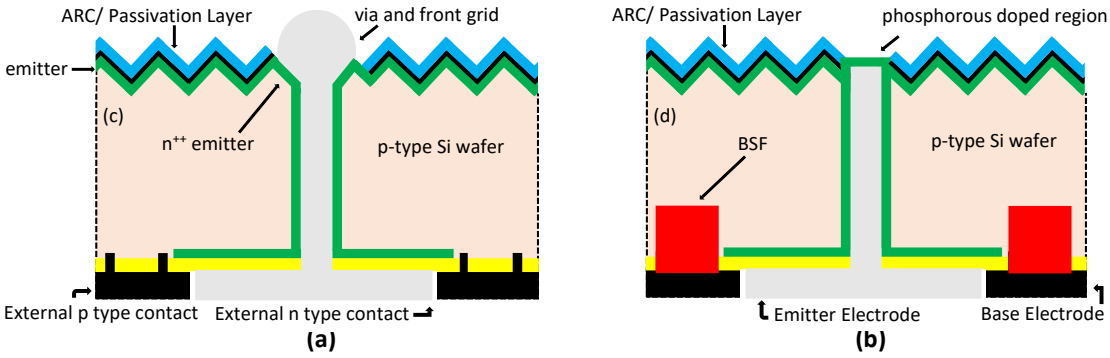

Figure 2.8: Cross sections of (a) Metal Wrap through cells (b) Emitter Wrap through cells (adapted from [62] and [15])

When a solar cell is partially shaded in a solar module, it can be forced to operate in reverse-bias and hence, dissipates power in the form of heat. This usually produces temperatures greater than 50 °C in the solar cell. Type II and type III breakdowns cause a negative temperature coefficient for voltages of $V < -12.5\,V$, whereas type I breakdown causes positive coefficient for $V < -6\,V$. In negative temperature coefficient region, the current produced varies inversely with temperature. Similar to the forward currents, the current flowing in reverse biased conditions vary proportionally with illumination. This mainly happens due to laterally distributed currents from regions of the cell which are breakdown free [19].

Ideally, power dissipated in partially shaded conditions is distributed equally over the entire cell. But, this is not always true; in certain solar cells, the heat is focused at certain defective regions causing irreversible damage. This damage is termed as hotspot formation and is discussed in detail in the upcoming section[8][35].

2.4.3. FORMATION OF HOTSPOTS

There is no standard definition for hotspot in the PV industry. Many papers define hot spot as the localized heating of a segment of the solar cell due to secondary breakdown [32], [34], [71]. Nevertheless, the term hot spots can be assigned to the heating up of solar cell even in the absence of secondary breakdown. A few researchers also define hot spot as the phenomena of increase in temperature to a higher level relative to it's surroundings[35].

Hot-spots occur when a large number of series connected solar cells cause a shaded cell to operate in high reverse bias. The shaded cell dissipates a significant amount of power which leads to localized overheating.The IV curves of unshaded and shaded solar cells can be used to visualize the power dissipation in the shaded cell(s) and to obtain the overall IV curve as shown in figure 2.9. This method is only applicable in short-circuit conditions and when the unshaded cells receive an equal irradiance. Consider the case where one cell is heavily shaded and is connected in series with 6 unshaded cells. First, the IV curve of the shaded solar cell in both forward and reverse bias should be obtained. In short-circuit conditions, the total power generated by the unshaded cells is dissipated in the shaded cell(s) and represents the worst-case scenario. Consequently, by mirroring the IV curve of the unshaded cells in the y-axis, the operating point of the unshaded cell can be identified as the intersection of it's IV curve and the reflected curve. The marked area in 2.9 (b) corresponds to the power dissipated in the shaded cell. Note that the unshaded solar cells have a higher current and voltage due to the higher incident irradiance and the series connection of multiple unshaded solar cells respectively. When many unshaded cells are connected in series, the shaded cell is forced to operate in high reverse bias which significantly increases the power dissipation [55].

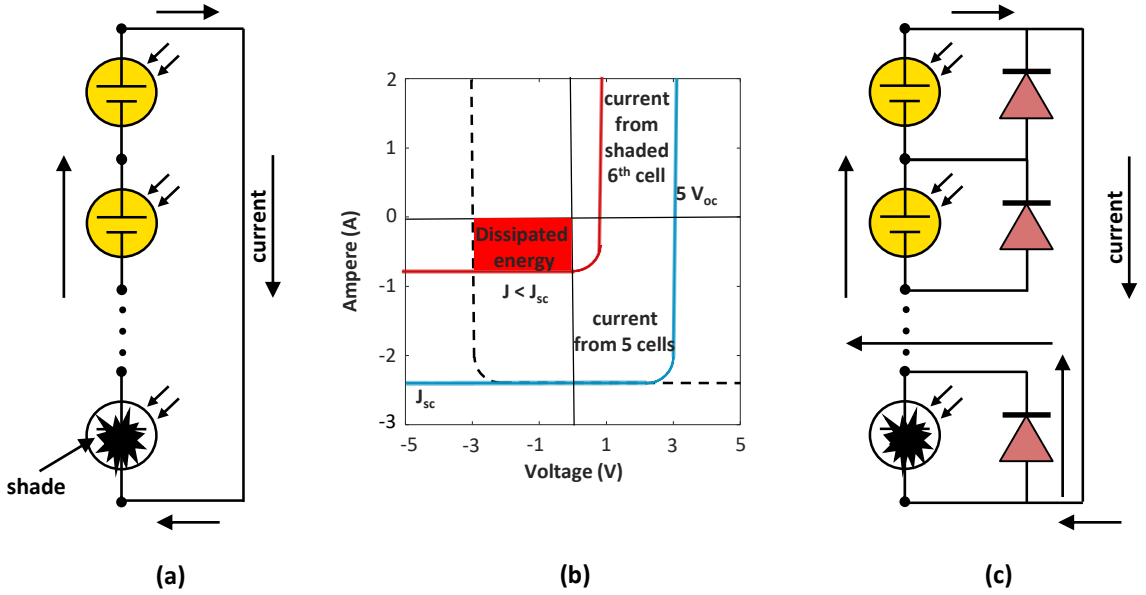

Figure 2.9: (a) A string of six (short circuited) solar cells of which one is partially shaded. (b) This has dramatic effects on the IV curve of this string. (c) Bypass diodes can solve the problem of partial shading. adopted from [55]

Severe hot-spot heating results in faster degradation of the solar cell. Moreover, it can cause permanent damage such as cell cracking and melting of solder. The important question is : at what conditions does permanent damage occur to the cell and accelerate the degradation rate? The typical rating of a solar module is around 85 °C. Increase in temperature of a solar cell can cause a thermal breakdown, which can produce high internal temperatures as high as 400 °C [4] [33]. At a temperature greater than 150 °C, the encapsulant and isolative material around the cells could get damaged [20] [25] [66]. The destruction of encapsulant, exposes the cells to environmental elements which can cause corrosion and additional damage to the cells leading to PV degradation [35].

Not only do hotspots compromise on reliability, but they are also a safety concern. Hot spots can damage solar panels and possibly lead to fires [50]. The general assumption is that using bypass diodes, protects cells from hotspots. Multiple field experiments on devices using bypass diodes

have shown that hot spotting still occurs, leading to accelerated panel degradation [13][52].

2.5. METHODOLOGIES TO IMPROVE SHADE RESILIENCE

Partial shading in solar modules could cause significant power losses and lead to the formation of hotspots. A joint effort by universities and corporations succeeded in the development of techniques to enhance the shade resilience of a solar module. In this section commercially applied methodologies along with methodologies which are in research phase are discussed. The emphasis is on the module level rather than the system level.

2.5.1. ONE BYPASS DIODE PER CELL

Using one bypass diode per cell instead of using three for the entire solar module reduces the power loss and chance of hot-spots in solar modules. This can be explained with an example: when a cell in a this kind of a module is shaded, only that particular cell is bypassed, unlike the conventional module, where shading of one cell leads to bypassing of the entire string. The decrease in power dissipation results in lesser heating of the bypass diode, improving the reliability of the module [24]. Although adding more bypass diodes would in principle improve the shade resilience of a solar module, adding too many bypass diodes eventually does not contribute to increase in shade resilience any further, especially if diodes have a high forward voltage drop (i.e. comparable to the V_{mpp} of a solar cell).

When a conventional bypass diode is activated it usually dissipates 4 W of power. This power loss is proportional to the forward voltage across the bypass diode. A modern silicon diode has a standard voltage of 600 mV, while a conventional schottky diode has a forward voltage of approximately 400 mV. Companies such as Texas instruments are developing active bypass elements which have 10 times lower forward voltage [29] than the usual diodes. The power loss of these so-called smart or active bypass diodes is therefore significantly reduced. This allows more bypass diodes to be introduced while the conduction losses remain reasonable.

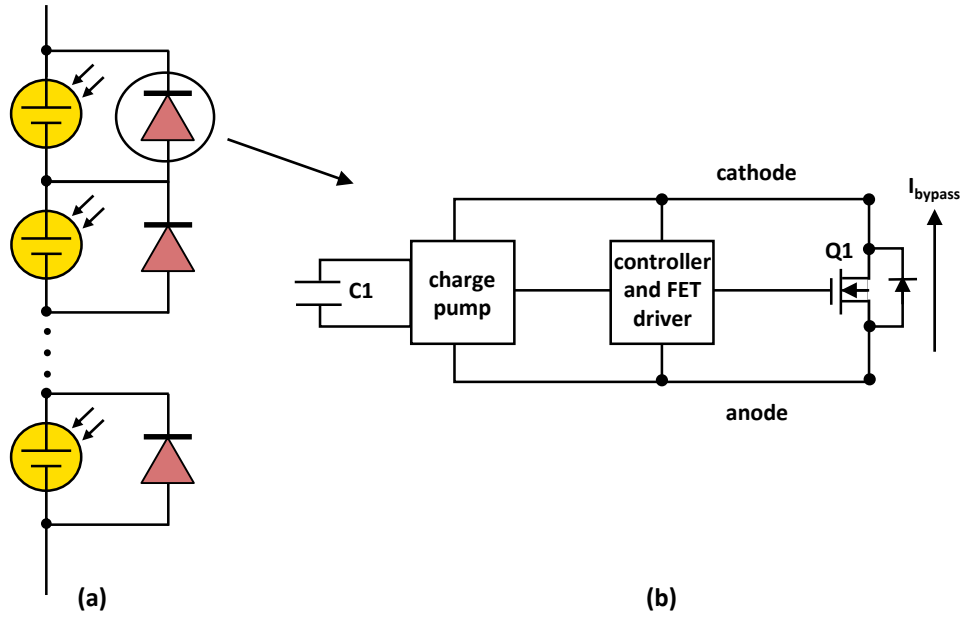

Figure 2.10: (a) Represents a solar module with one bypass diodes per cell (b) block diagram of smart bypass diode [29]

Smart bypass diodes have allowed to produce modules with one diode per cell which looks as shown in Figure 2.10 (a). In an experiment carried out by Pannebakar various topologies such as 1 BPD per cell and 1 BPD for every three cells have been examined. The 1 BPD per cell nearly has a complete linear response to various shadow patterns i.e extremely low output power loss during shading conditions. In this type of module, the power loss under partial shading is limited [46].

The main disadvantage of using smart bypass diodes is: they are expensive to introduce on a wide scale at the present time. A Schottky diode costs $0.16 while a smart bypass diode costs around $1.50. However, major cost reductions are tend to be practical with the growing economies of scale. There are yet a few more drawbacks, with a configuration such as one bypass diode per cell : Manufacturing and designing the electric circuits of modules with one bypass diode per cell could be highly complex. With increase in number of components, the number of components that could get damaged increases. Finally, the area of the module increases which could have an effect on the performance ratio [46], where the performance ratio of a solar module is given by :

$$\mathrm{PR} = \frac{\mathrm{E_{out}}}{\mathrm{G} \times A \times \eta_{\mathrm{STC}}} \tag{2.13}$$

$\mathrm{E_{out}}$ is the energy output (kWh) of the solar module, G is the irradiation in the plane of array ($\mathrm{kWhm^{-2}}$) and A is the area of the solar module ($\mathrm{m^2}$) and η_{STC} is the nominal efficiency of the solar module. The denominator is numerically equivalent to the energy which would be produced if the system is always running with its nominal efficiency as defined by the nameplate nominal power (kWh).

2.5.2. PARALLEL CONNECTIONS OF SOLAR CELLS

Cells in commercial solar modules are usually connected in series. These strings carry the same current which cannot exceed the current of a single cell and the module voltage is the sum of the individual cell voltages as shown in Figure 2.11(a). In absence of bypass diodes, the current through a series connected string is limited by the worst performing cell, as shown in Figure 2.12(a). As a result, the series architecture is hardly resilient to partial shading which occurs frequently in urban landscapes.

In contrast to series connected cells, the cells connected in parallel operate at the same voltage and the module current is the sum of the individual cell currents as shown in Figure 2.11(b) and Figure 2.12(b) shows the performance of the module with one of the cells being shaded. Power losses in the module can be calculated as:

$$\mathrm{P} = \mathrm{I^2R} \tag{2.14}$$

where, I is the output current and R is the resistance of the cables through which current flows. Due to the aggregation of current from various cells, the current adds up resulting in significant resistive power losses. Thicker cables are required to carry higher current, which further increases the costs and impacts the levelised cost of electricity (LCOE) of solar energy.

Consequently, connecting all cells in series would result in the best performance under uniform irradiance, because the resistive power losses are minimized. While, connecting all cells in parallel provides maximum shade resilience, because shaded solar cells cannot limit the current of unshaded cells and the voltage hardly varies with irradiance as mentioned in 2.4.1. But, the main disadvantage of a parallel connection is that it significantly increases the current and therefore the resistive power losses and cable costs.

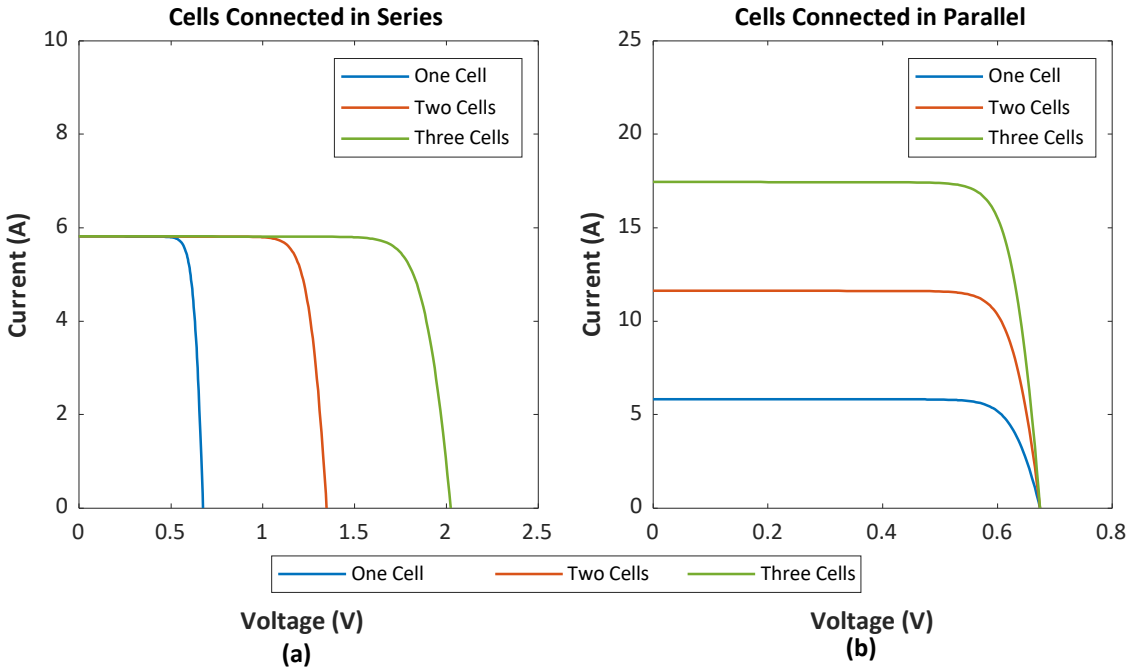

Figure 2.11: IV curves of (a) series and (b) parallel connected solar cells

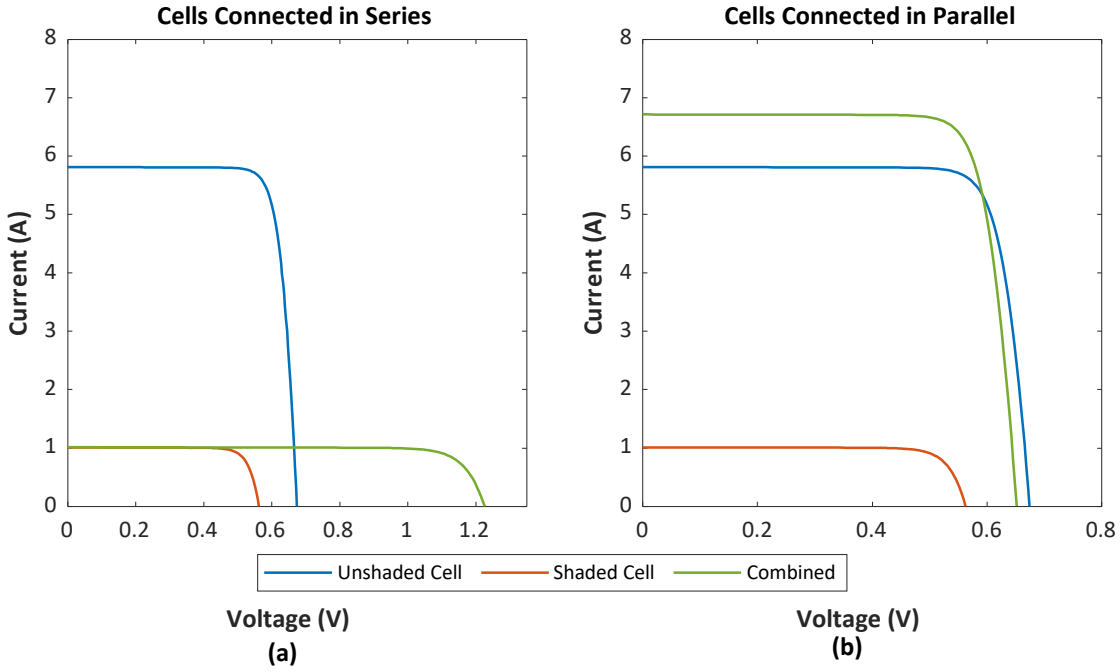

Figure 2.12: Impact of current and voltage mismatch on the IV curve when a shaded and unshaded solar cell are connected in (a) series and (b) parallel

2.5.3. ALTERNATIVE SOLAR MODULES

A solar module consists of interconnected solar cells. The way in which these cells are connected is described by their topology or architecture. The most common topologies are series, parallel, series-parallel, total cross-tied, bridge-linked and honeycomb[14]. As discussed in 2.5.2 the series architecture is hardly resilient to partial shading whereas in parallel connections there is a signifi-

cant increase in current and hence, resistive power losses and additional cable costs. Hence, it is found that series connections are preferrable only when there is uniform incident irradiance, while parallel connections are preferrable under partial shading conditions.

The series-parallel (SP) topology is a static solar module reconfiguration topology which is middle ground between connecting all cells in series or parallel. The aim is to minimize the power losses while maximizing the shading resilience. In this topology, cells are connected in series to form strings and multiple strings are then connected in parallel as shown in Figure 2.13(a) [48]. Non-uniform irradiance will now only affect the current of the strings containing the (partial) shaded cells. Compared to connecting all cells in parallel, the current and therefore the resistive power losses will be lower. The optimal configuration depends on the shading conditions and system requirements.

The total cross-tied (TCT) topology is another static module architecture to balance between shading resilience and power losses[49]. In this topology cells are connected in parallel to form rows and multiple rows are then connected in series as shown in Figure 2.13(b). Research shows that solar modules in urban landscapes which have a TCT topology generally outperform a SP architecture [65],[12].

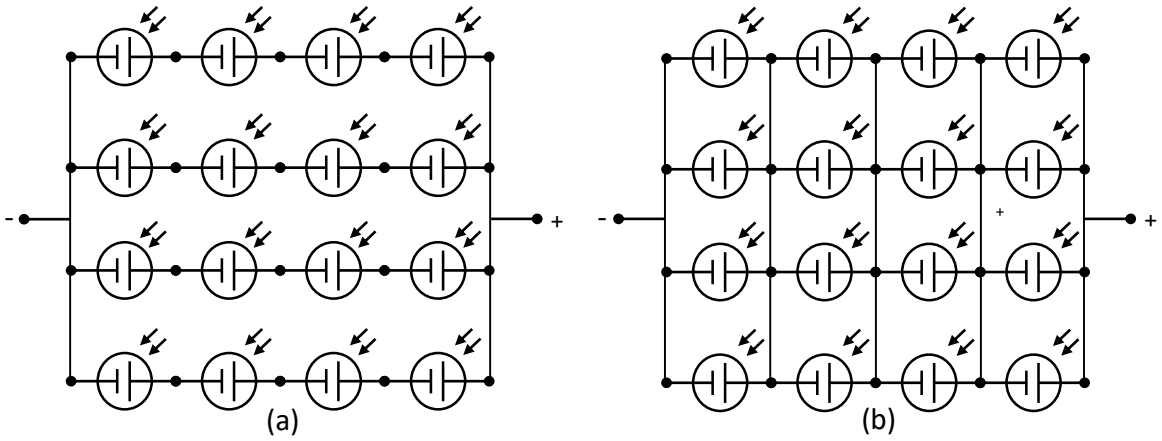

Figure 2.13: (a) Series-Parallel and (b) total cross-tied topology

Bypass diodes and parallel topologies are static techniques to improve the shade resilience of solar module and have hardwired interconnections. In contrast, reconfigurable solar modules are proposed that dynamically change the cells interconnection in real time. These topologies use switching to change interconnections in real time. The switching moments can be at regular or variable time intervals and should be chosen carefully to minimize mismatch losses. Dynamic topologies can result in higher shade resilience compared to static techniques. Dynamic topologies are mostly implemented on system level and hence, are out of scope of this report.

The above mentioned reconfigurable topologies allow the PV generator to operate under severe partial shading conditions. However, complexity and costs are the main disadvantages of using these kind of systems.

2.5.4. COMMERCIALLY AVAILABLE LOW BREAKDOWN VOLTAGE SOLAR CELLS

To improve shade resilience of a solar module various methodologies such as using active bypass elements, one bypass diode per module and parallel connection of solar cells. However, smart by-

pass diodes are extremely expensive at the moment. Complex manufacture and designs of electrical circuit are involved in one bypass diode per cell topology. Also with the increase in number of components the reliability of the functioning of components reduces. Ohmic losses in parallel connections are extremely high while in alternative solar modules are complex to build and expensive.

A technology which is cost effective and doesn't involve in complex manufacturing process would be ideal for partial shading conditions. From the active bypass elements it is clearly understood that having a low voltage leads to lesser losses.Therefore, in principle it's worth exploring characteristics of solar modules manufactured using low reverse voltage solar cells. **To the best of my knowledge there is yet no study done to assess the improvements that can be obtained with low breakdown voltage solar cells.**

Ideal solar cells would have zero reverse breakdown voltage. In such a case, we do not need bypass diodes in the system. This is going to eradicate the problems such as hotspots and power dissipation. However, in practice it's impossible to achieve a solar cell with a reverse breakdown voltage of 0 V. Nevertheless, solar cells are available in the market with breakdown voltages as low as $-5.5\,\mathrm{V}$ [57] (Sunpower Maxeon gen 2 solar cells) and $-3.2\,\mathrm{V}$ [58] (Sunpower Maxeon gen 3 solar cells), and lower breakdown voltages might be reached with proper design of the PV cell. Hence, this thesis revolves around analysing this concept by using simulations as a tool.

3

IDEAL ELECTRICAL POTENTIAL OF LOW BDV SOLAR CELLS

The chapter starts by discussing the concept of shading linearity (SL) with examples. An overview of the parameters used in the simulation framework for a case study is presented. Using the simulation model the reverse characteristics of solar cells are manipulated independently from the forward characteristics and performance of solar module has been evaluated. This is done for several synthetic shading patterns as well as realistic shading patterns. A detailed sensitivity analysis is carried out to analyse the validity of the results.

3.1. SHADING LINEARITY

Partial shading of photovoltaic modules is a common phenomena which occurs in day to day life, and is liable for around 25 % of the performance ratio of solar modules [4]. Ideally, we would like the solar modules to follow shading linearity condition during partial shading.

3.1.1. DEFINITION OF SHADING LINEARITY

According to the concept of shading linearity, the losses in a solar module are proportional to the fraction of the module shaded irrespective of orientation and distribution of shade. Mathematically, shading linearity is a plot drawn with normalised average irradiance (NAI) on the x-axis and normalised output power on the y-axis which is a bijective function like the one shown in figure 3.1(b). NAI is defined as the ratio of irradiance incident on the module at a given moment to the STC irradiance.

$$\text{Normalized Average Irradiance(NAI)} = \frac{\int\int G_{x,y} \cdot dx \cdot dy}{G_{STC} \cdot A} \tag{3.1}$$

$G_{x,y}$ is the irradiance incident on solar module shown in figure 3.1 (a) as a function of it's position in the x-y plane. G_{STC} is the irradiance at STC i.e. $1000\,W\,m^{-2}$ and A is the area of the module, which is here assumed to be product of area of one cell and number of cells. The (NAI) depends on real time irradiation hence, it accounts for all possible shading conditions such as shading due to clouds, dust particles, trees, other buildings, bird droppings etc.,

NOP is defined as the ratio of the maximum power generated by the module at a given instant to the power output at STC.

$$\text{Normalized Output Power(NOP)} = \frac{P_{MPP}(t)}{P_{STC}} \tag{3.2}$$

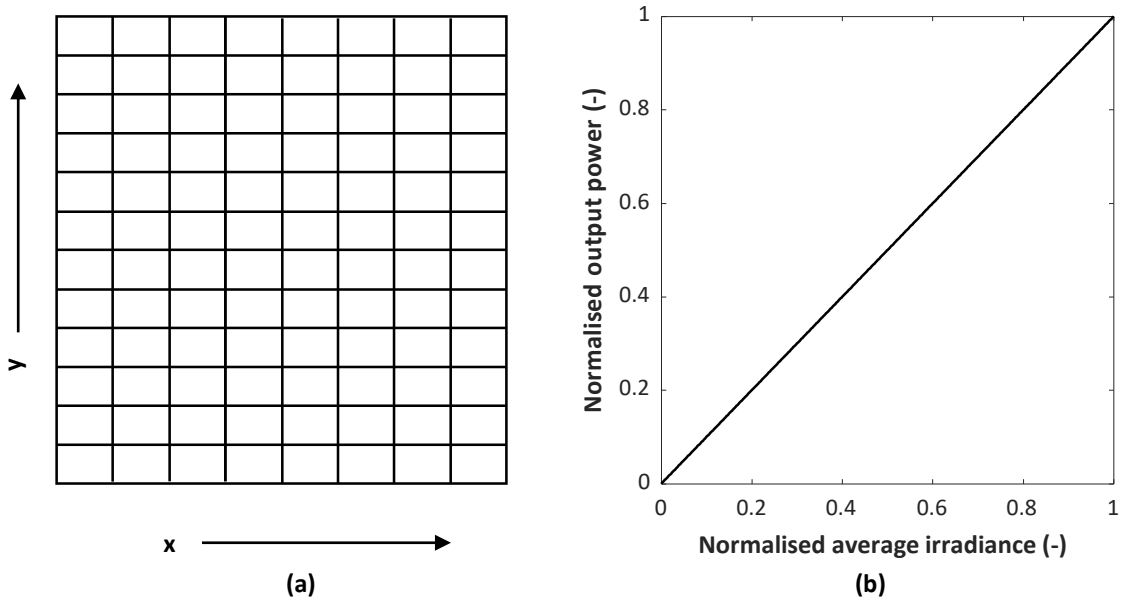

Figure 3.1: (a) Layout of a solar module (b) Shading linearity plot

Achieving shading linearity in real life situations, is not possible because with change in intensity and geometry or location of shade on conventional solar modules , there are multiple power output values for the same NSV. This has been clearly explained with an example.

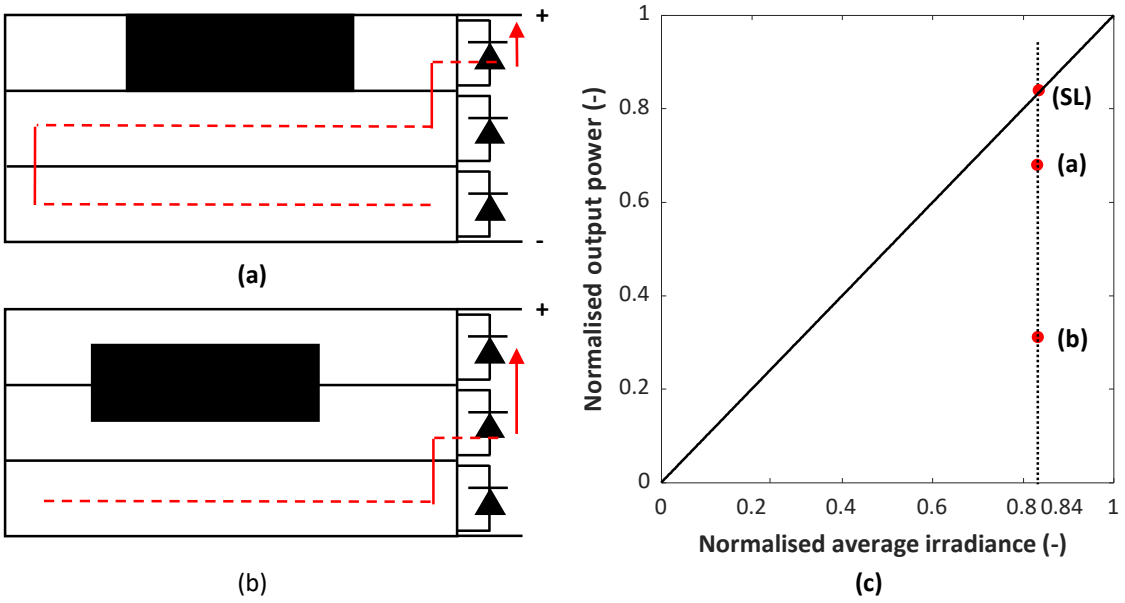

Figure 3.2: (a) One row and (b)two rows of solar module partially shaded (c) Shading linearity plot

Figure 3.2 (a) represents a conventional solar module with 3 BPDs and a shade with an area equal to 16.66 % of module area blocks the first row. Therefore, the power is generated by the other two rows

while the shaded row is bypassed and is equal to $\frac{2}{3}$ of the maximum power represented in figure 3.2 (c). The BPDs are assumed to be ideal and the shaded & unshaded parts are assumed to have uniform intensity throughout i.e $0\,W m^{-2}$ and $1000\,W m^{-2}$ respectively. As per the concept of shading linearity the power output of the module should be equal to the non shaded amount of the solar module i.e 83.33 % in this case. However this is not achieved because of the presence of BPDs which bypass the whole row, even though only half a row has been shaded.

Figure 3.2 (b) represents a similar solar module with the same shade area, but blocking the first two rows. Now two BPDs are bypassed and only a $\frac{1}{3}^{rd}$ of the maximum power is the output as shown in figure 3.2 (c). From this example, it is observed that for the same NAI values there are multiple NOP values making it a non bijective function.

Using 1 BPD per cell is a solution for achieving SL however, as discussed earlier it is economically not feasible at the moment and complex to build. To avoid the problem of bypassing, the BPDs could be avoided but this often leads the shaded solar cells to operate in the reverse bias and dissipates power equivalent to the product of current and reverse breakdown voltage. Solar cells with zero breakdown voltage would have zero losses and would be ideal to achieve SL. Nonetheless, manufacturing solar cells with zero BDV is impossible due to the presence of defects, but it is possible to produce solar cells with relatively low BDV than conventional solar cells. Therefore in the upcoming sections performance of solar modules made of solar cells whose reverse characteristics have been manipulated independently from the forward characteristics is analysed.

3.2. SIMULATION PARAMETERS

The conventional (reference) and the simulated modules are modelled in MATLAB Simulink. The solar modules considered in this report contain 96 solar cells with a size of $125\,mm^2$. The single diode five parameter solar cell model is adjusted to include the reverse characteristics associated with shading. This is done by connecting the combination of a voltage controlled switch, resistor and diode in parallel with the current source [69] making it an 8-parameter model as shown in the figure 3.3(a). The values used in this eight-parameter model are given in Table 3.1.

Parameters	**Symbol**	**Values**
Series Resistance	R_S	$3.9\,m\Omega$
Shunt Resistance	R_{SH}	$6.54\,\Omega$
Saturation Current	I_0	0.92 nA
Ideality Factor	n	1
Photogenerated Current	I_{PH}	5.81 A
Saturation Current(reverse)	I_{01}	1 fA or 1 aA
Ideality Factor (reverse)	n_1	0.1 or 12.6
Reverse Bias Voltage	V_{RB}	-1 V or -14 V

Table 3.1: Solar cell modelling parameters

The one diode model is chosen for this simulation since it is faster and results from these simulations are only used for analysing and estimation purposes. The values I_{01} and n_1 have no physical meaning but are used for simple use and faster calculations. The voltage controlled switch in 3.3(a) is used to switch the operating point from forward to reverse bias.

The IV curves of these solar cells in both reverse (breakdown voltage of -1 V and -14 V) and forward

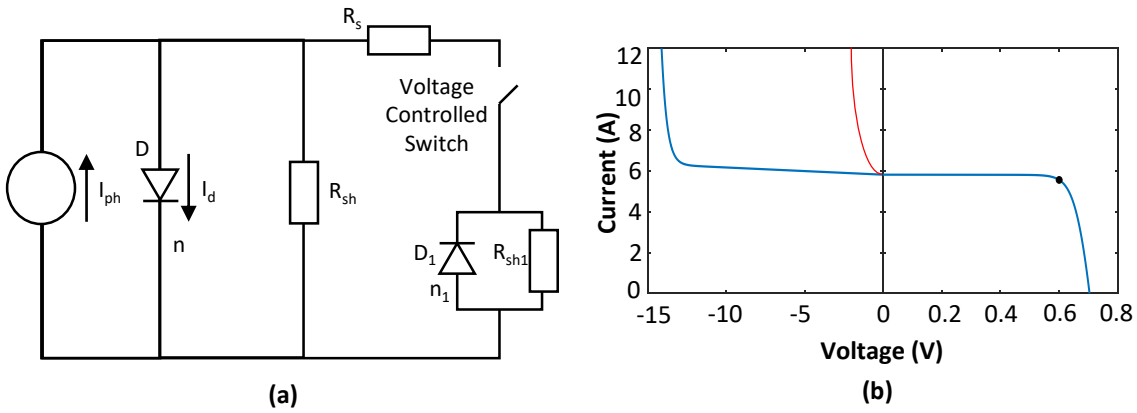

Figure 3.3: (a) 8 parameter model of solar cell (b) IV curves of solar cell with low and high breakdown voltages

bias are shown in figure 3.3 (b). All simulations are performed at a cell temperature of 25 °C which corresponds to the standard test conditions (STC). In the electrical simulations, the temperature effects described previously are not taken into account since it wouldn't have much impact on comparative studies.

Parameters	Symbol	Values
Open-circuit Voltage	V_{oc}	0.70 V
Short-circuit Current	I_{sc}	5.81 A
Power at MPP	P_{MPP}	3.33 W
Voltage at MPP	V_{MPP}	0.60 V
Current at MPP	I_{MPP}	5.56 A
Fill Factor	FF	0.82
Efficiency	η	21.77 %

Table 3.2: Simulation external parameters

The IV curve under forward bias can be used to determine the external parameters of the solar cells. These are listed in table 3.2. The power produced by each solar cell at STC is around 3.33 W.

3.3. SOLAR MODULE TOPOLOGIES

To put the proposed (solar module made of low reverse voltage solar cells) solar module into perspective, its performance is compared with two relevant reference topologies shown in Figure 3.4. The blue solar cells represent the size and orientation of a single subgroup. The 96 cell solar module is chosen because, the initial plan was to build a solar module with low reverse BDV cells. The laminator available at the PVMD group could accomodate for a maximum of 4 by 4 cells. Therefore 96 cells have been chosen. Conventional solar modules have 3 BPDs so one of the topologies imitated them as shown in figure 3.4(a). In this topology, a bypass diode is connected in parallel with each of the three series connected subgroups. A similar reference topology is obtained when switching to six subgroups as shown in figure 3.4(b). The 6 BPDs topology have been chosen because it is geometrically more shade resilient compared to the 3 BPD topology.

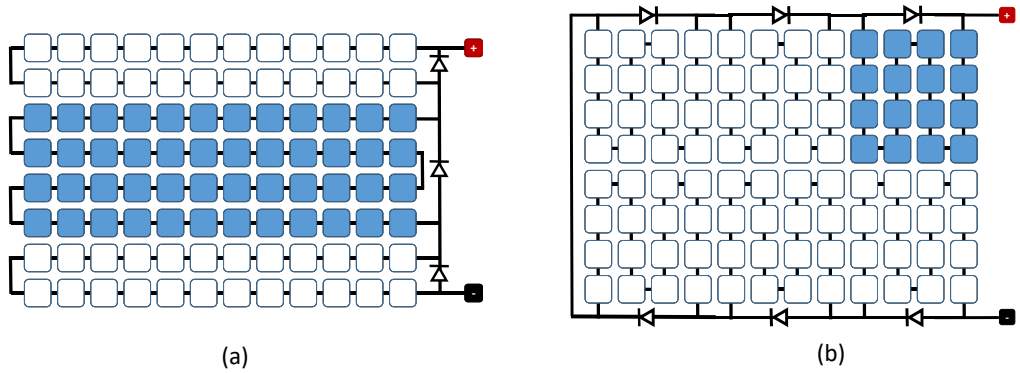

Figure 3.4: Module Configurations : (a) 96 cell module with three bypass diodes (b) 96 cell module with six bypass diodes

3.4. SYNTHETIC IRRADIANCE VALUES

3.4.1. METHODOLOGY

Simulations of different synthetic shading patterns on a solar module have been generated using Matlab. The synthetic patterns values considers many shading patterns such as horizontal, vertical and diagonal shading. All these shading patterns are further divided into progressive and block shading. By this attempt, majority of all the possible shading patterns that could occur in real life have been recreated.

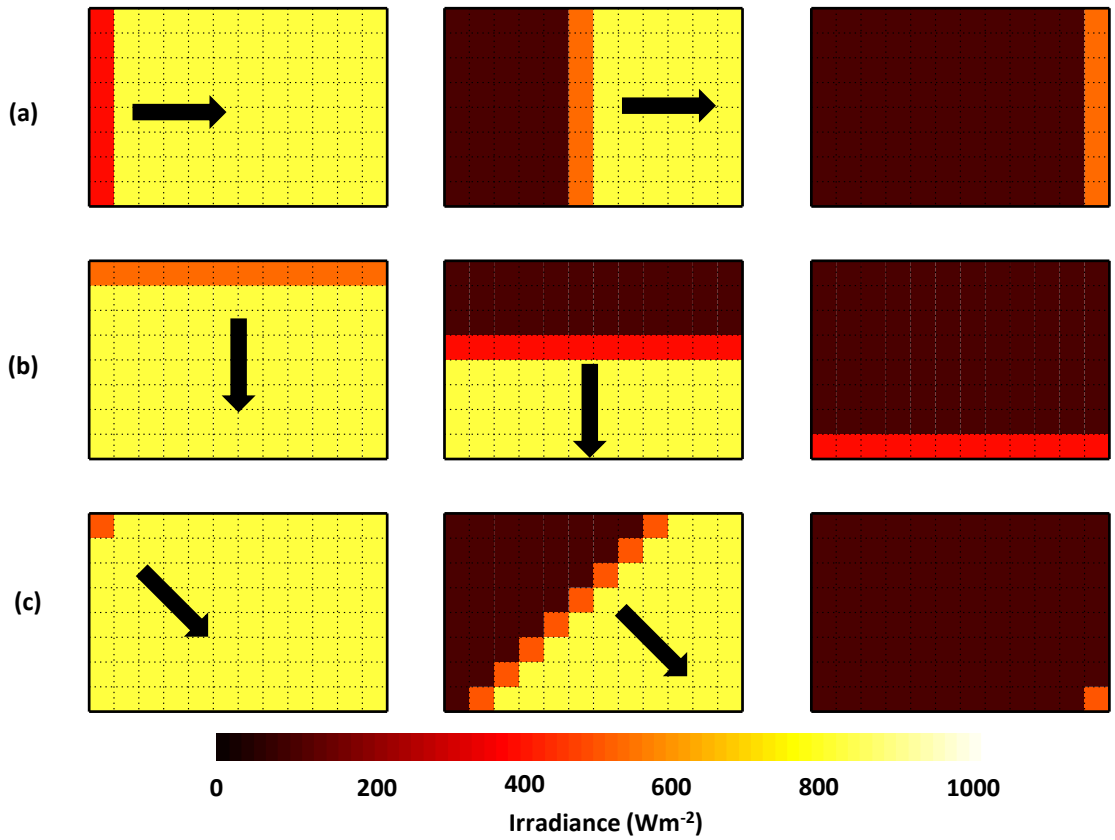

Figure 3.5: (a) Vertical (b) horizontal and (c) diagonal progressive shading

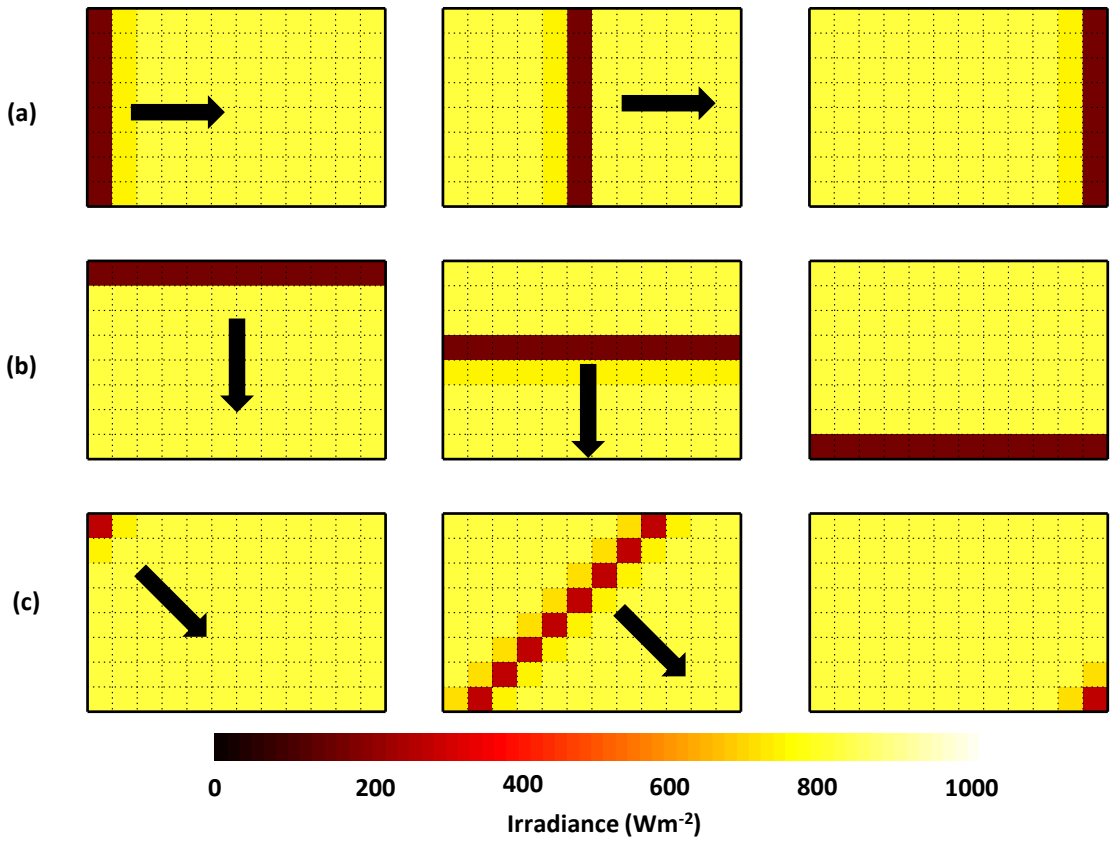

Figure 3.6: (a) Vertical (b) horizontal and (c) diagonal block shading

Each shading pattern on a solar module divides it into two regions : shaded and unshaded region. The range of their irradiance values, have been given in the table 3.3. The shade pattern is also divided into horizontal, vertical and diagonal shading based on the orientation of the shade. The shade moves from one side to other in case of horizontal and vertical shading, whereas in diagonal shading, the shade moves from one corner to another. Row shading is also called as horizontal shading is simulated by considering the angle of shade to be 0°, whereas for column/vertical shading the angle considered is 90°. For diagonal shading we chose multiple angles : 30°, 45°,60°. If the shade starts at one end of the module and eventually shades the entire module, then it is called progressive shading. A typical example of progressive shading would be shading due to immobile objects such as trees, chimneys or neighbouring buildings. In the table, the progressive shading has been represented with a width equal to zero. If a block of shade with a certain width advances from one side of the module towards another side, then it is called block shading. Shading due to mobile objects such as clouds or birds could result in block shading. The percentage of shading on the module remains constant in block shading, since the same amount of shade moves over the module. For this report, we chose two different widths of block shade and are represented by widths = 1,2 in the table 3.3. The progression of the shade from one side to another side, or from one corner to another corner are shown at different time intervals and is denoted by time intervals in the table. Considering all these cases the total number of simulations comes out to be 9000. A brief summary of all the different shading patterns has been represented in table 3.3.

Parameters	Range of Values	Number of Values
Unshaded Irradiance (Wm^{-2})	[200;1000]	5
Shaded Irradiance (Wm^{-2})	50: Unshaded Irradiance	12
Angle (degrees)	0°,30°,45°,60°,90°	5
Width	0,1,2	3
Time intervals	10	10
Total	5x12x3x5x10	9000

Table 3.3: Shading Parameters

3.4.2. RESULTS AND ANALYSIS

From the above procedure irradiance values for each cell of an 8×12 solar module for 9000 different shade patterns are generated. These values have been fed into the simulink models which have been discussed in 3.2 for two solar module topologies (96 cell 3 BPDs model and 6 BPDs). The model calculates the maximum power point for each of the shade patterns. The model is run multiple times, each time modifying the reverse characteristics. For this analysis, we have used a reverse breakdown voltage of 1 V and 14 V respectively. The reverse breakdown voltage value 14 V represents conventional solar cells and the value of 1 V is hypothetical. The change in reverse characteristics of a solar cell definitely has an impact on the forward characteristics however, this first analysis only focuses on the effects of varying reverse characteristics by assuming that the forward voltage in both the cases is unchanged.

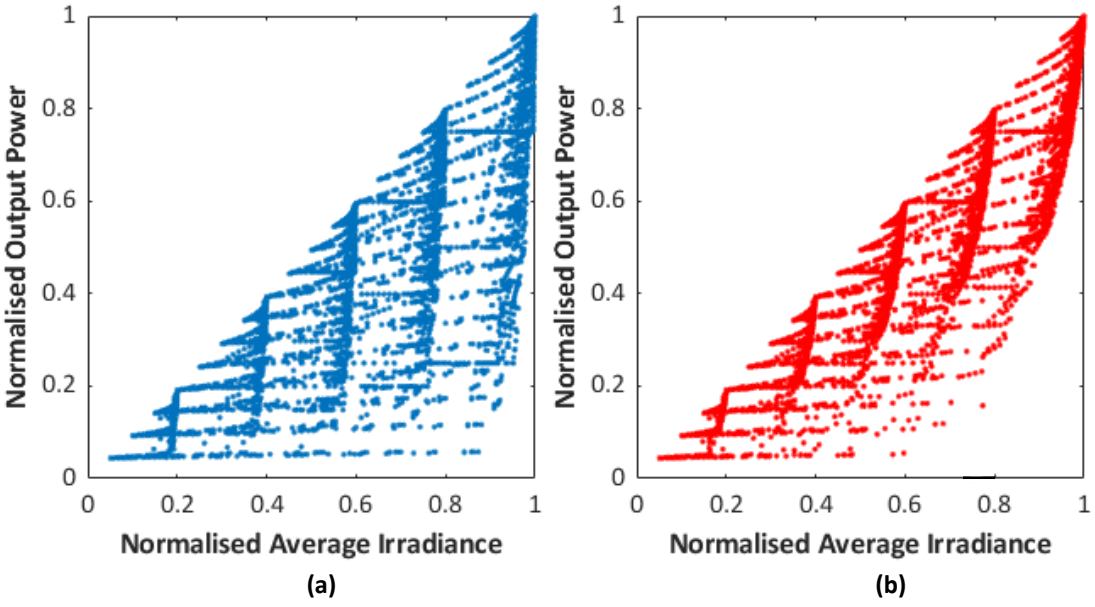

Figure 3.7: Shading linearity of 3 BPD module for (a) V_{rev} = 14V and (b) V_{rev} = 1V for synthetic irradiance values

After running the simulations for a module with 3 BPDs, the shade linearity for both reverse breakdown voltages have been plotted as seen in figure 3.7. A considerable amount of points are seen at the right bottom parts of each plots. This means that for a normalised average irradiance close to 1 has a normalised power output close to 0. A small amount of shade ensuring bypassing of two arrays due to turning on of BPDs is a possible explanation. However these points reduce when low BDV solar cells are simulated as seen in 3.7(b). Blue colour points in the plots indicate simulations

run for reverse BDV of −14 V while red colour points represent reverse BDV of −1 V.

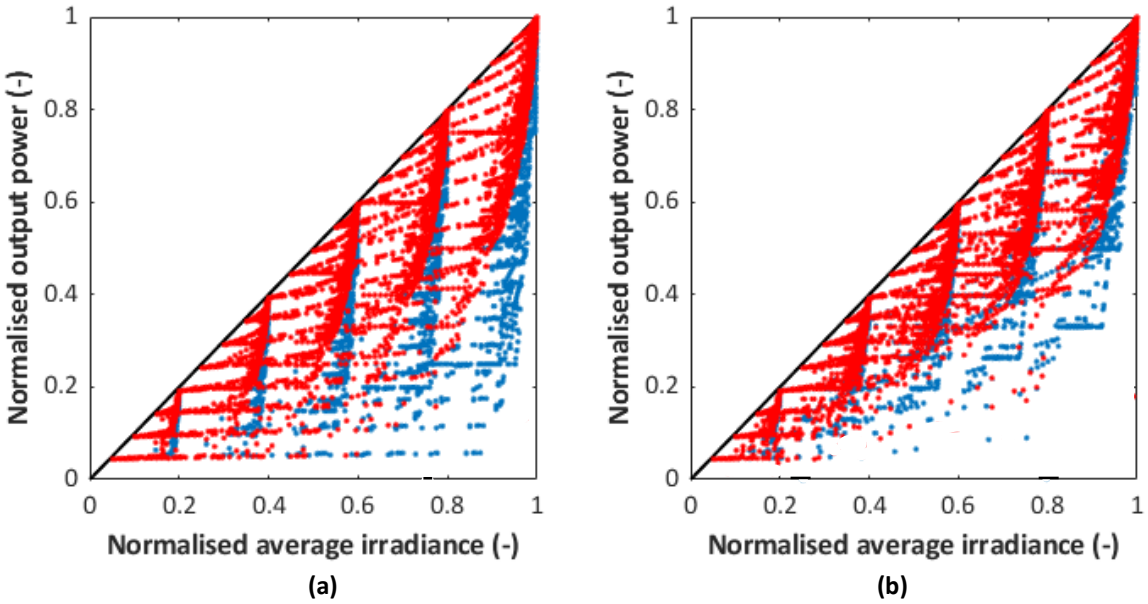

Figure 3.8: Comparison of shading linearity for V_{rev} = −14 V and V_{rev} = −1 V (a) 3 BPDs (b) and 6 BPDs for synthetic irradiance values

Since the forward characteristics remain unchanged only the reverse characteristics are accountable for any change in the power output in the simulations. Theoretically, for a module made with low reverse breakdown voltage cells, a higher number of solar cells need to be shaded to activate the bypass diodes when compared to conventional solar modules. This means that the losses due to bypassing of array reduce upto a certain extent which in turn improves power output which is reflected in figure 3.8. The increase in power is indicated by the vertical translation of each blue point to become a red point thereby improving shading linearity. Therefore we validate that by using low reverse BDV cells, a better performing solar module can be made.

In the synthetic irradiances approach, a lot of shading patterns have been considered out of which only a few patterns occur in real life. In the next section a more realistic irradiance values are calculated using forward ray tracing method on a particular rooftop in Rotterdam. A similar process is repeated to continue with our validation procedure.

3.5. REAL LIFE IRRADIANCE VALUES

3.5.1. METHODOLOGY

A rooftop in Rotterdam facing Southwest with a tilt of 56° has been chosen for this purpose as shown in Figure 3.9.The size of the rooftop when expressed in terms of solar cells turns out to be 36 × 88. This means, a solar module comprising a size of 36 rows and 88 columns can be fit on the rooftop. The irradiance for each cell on the roof has been calculated for every ten minutes over a year using ray scattering techniques.

In the Figure 3.10a and Figure 3.10b the most illuminated and most shaded region of the whole roof with an annual irradiation of 909.81 kWh m^{-2} and 480.30 kWh m^{-2} have been indicated. The most illuminated region could give us a pessimistic result since there would be little shading fur-

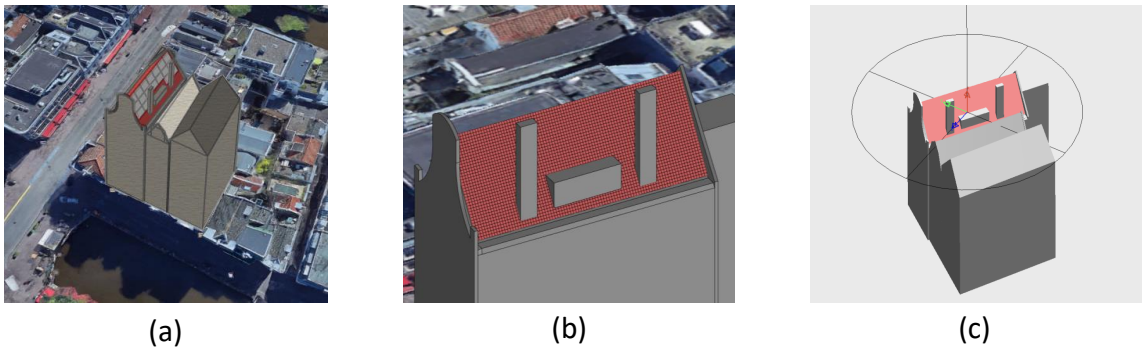

Figure 3.9: (a) Building in Rotterdam whose rooftop is used for the following analysis (b) Straight view of the rooftop (c) Ray tracing of the rooftop to find irradiance [5]

ther having little impact over the power output during partial shading. In the same manner the most shaded region could give highly optimistic results. Therefore, the region highlighted in Figure 3.10c which is somewhere in between the highly illuminated and shaded regions with irradiation of 648.66 $kWh\,m^{-2}$ has been chosen to place the solar module. The position is placed at the 10^{th} row and 15^{th} column and is repeatedly shaded throughout the year, by the pillar on the roof.

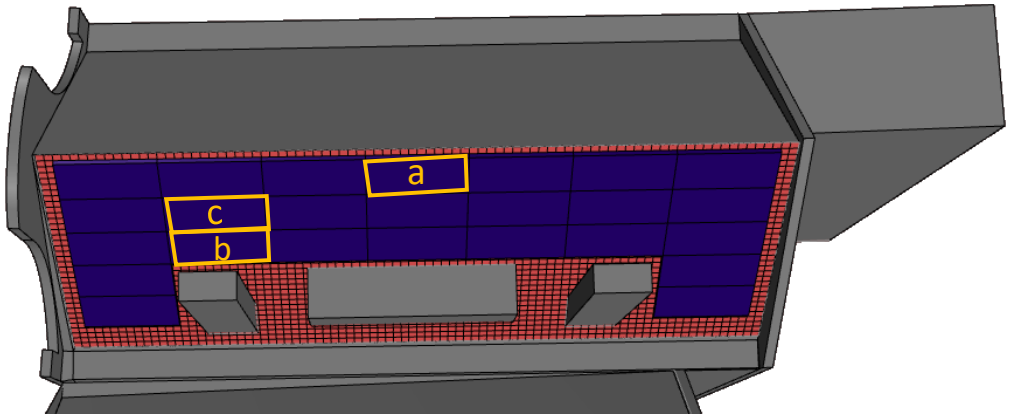

Figure 3.10: Chosen solar module locations on the rooftop (a) Most illuminated (b) least illuminated and (c) intermediately illuminated [5]

Azimuth angle of the module (A_m) is the angular measurement in the spherical coordinate system in which 0° denotes North, 90° denotes East, 180° denotes South and 270° denotes West. In this case, the azimuth angle is 236° i.e the module is facing South-West.The tilt of the module (θ_m) is the angle at which the roof is inclined with respect to the ground. The altitude of the module is the complementary to the tilt i.e ($a_m = 90 - \theta_m$). Hence, thee tilt and altitude of the solar modules on the roof are 56° and 34° respectively. Albedo is the amount of light reflected from a surface. The albedo for this urban landscape is chosen to be 0.15.

The forward ray tracing method has been used for calculation of irradiance on the solar rooftop from an urban environment and there is solar illumination at these locations are available for slightly more than half the time instances. Sensitivity maps on each cell of the roof are used to perceive the variation of irradiance at different moments.Figure 3.11 shows the sensitvity map and the annual

Parameters	Values
Azimuth of Module (A_m)	236 °
Tilt of module (θ_m)	56 °
Albedo	0.15

Table 3.4: Solar module orientation

irradiation at locations A,B,C.

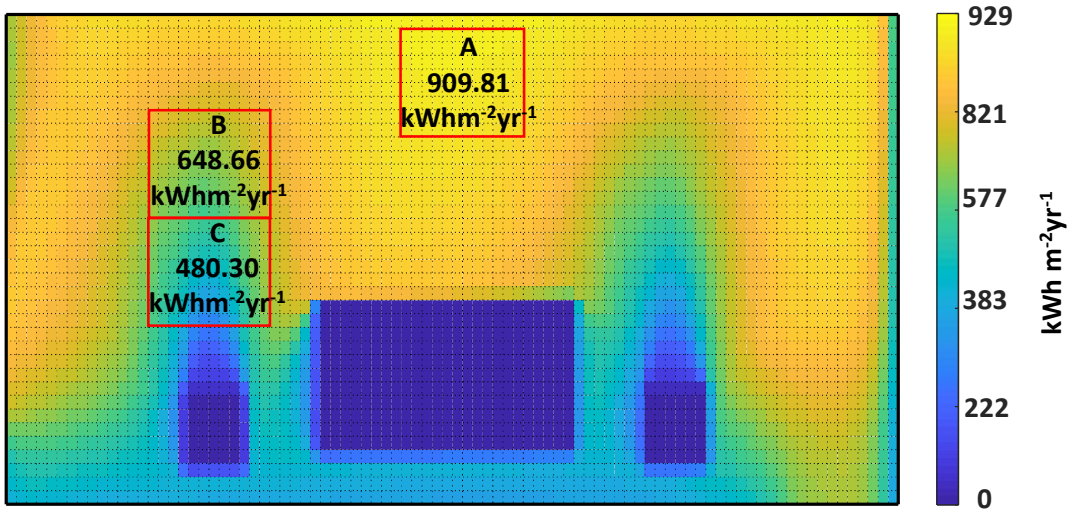

Figure 3.11: Sensitivity map showcasing the annual irradiation at the chosen locations

3.5.2. ROUGH ESTIMATE OF ENERGY PAYBACK TIME ON ROOFTOP

To calculate payback of advanced crystalline modules by 2020, researcher Mann performed a prospective life cycle assessment analysis and included only cradle to gate stages of the modules, neglecting the BOS and disposal (grave) stage. Static scenarios have been used to reckon BOS in the calculation of Energy Pay Back Time (EPBT). Due to the stochastic approach of this study, parametric and scenario uncertainties have been included. In this study, two types of PV systems were considered: rooftop and ground mount PV plant. In each of these cases calculations were made for three modules. The efficiency of these modules range from 20-23.5 % considering frameless encapsulation without lamination foil. The estimates of electricity use for Rooftop PV systems range from 839-929 $MJ\,m^{-2}$ (233.07 - 258.07 $kWh\,m^{-2}$) and for the ground mount ranges from 867-899 $MJ\,m^{-2}$ (240.8526 - 249.7422 $kWh\,m^{-2}$). The energy payback for this has been calculated to be in the range of 0.7 - 0.9 years for rooftop and 0.7 - 0.8 years for ground mount considering the annual Insolation of southern europe (1700 $kWh\,m^{-2}year^{-1}$) [41].

These calculations are a bit optimistic, when compared to calculations made by other researchers, especially due to the timeline of the research. Based on energy analysis Dutch researcher Alsema, calculated a payback of 4 years assuming 12 % efficiency and 2 years for 14 % efficient modules[3]. Palz and Zibetta's calculation also resulted in a payback time of 2 years [45], whereas Knapp and Jester carried out experiments for single -crystal-silicon modules at a manufacturing facility and

computed the energy payback time to be around 3.3 years [36]. Therefore, it can be roughly said that the energy payback time of a PV system is 2 years at an insolation of 1700 $kWh\,m^{-2}year^{-1}$.

The insolation on the position which has been chosen on the rooftop to carry out this experiment is 675.61 $kWh\,m^{-2}year^{-1}$. So, the question is does it make sense to have a solar module installed here? It's absolutely worth installing a module at that position because, the payback time turns out to be 5 years, which is pleasantly enough. Building integrated Photovoltaics have been on a rise recently, and solar facades is an integral part. A facade facing eastwards in the same location as the rooftop, has lower insolation levels than the chosen rooftop solar module position.

3.5.3. RESULTS AND ANALYSIS

The irradiance values for each cell of the 8 × 12 solar module located at B have been fed into the 8-parameter simulink models discussed earlier. The model is run multiple times, modifying the reverse characteristics, keeping the forward characteristics of the solar cell unchanged. For this analysis we have used a reverse breakdown voltage of 1V and 14V respectively and output power for every 10 minutes for an year has been calculated. This data has been further used to plot shade linearity curves, calculate yield, mean square deviation and root mean square deviation with respect to ideal conditions.

SHADING LINEARITY

From the plots 3.12, it can be seen that the Normalised Average irradiance ranges from to 0 % to 70-75 % accounting for partial shading. In figure 3.13 the red dots indicate the power output of V_{rev} = −1 V (simulated module) and blue dot indicates V_{rev} = −14 V (conventional). The blue dots seem to move vertically upwards with change in reduction of reverse BDV improving the shading linearity irrespective of number of diodes. This indicates that either increasing BPDs or using low BDV cells improves shade linearity. To validate this the mean bias deviation and root mean square deviation has been calculated.

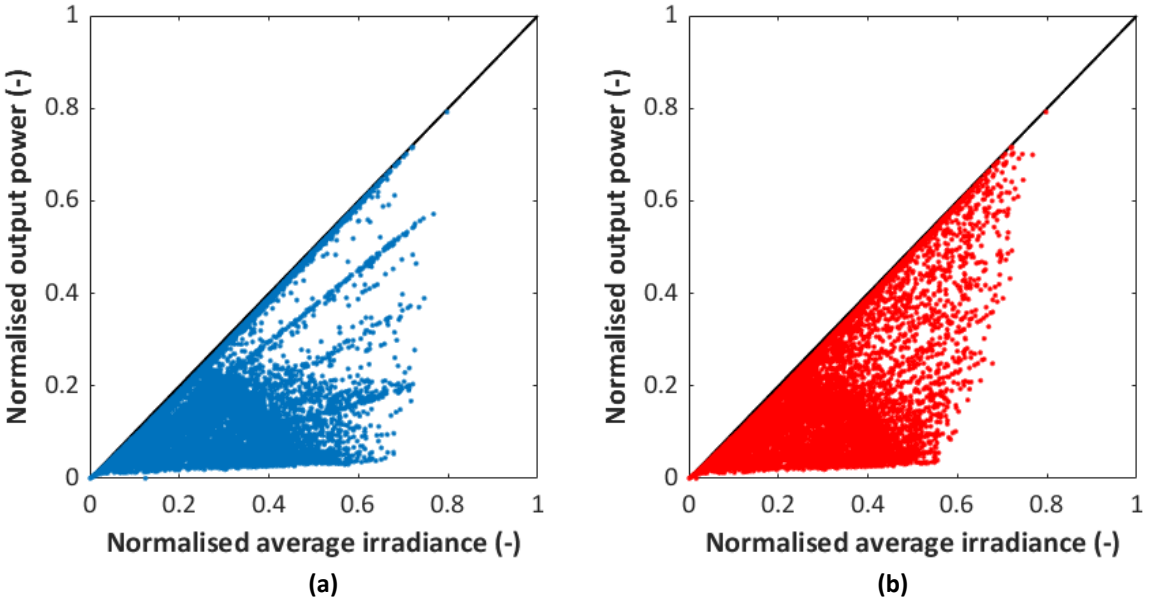

Figure 3.12: Shading linearity of 3 BPD module (a) with V_{rev} = −14 V (b) and with V_{rev} = −1 V for realistic irradiance values

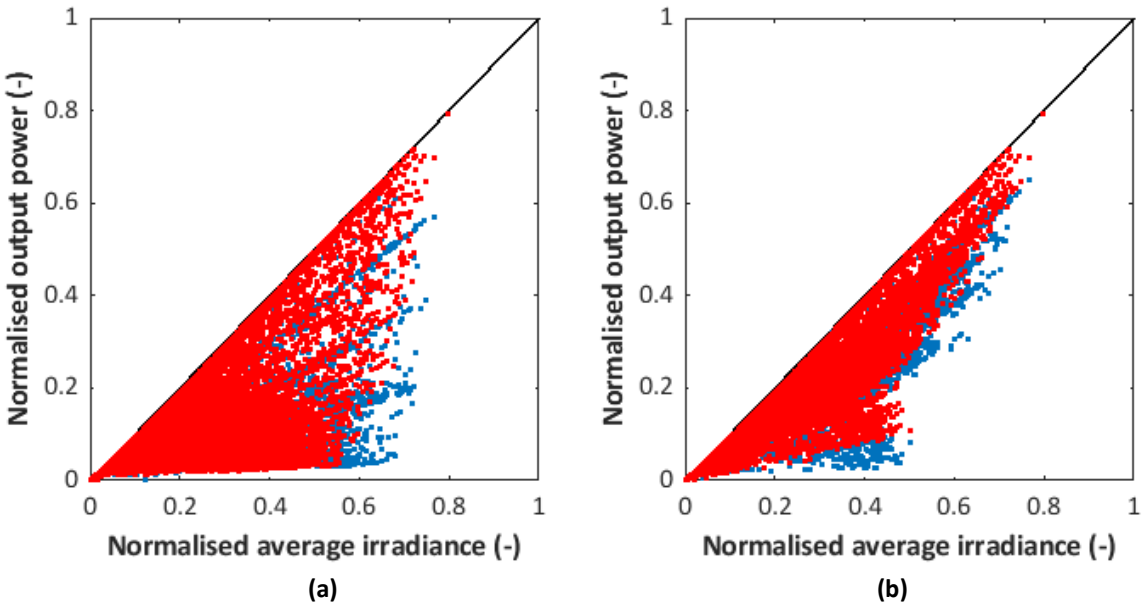

Figure 3.13: Comparison of shading linearity for $V_{rev} = -14\,V$ and $V_{rev} = -1\,V$ (a) 3 BPDs (b) and 6 BPDs for realistic irradiance values

DEVIATION FROM IDEALITY

In order to assess the improvement of shading linearity for different models, the following statistical parameters have been used: mean bias deviation (MBD) and root mean square deviation (RMSD), which indicate the deviation between the ideal values and those estimated by the models, being the expressions of these parameters [67]:

$$MBD = \frac{\sum_{i=1}^{N}(y_i - x_i)}{N \cdot \bar{x}} \tag{3.3}$$

$$RMSD = \frac{[\sum_{i=1}^{N}(y_i - x_i)^2]^{\frac{1}{2}}}{N \cdot \bar{x}} \tag{3.4}$$

where y_i is the i-th NOP ideal value, x_i the i-th simulated NOP value, $\bar{x}$ the mean of the simulated NOP value and N the total number of data points analysed.
The MBD and RMSD give the difference between the simulated and ideal value. Higher value of deviation indicates that the simulated values are farther from ideality. All the statistical indicators are normalized in order to facilitate fair comparison.

Figure 3.14 shows the MBD vs season plots of the 3 BPD and module configurations and each module is made of cells with reverse voltages of 1V (simulated module) and 14V (conventional module). In both the plots a similar trend can be seen and clearly the simulated modules have a lower deviation from ideality than the conventional modules. The deviations are calculated on a monthly basis to analyse the impact of seasonal changes. During the winter months when the irradiation is lower (December and January) the performance gain of the simulated module when compared to the conventional module is higher than summer months when the sky is clearer and irradiance is higher(June and July). Similarly in the RMSD plots as shown in Fig 3.14, the simulated modules are more dominant than the conventional module configuration verifying the MBD plots.

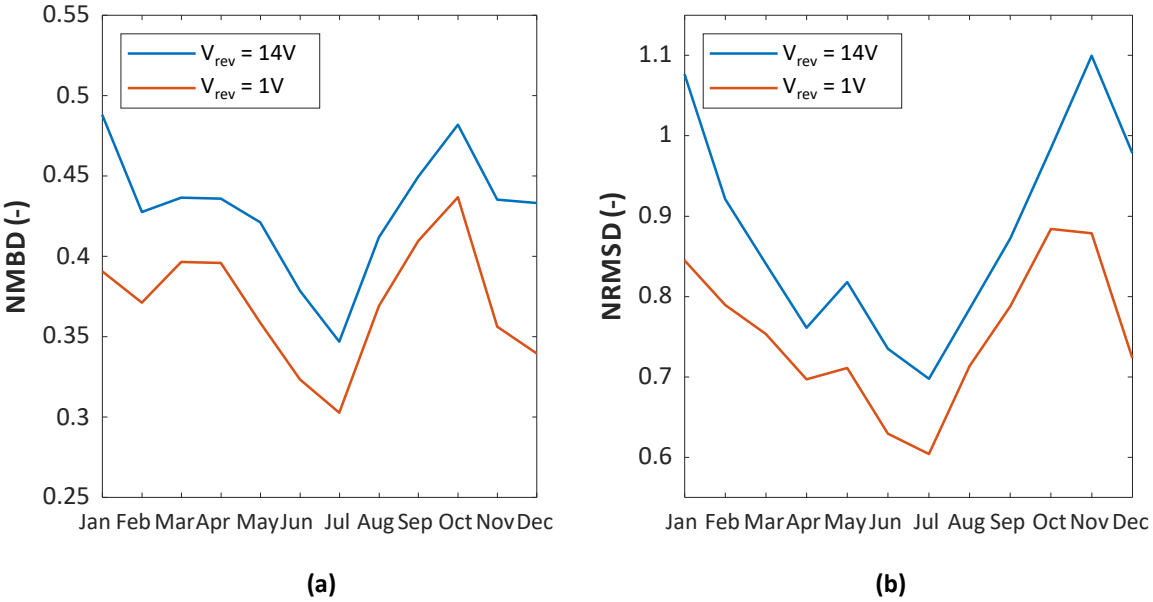

Figure 3.14: (a) Mean bias deviation and (b) root mean square deviation of solar module made with simulated cells and conventional cells with 3 BPDs

YIELD

Specific yield is defined as the amount of energy (kWh) produced per kilo watt peak (kWp) of module capacity over a year. Specific Yield (kWh/kWp) is one of the performance metrics most widely used in solar systems of all sizes and in this case used to compare performance of different module configurations[72]. The V_{mpp} of the solar cell is 0.60 V and the I_{mpp} is 5.56 A which makes the capacity 0.32 kWp for a 96-cell module.

Figure 3.15(a) shows the specific yield plots per month and the Figure 3.15(b) shows the annual specific yield for 3BPD module and 3BPD conventional module. The specific yield of the simulated module is higher for every month of the year than the conventional module even though the forward characteristics of the solar cell is assumed to be unchanged. The gain in yield is accounted for the reduction of losses when a module made of lower reverse BDV cells. It is also observed that the gain percentage in specific yield is greater during the months of low irradiance than during the months of higher irradiance proving that solar modules made of low BDV are optimal for use in partial shading conditions. The overall average specific yield improves by 8.81 % over a year when the 3BPD module is used.

Figure 3.16 shows the average specific yield plots for the 6BPD configuration. Except for the amount of increase in specific yield, the rest of the trends in these plots is the same. The average specific yield improves by 3.34 % over a year when the simulated 6BPD module is used. This implies that adding additional BPDs improves shade resilience of a solar module.

To put the above mentioned matter into perspective, the term operating efficiency is introduced.

Operative efficiency(η_{op})

The operative efficiency of a solar module is a parameter used to describe the efficiency of a solar module under real operating conditions and it is defined as the ratio of output energy yield of a module over a year to the maximum energy incident on the module :

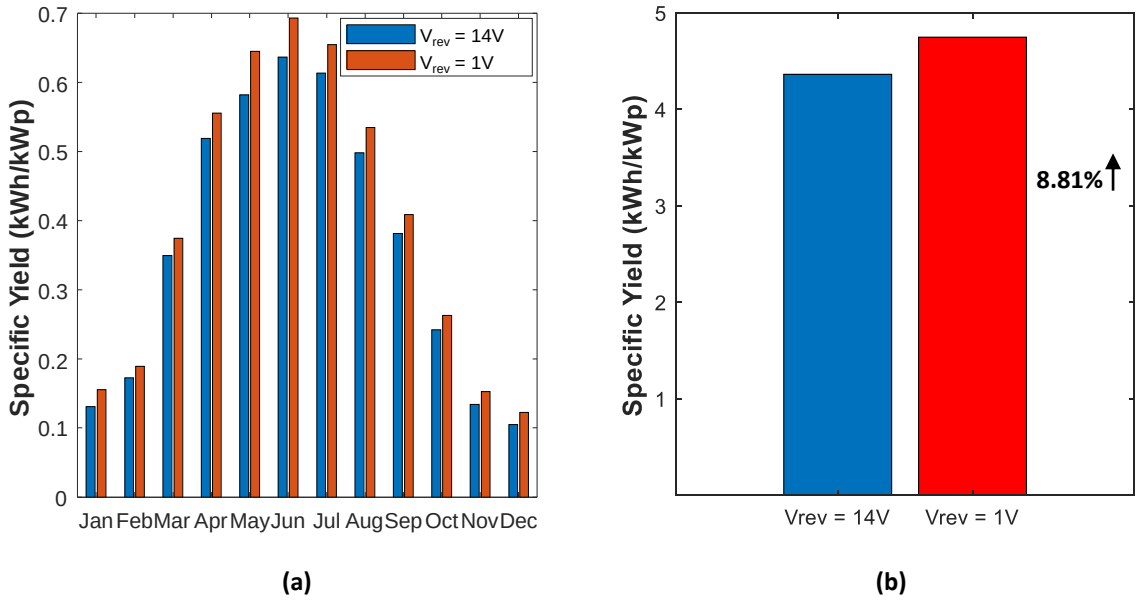

Figure 3.15: (a) Monthwise and (b) annual specific yield comparison between the conventional and the simulated module with 3 BPDs

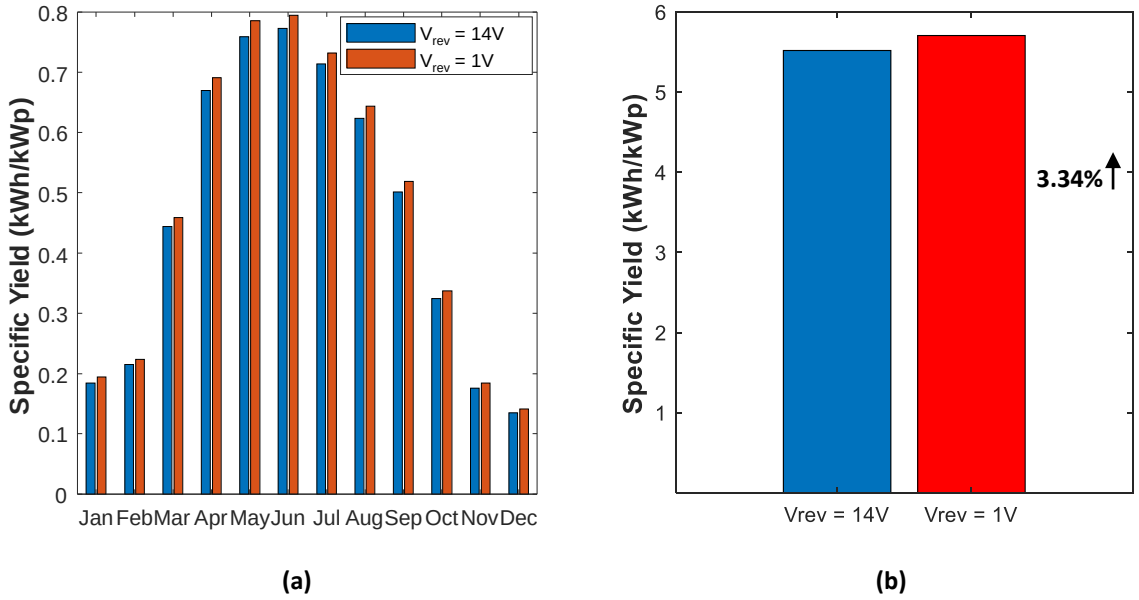

Figure 3.16: (a) Monthwise and (b) annual specific yield comparison between the conventional and the simulated module with 6 BPDs

$$\eta_{\mathrm{op}} = \frac{\int_{\mathrm{year}} \mathrm{MPP(t)} \cdot \mathrm{dt}}{\int_{\mathrm{year}} \mathrm{G_m}(t) \cdot \mathrm{A_m} \cdot \mathrm{dt}} \tag{3.5}$$

The operative efficiency of the 3BPDs configuration improves from 8.29% to 9.02% and for the 6BPDs configuration improves from 10.48% to 10.83% when we switch from the conventional to the simulated model.

3.6. SENSITIVITY ANALYSIS

Sensitivity analysis is a method used to determine the extent to which results are affected by changing certain variables in a model. In this thesis, variable that has been changed is the reverse breakdown voltage while the output results are the annual specific yield. The reverse breakdown voltage values have been manipulated, the whole time keeping the V_{mpp} in other terms the forward voltage unchanged. Figure 3.17 shows the analysis.

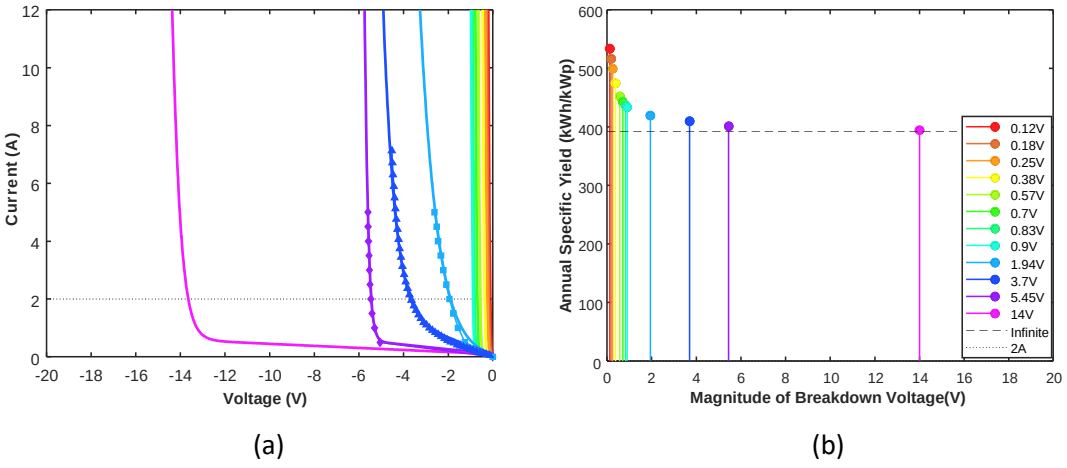

Figure 3.17: (a) Reverse voltages of various simulated solar cell models (b) and their corresponding yields

In figure 3.17(a) the coloured curves represents the dark, reverse IV curves of various solar cells. The curves which have markers represent measured solar cells gen 2, zebra and gen 3 with reverse BDV $-5.45\,V$,$-3.70\,V$ and $-1.94\,V$ respectively. The dotted line indicates 2A current, the corresponding voltage value is considered as the breakdown voltage. In figure 3.17(b) the coloured stems represents the annual specific yield of a 96 cell 3BPD configured solar module for the corresponding breakdown voltages shown in figure 3.17(a). While the dashed line represents the annual specific yield of the same module with ∞ breakdown voltage. Conventional solar cells have a breakdown voltage of -14V. The difference in annual specific yield of a cell with ∞ BDV and a conventional solar cell is not much. Therefore, cells with BDV in the range of [-14V $-\infty$ V] do not have much difference in their yields, hence they are not considered in the model.

In 3.17(b), a linear trend in growth of specific yield can be observed until a breakdown voltage of 0.57 V. After that an exponential rise in specific yield is observed. The reason behind this could be that the bypass diodes aren't able to turn on and the solar cells are operating at reverse BDV values thereby, reducing the losses due to bypassing of an entire array.

From table 3.5 it can be seen that there is an increase of 36.23 % in DC gain for cells with $-0.12\,V$ when compared with ∞ V cells. Similarly, with a $-0.90\,V$ solar cells there is a gain of almost 11 %. There is no solar cell with a reverse BDV of $-1\,V$ but it might be a possibility in the future that these kind of cells are manufactured. There are several companies such as AE solar manufacturing schottky diodes with a forward voltage of 0.30 V. For a reverse BDV of $-0.25\,V$ there is a DC gain of almost 27.49 %. From this it can be concluded that instead of having one bypass diode per cell which has a complex manufacturing process it's worth exploring how to manufacture very low reverse BDV cells.

Also, the solar cells with BDV -5.45 V, -3.70 V and -1.94 V represent measured sunpower solar cells.

Breakdown Voltage (V)	**Annual Specific Yield (kWh/kWp)**	**Relative gain w.r.t ∞ BDV**
-0.12	533.81	36.23%
-0.18	516.56	31.84%
-0.25	499.54	27.49%
-0.38	474.64	21.14%
-0.57	452.30	15.44%
-0.70	443.35	13.15%
-0.83	436.64	11.44%
-0.90	433.81	10.71%
-1.94	419.39	7.00%
-3.70	409.76	4.58%
-5.45	401.23	2.40%
-14.00	394.45	0.67%
∞	391.82	0

Table 3.5: Reverse Breakdown Voltages and corresponding yield

The relative increase in yield for each of these solar cells with respect to a solar cell with ∞ BDV is 2.40 %, 4.58 % & 7.00 % respectively. This is a significant gain in yield and hence shows that it is worth exploring the yield of commercially available low BDV solar cells with a much more accurate model.

4

EXPERIMENTAL MODELING OF COMMERCIALLY AVAILABLE LOW BDV SOLAR CELLS

In the previous chapter, simulations were run based on one diode model of solar cell. The model possessed multiple values of breakdown voltage while the forward characteristics were assumed to be unchanged. In this chapter, the main aim is to characterize a new and much more accurate solar cell model. For this, IV curve measurements of various solar cells are measured both in dark and illuminated conditions.

4.1. METHODOLOGY & MEASUREMENTS

The main aim is to characterise the available Sunpower Maxeon solar cells by taking IV measurements in (i) dark; and (ii) under varying illumination and varying temperature for both forward and reverse bias.

4.1.1. CELL PHYSICAL CHARACTERISTICS

The wafer of the solar cells used for this thesis are made up of monocrystalline silicon. The front face of the solar cell has a uniform, black antireflection coating and since the cell is an all back contact, the back is made of copper metal grid, coated with tin. The area of the cell is 153 cm^2 , thickness is 150 μm and has a weight of around 6.5 g. Tin-plated copper strain-relieved interconnect tabs are usually used since they are easily solderable and compatible with lead-free processing. Hence, two of these connectors are soldered to the terminals of the cell and one end of the connectors is soldered with wires that are connected to the DC load.

4.1.2. LIMITATIONS OF MEASUREMENT SETUP

There were certain limitations in making these measurements: Most of the equipment available with the PVMD group at TU Delft are used for measuring cells with small surface area. Hence, the equipment could only measure low levels of current. Out of the available electronic DC loads the maximum measurable limits of current is by a Keithley 2601 sourcemeter which had a current range of -3A to 3A and voltage range is -5.9V to 5.9V. With the help of the chief technician Remko Koornheef, a crude software has been built in LabView and IV sweeps of the various solar cells were made. There were some errors in the measurement values close to 0 A which appear in the form of discontinuity in the IV curves however the important measurement values have not been tampered. The error values have been replaced by new values generated using the method of interpolation.

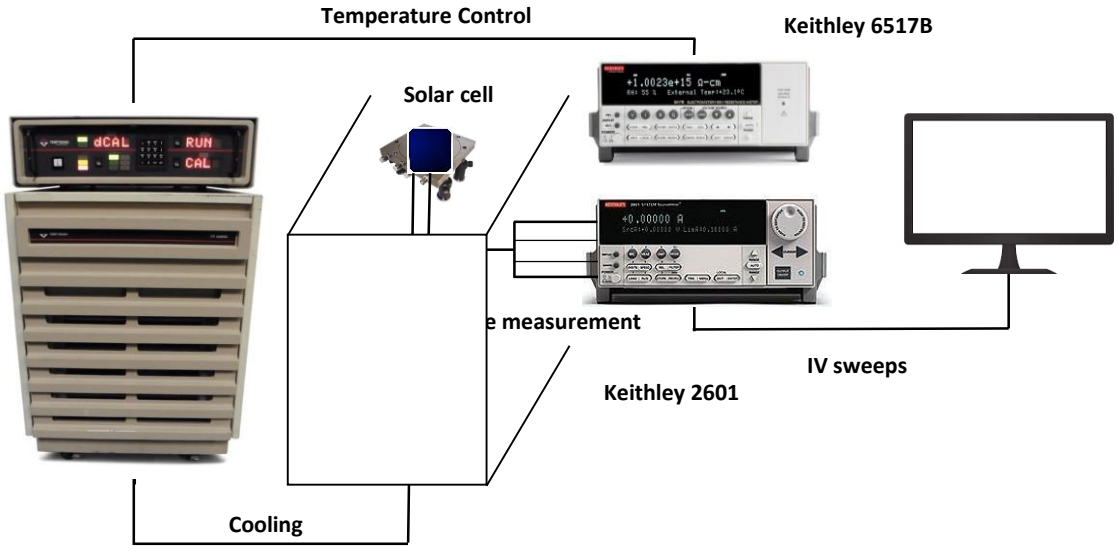

Figure 4.1: Setup for the dark IV curve measurements

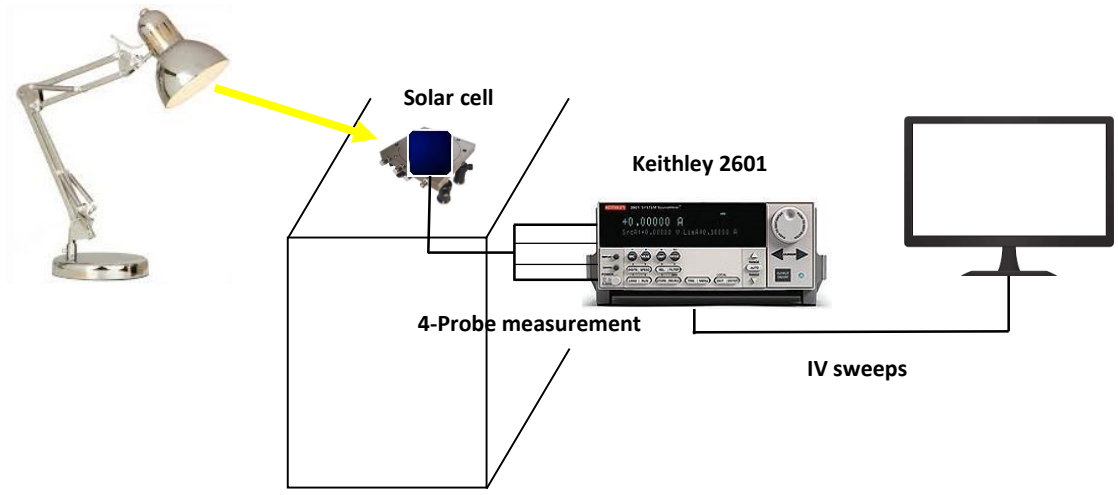

Figure 4.2: Setup for the illuminated IV curve measurements

4.1.3. DARK IV MEASUREMENTS IN REVERSE BIAS

Measurements for 10 solar cells of each type at five different temperatures (20 °C, 40 °C, 60 °C, 80 °C, 100 °C) have been taken. A temptronic thermal inducing vaccuum platform is used to vary the temperature and is controlled by Keithley 6517 B electrometer. In Figure 4.3 (a) the dark reverse characteristics of 10 gen 2 solar cells at a constant temperature of 60 °C(Although the measurements have been taken for 5 different temperature values, 60 °C has been randomly chosen and plotted)

are plotted and are roughly the same. The reverse characteristics of all the cells at different temperatures have been measured and look more or less similar when compared amongst cells. Figure 4.3 (b) shows the reverse characteristics of one of the gen 2 solar cells at the various temperatures. As the temperature increases the dark reverse characteristics improve i.e the breakdown voltage reduces by a tiny amount. However, in gen 2 cells (not only for the cell shown in figure 4.3(b) but also the other 9 cells that are measured) there is a significant change at the knee of the IV curves.

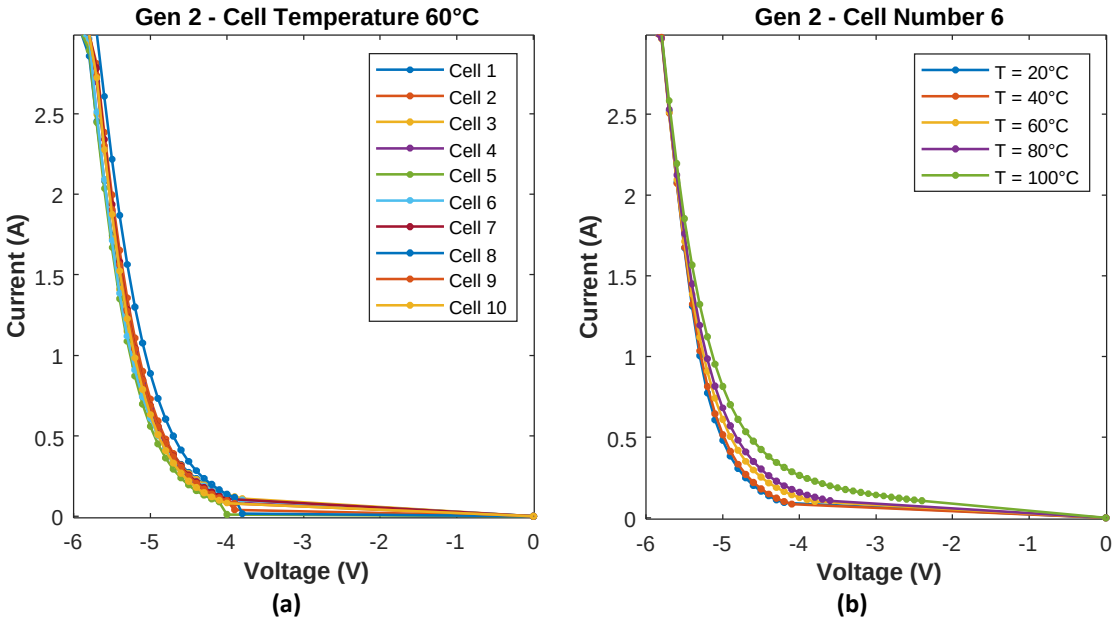

Figure 4.3: Dark measurements (a) different gen 2 cells at constant temperature (b) same gen 2 cell at different temperatures

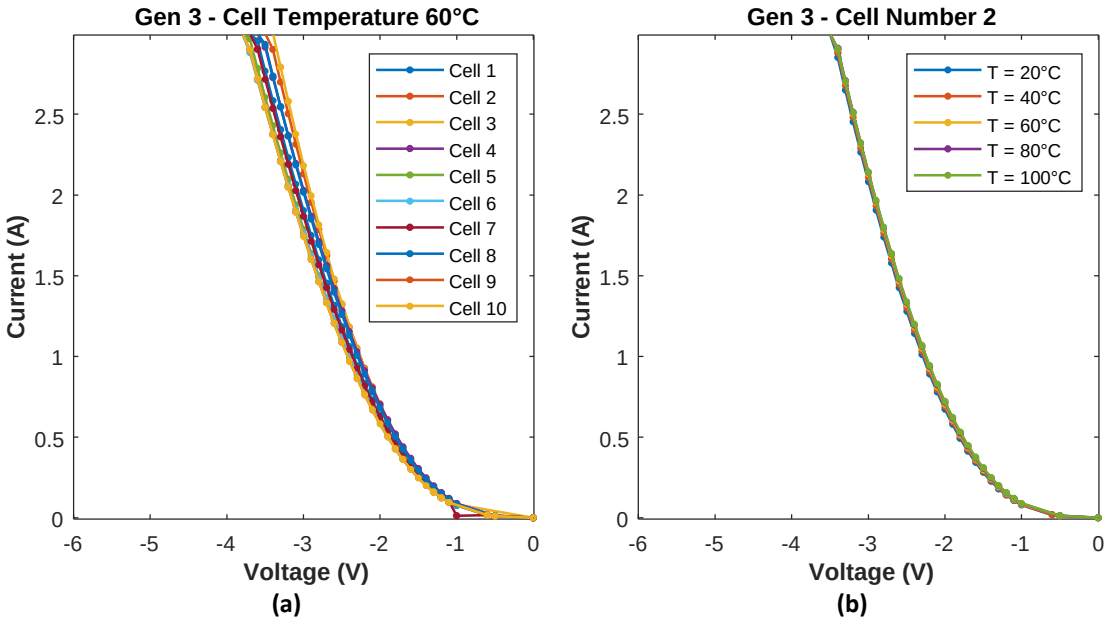

Figure 4.4: Dark measurements (a) different gen 3 cells at constant temperature (b) same gen 3 cell at different temperatures

Similarly figure 4.4 shows the dark reverse characteristics of sun power gen 3 solar cells. From figure 4.4(b) it can be seen that gen 3 cells also show a positive temperature coefficient however at the knee the IV curves are almost overlapping unlike the gen 2 solar cells. It is also to be noted that gen 2 cells have a hard breakdown compared to gen 3 cells.

The low reverse breakdown and positive temperature coefficients indicate the dominance of zener breakdown mechanism in both the solar cells. However, the behaviour at the knees of the IV curves cannot be supported from the scope of the literature. However, it can be speculated that with rise in temperature, the breakdown shifts from a hard to softer breakdown.

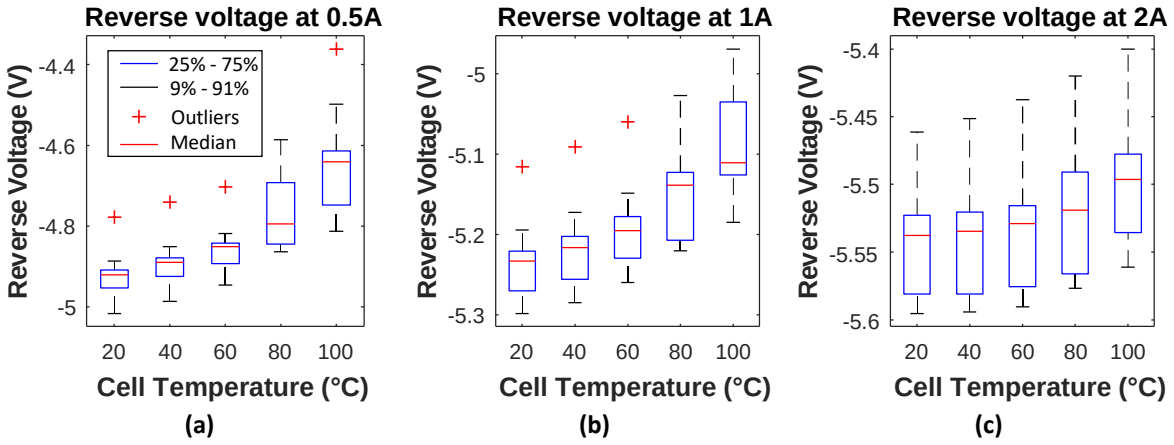

Figure 4.5: Box plots for 10 different gen 2 solar cells representing reverse voltage plotted against temperature measured at (a) 0.5 A (b) 1 A (c) 2 A

Figure 4.5 and Figure 4.6 represent the dark IV curves in terms of box plots for 10 gen 2 cells and 10 gen 3 cells respectively. In these plots the reverse voltage is plotted against variable temperatures at three different currents 0.5A, 1A and 2A. As defined in the previous chapters, the breakdown voltage corresponds to the voltage at 2A. From these plots the reverse breakdown voltage for a gen 2 cell ranges from -5.6V to -5.4V for temperatures between 20 °C - 100 °C. Similarly for gen 3 cells the breakdown voltages ranges from -3.2V to -2.9V.

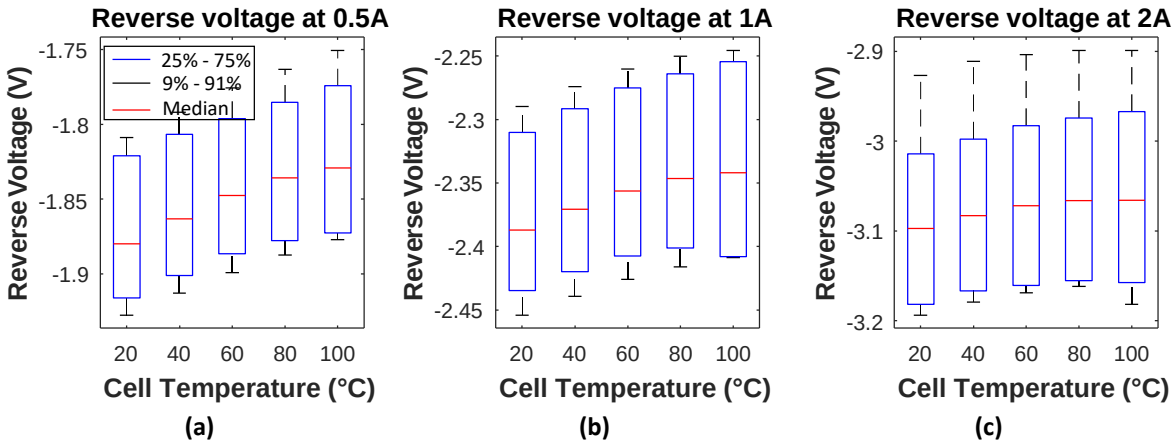

Figure 4.6: Box plots for 10 different gen 3 solar cells representing reverse voltage plotted against temperature measured at (a) 0.5 A (b) 1 A (c) 2 A

4.1.4. IV MEASUREMENTS AT VARYING IRRADIANCE AND VARYING TEMPERATURE

Measurements for 3 solar cells of each type at four different irradiances and temperatures ranging from 0 to 350 $W m^{-2}$ and 30 °C and 40 °C have been taken. Figure 4.7 represents the change in reverse BDV voltage of gen 2 and gen 3 cells. The temperature range is chosen only upto 350 $W m^{-2}$ due to the limitation of measurement equipment which measures high current.

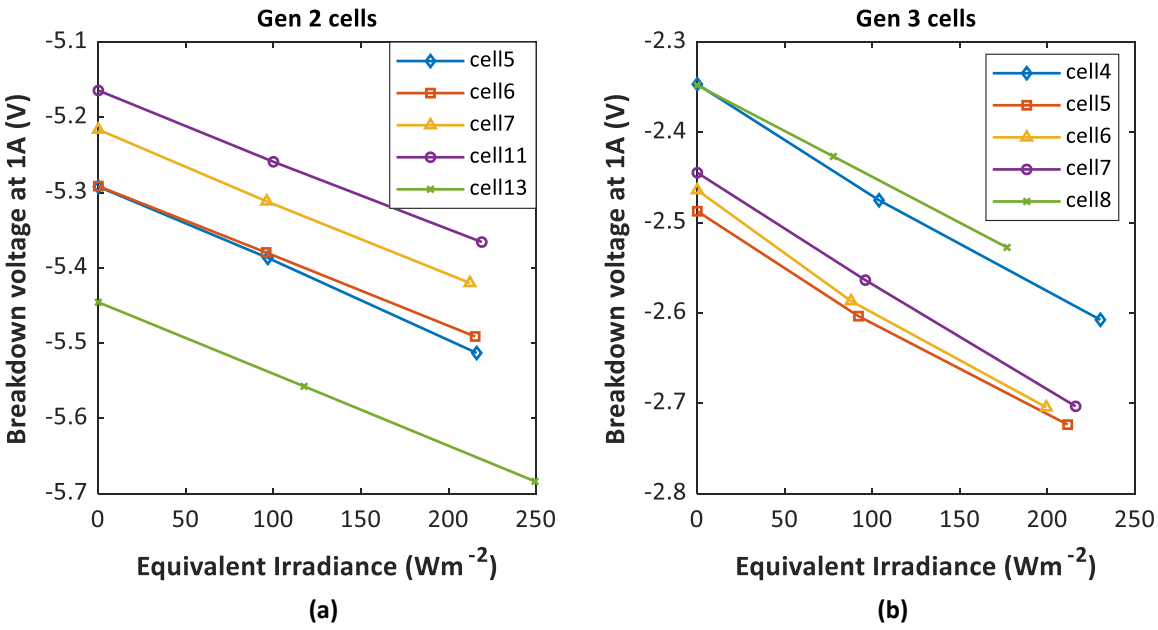

Figure 4.7: Change in breakdown voltage with irradiance of (a) gen 2 and (b) gen3 cells.

4.2. CHOICE OF MODEL

As discussed in section 2.5 there are two main solar cell models: the one diode model with five parameters and the two diode model with seven parameters. The one diode model is usually the first choice tool for researchers owing to its simplicity which comes from the fact that there are lesser unknown parameters to analyse and extract. However, the one diode model neglects the recombination losses in the depletion region which are significant at low voltages. Therefore, this model when exposed to weather changing conditions such as partial shading which causes lowering of irradiance levels and higher cell temperatures, suffers from inaccurate description of cell behaviour[54].

Alternatively, a two diode model requires a computation of seven parameters, making it more complex and time consuming, hindering this model from being widely used. However, the two diode model delivers more accurate results even at the vicinity of the open circuit voltage V_{oc}. From literature one diode model shows degraded behaviour for both multicrystalline and monocrystalline solar cells at low solar irradiance whereas two diode model exhibits greater accuracy than the one diode model[64].

The modelling of solar cells should describe their behaviour according to the conditions of use. A monocrystalline silicon solar cell is being used to simulate modules in an urban setting where partial shading is common. Hence, the two diode model is more practical for this application.

4.3. SOLAR CELL FITTING

The fitting of the two diode model has been divided into two parts: fitting the forward characteristics and fitting the reverse characteristics respectively.

4.3.1. FORWARD PARAMETERS FITTING

As discussed earlier, a two diode model has seven unknown parameters namely: photogenerated current (I_{ph}), diode reverse saturation currents (I_{01} & I_{02}), diode ideality factors (n_1 & n_2) shunt resistance (R_{sh}) and series resistance (R_s). From the datasheet there are three known points on the forward IV curves: the maximum power point, short circuit current and open circuit voltage. Therefore a fitting model proposed by Hovinen is adapted in this report [26].

Due to the non ideal recombination and parasitic series and shunt resistance, the ideality factor is voltage dependant. The ideality factor is controlled by shunt path across p-n junctions at low voltages i.e at low irradiance levels causing a large peak in the ideality factor curve as shown in figure 4.8. While the ideality factor is stable at intermediate voltages and at high voltages, it is governed by series resistances[42].

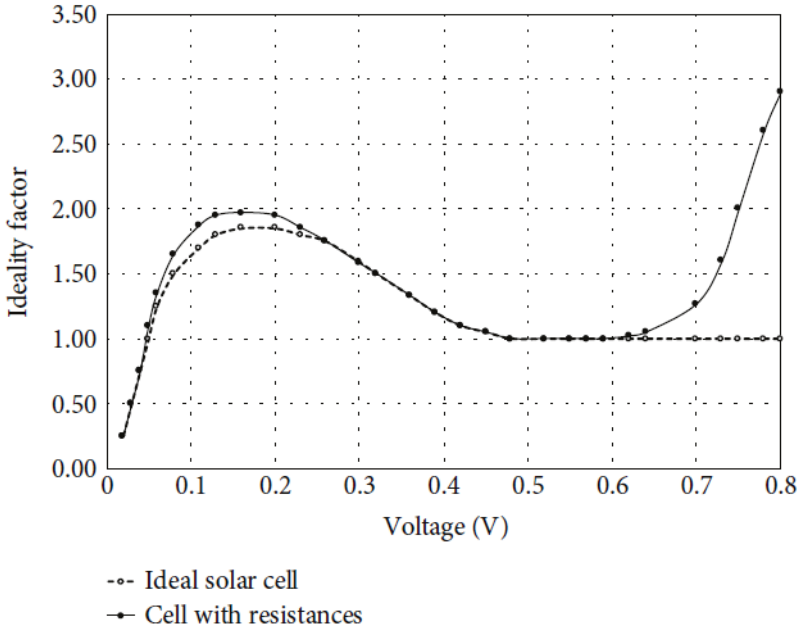

Figure 4.8: Dependence of ideality factor on voltage [42]

The ideality factor ranges in between 1 and 2. To reduce the complexities while fitting, voltage dependent ideality factor values are replaced by constants. The ideality factors n_1 and n_2 are equal to 1 and 2 representing diffusion and recombination current respectively.

With two fixed parameters, there are five more to be determined. To find the other parameters the current equation for the two diode model is written as an explicit function of current and voltage.

$$f(I,V) = I - I_{ph} + I_{01}\left(\exp^{\left(\frac{V+IR_s}{n_1V_t}\right)} - 1\right) + I_{02}\left(\exp^{\left(\frac{V+IR_s}{n_2V_t}\right)} - 1\right) + \frac{V+IR_s}{R_{sh}} = 0 \tag{4.1}$$

Then the equation 4.1 is partially differentiated as shown in equation 4.2 to obtain:

$$\frac{dF}{dI} + \frac{dF}{dV}\cdot\frac{dV}{dI} = 1 + \left(R_s + \frac{dV}{dI}\right) \times \left(\frac{I_{01}}{n_1V_t}\exp\left(\frac{V+IR_s}{n_1V_t}\right) + \frac{I_{02}}{n_2V_t}\exp\left(\frac{V+IR_s}{n_2V_t}\right) + \frac{1}{R_{sh}}\right) = 0 \tag{4.2}$$

where V_t is the thermal voltage given by:

$$V_t = \frac{kT}{q} \tag{4.3}$$

k being the boltzmann constant, T is the cell temperature and q the electron charge. The diode shunt resistance is determined directly from the IV curve slope at the short circuit (V = 0) point as:

$$\left(\frac{dI}{dV}\right)_{V=0} = \frac{1}{R_{sh0}} \tag{4.4}$$

Using equation 4.4, four parameters (I_{ph},I_{01},I_{02},R_{sh}) can be written in terms of the fifth parameter (R_s). Equations can be found in appendix. The possible solutions of R_s is then iterated by initialising it with a value of 1 mΩ and increasing it progressively. The value of R_s is chosen in such a way that the fitted IV curve has the minimum root mean square error from the measured IV curve.

Parameters	$\mathbf{I_{ph0}}$ (A)	$\mathbf{I_{s1}}$ (A)	$\mathbf{n_1}$ (-)	$\mathbf{I_{s2}}$ (A)	$\mathbf{n_2}$ (-)	$\mathbf{R_s}$ (Ω)	$\mathbf{R_{sh}}$ (Ω)
Gen 2	6.32	1.96e-11	1	1.56e-6	2	2.3e-3	306.76
Gen 3	6.15	3.99e-12	1	5.73e-7	2	2.2e-3	192.53

Table 4.1: Values of fitting parameters of the double diode model for gen 2 and gen 3 cells

4.3.2. TEMPERATURE DEPENDENCE OF SOLAR CELL PARAMETERS

The solar cell parameters depend on temperature. In the seven parameter model, the two diode ideality factors (n_1 & n_2) are still assumed to be constant and independent of temperature. The solar cell block from simulink provides the following relationships between the photogenerated current (I_{ph}), diode reverse saturation currents (I_{01} & I_{02}), shunt resistance (R_{sh}), series resistance (R_s) and temperature as follows:

$$I_{ph}(T) = I_{ph} \times (1 + TIPH1 \times (T - T_{STC})) \tag{4.5}$$

where, TIPH1 is the first order temperature coefficient for I_{ph} who's value is taken from the datasheet and T is the solar cell simulation temperature which ranges from −10 °C to 80 °C.

$$I_{01}(T) = I_0 \times \left(\frac{T}{T_{STC}}\right)^{\left(\frac{TXIS1}{n_1}\right)} \times \exp\left(\frac{Eg \times \left(\frac{T}{T_{STC}} - 1\right)}{n_1 \times V_t}\right) \tag{4.6}$$

$$I_{02}(T) = I_0 \times \left(\frac{T}{T_{STC}}\right)^{\left(\frac{TXIS2}{n_2}\right)} \times \exp\left(\frac{Eg \times \left(\frac{T}{T_{STC}} - 2\right)}{n_2 \times V_t}\right) \tag{4.7}$$

TXIS1 and TXIS2 are the temperature coefficients for the saturation current which indicates how saturation current changes with temperature and TXIS1 = TXIS2 = 3. E_g is the band gap energy of silicon which ranges from 1.11 eV and 1.14 eV. For the solar cell simulation range, the E_g is chosen to be 1.12 eV. Finally the series and shunt resistances are:

$$R_s(T) = R_s \times \left(\frac{T}{T_{STC}}\right)^{TRS1} \tag{4.8}$$

$$R_{sh}(T) = R_{sh} \times \left(\frac{T}{T_{STC}}\right)^{TRSH1} \tag{4.9}$$

TRS1 and TRSH1 are the temperature exponents for the series and shunt resistance. The series and shunt resistances are assumed to be not effected by temperature hence, TRS1 = TRSH1 = 0. However,

Temperature coefficients	TIPH1	TXIS	E_g (eV)	TRSI & TRSH1
Gen 2	4.1139e-04	3	1.12	0
Gen 3	4.7154e-04	3	1.12	0

Table 4.2: Values of temperature coefficients of the double diode model for gen 2 and gen 3 cells

in reality resistances are sensitive to temperature. All the temperature coefficienct values are given in table 4.2
Using these fitting parameters the solar cells are replicated and their fitted external parameters are compared with the datasheet paramters in tables 4.3 and 4.4.

Gen 2	P_{mpp} (W)	V_{mpp}(V)	I_{mpp}(A)	V_{oc}(V)	I_{sc}(A)
Datasheet	3.46000	0.58000	5.98000	0.68000	6.32000
DDM (sim)	3.44630	0.57498	5.99390	0.67704	6.32000
Deviation (%)	0.39753	0.87307	-0.23190	0.43720	0.00000

Table 4.3: Values of external parameters generated from the double diode model for gen 2 cells

Gen 3	P_{mpp}(W)	V_{mpp}(V)	I_{mpp}(A)	V_{oc}(V)	I_{sc}(A)
Datasheet	3.63000	0.62100	5.84000	0.72100	6.15000
DDM (sim)	3.60860	0.61505	5.86710	0.71783	6.15000
Deviation (%)	0.59303	0.96740	-0.46190	0.44161	0.00000

Table 4.4: Values of external parameters generated from the double diode model for gen 3 cells

From these tables, it is seen that the deviation of the double diode model simulated parameters from the datasheet values is less than 1 % and hence can be concluded that the simulated cell is pretty much representative of actual cell.

4.3.3. REVERSE PARAMETERS FITTING

The fitting of the reverse parameters was considered to follow the Bishop's approach. The main difference between Bishop's approach and the rest is that, Bishop considers that currents components affected by the breakdown process are those from the shunt resistance while the rest of them (such as Hartman, Lopez pinada models) consider primary currents [2] as seen in figure 4.9. The leakage current J_{sh} is the current through the shunt resistance and controls the cell reverse characteristics. This means that only a part of the current component shold be affected by avalanche multiplication. Therefore the Bishop's model in which the leakage current J_{sh} is multiplied by a non-linear factor [7] as shown in figure 4.9(a). is more widely used [2].
A good model should have a simple function ($M(V_j)$) so that temperature and irradiance coefficients can be added, and should reflect the measurements made at different irradiances and temperatures. Finally, the IV curve should be continuous and differentiable while transitioning between the forward and reverse bias i.e the slope $\left(\frac{dI}{dV}\right)_{V=0} = \frac{1}{R_{sh0}}$ should be constant.

A few exponential and polynomial functions have been used to try and replicate the reverse IV curves but maintaining a constant slope at the point V = 0 was difficult to achieve. This is due to the increase in slope of the IV curve of gen 3 solar cell compared to the gen 2 cell. It can also be argued that in low BDV cells zener breakdown mechanism is dominant. This is also supported by the positive temperature coefficient obtained in figure 4.11(a) . The bishop model is designed for reverse characteristics in which avalanche breakdown mechanism are predominant. Hence, there

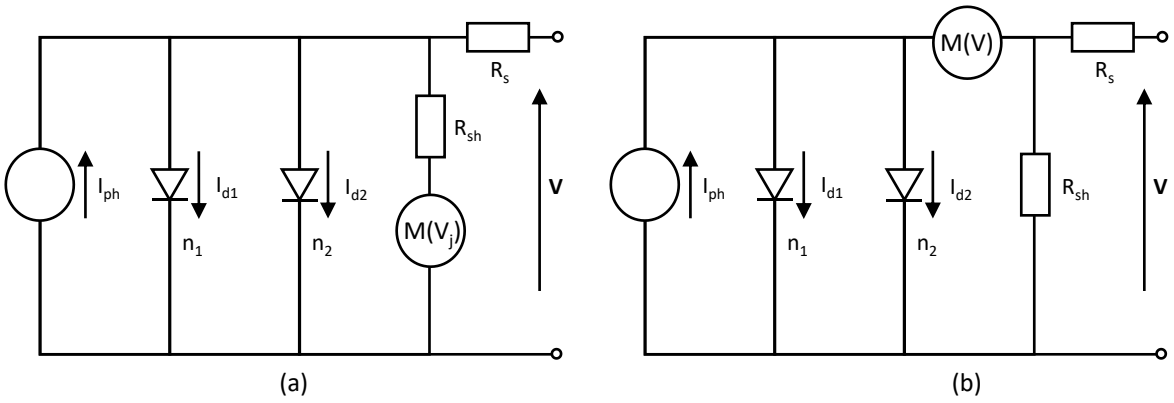

Figure 4.9: (a) Bishop model [7] (b) other models for fitting reverse characteristics of solar cells [2]

might be a requirement of a completely new model.

Due to the limitation of measurements and also in view of time, the temperature and irradiance dependency of reverse IV curves has been ignored. Instead a measured dark IV curve at 25 °C is manually fitted to the forward IV curve.

4.4. IMPACT OF NEGLECTING TEMPERATURE AND IRRADIANCE EFFECTS ON REVERSE IV CURVES

The temperature coefficient (change in reverse BDV w.r.t temperature) and the irradiance coefficient (change in reverse BDV w.r.t irradiance) are analysed to find the impact on reverse IV curves. Figure 4.10 represents the voltage gradient w.r.t temperature and irradiance.

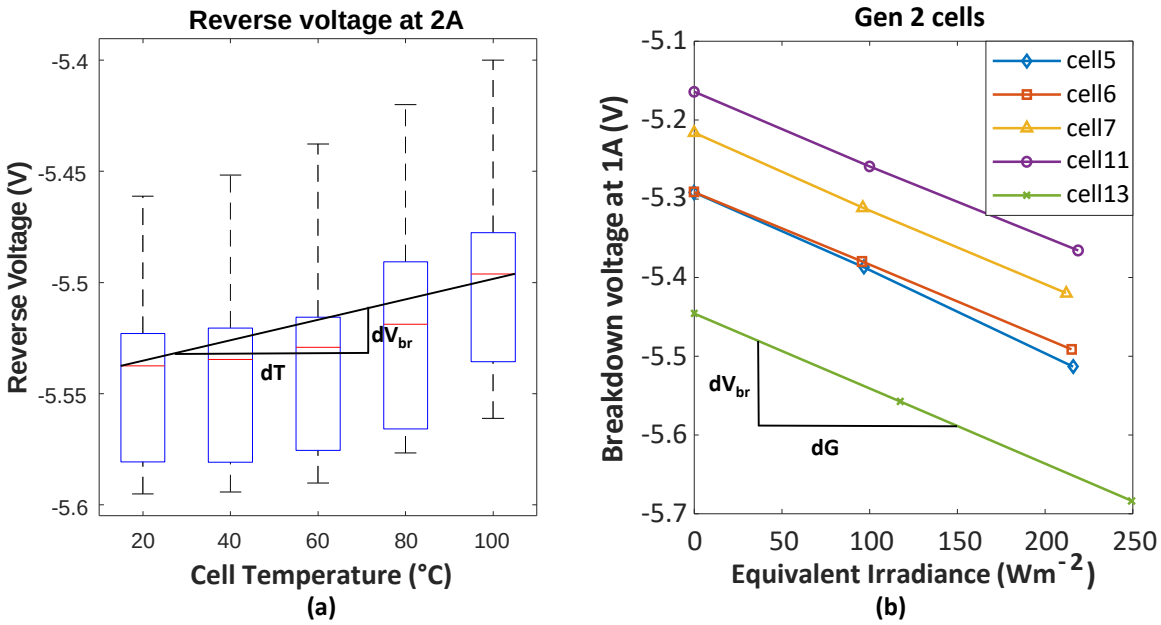

Figure 4.10: Rate of change of breakdown voltage (a) w.r.t temperature and (b) w.r.t irradiance

The temperature and irradiance coefficients for five different cells have been plotted in figures 4.11 and 4.12. The dashed line in all the plots represents the mean of the gradients. The measured

temperature coefficient is positive i.e the magnitude of reverse BDV of the solar cell decreases with increase in temperature and is equal to 0.0004 V/ °C for gen 2 cells and around 0.00047 V/ °C for gen 3 cells from figure 4.11. This means that for a change in 100 °C in temperature, the reverse BDV of gen 2 and gen 3 cells improve by 0.04 V and 0.047 V which is not very significant.

The measured irradiance coefficient is negative i.e the magnitude of reverse BDV of the solar cell increases with increase in irradiance assuming the same trend is followed even at higher irradiances. The irradiance coefficient is equal to 0.00095 V/ Wm^{-2} for gen 2 cells and around 0.00115 V/ Wm^{-2} for gen 3 cells from figure 4.12. This means that for a change in 1000 Wm^{-2} irradiance, the reverse BDV of gen 2 and gen 3 cells reduces by 0.95 V and 1.15 V which seems very significant. However, the solar cells are not always operating at STC. Especially in partial shading conditions when there are chances of the cells operating in reverse bias, the change in irradiance is much lower. This makes the change in reverse BDV a little bit less significant.

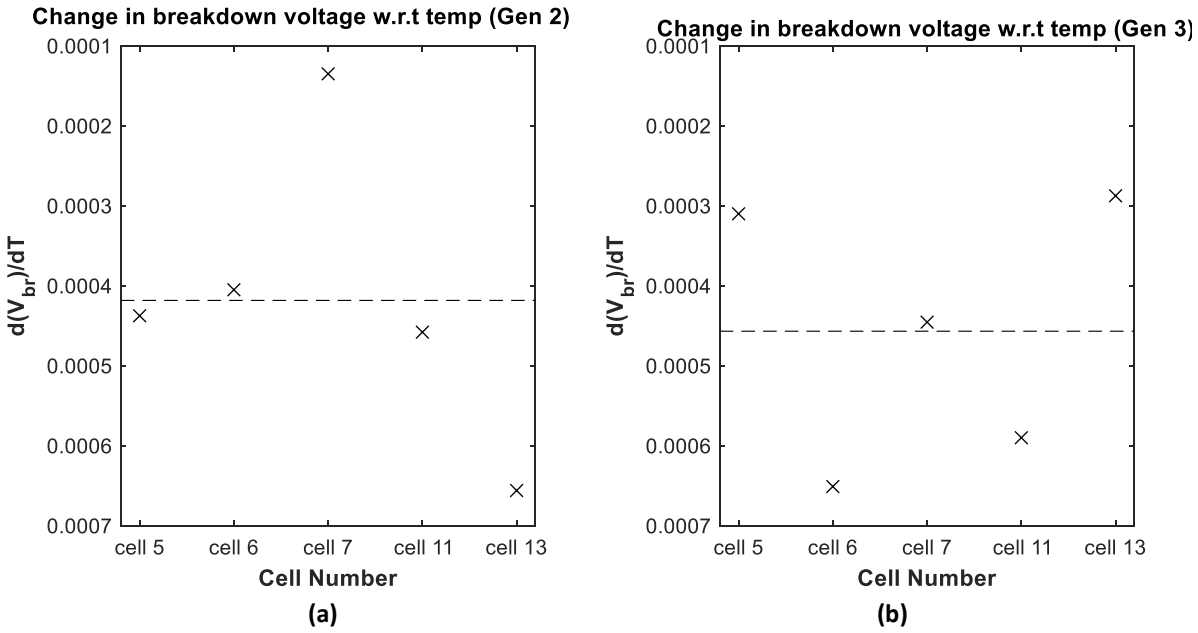

Figure 4.11: Rate of change of breakdown voltage w.r.t temperature for (a) gen 2 and (b) gen 3 cells

The effects due to positive temperature coefficient might compensate a small part of the negative irradiance coefficient. Therefore it can be said that the effect of neglecting temperature and irradiance effects on reverse characteristics is quantitatively not accurate. However, owing to the small temperature and irradiance coefficients, a solar cell model in which the reverse characteristics are independent of temperature and irradiance can be used for qualitative analysis.

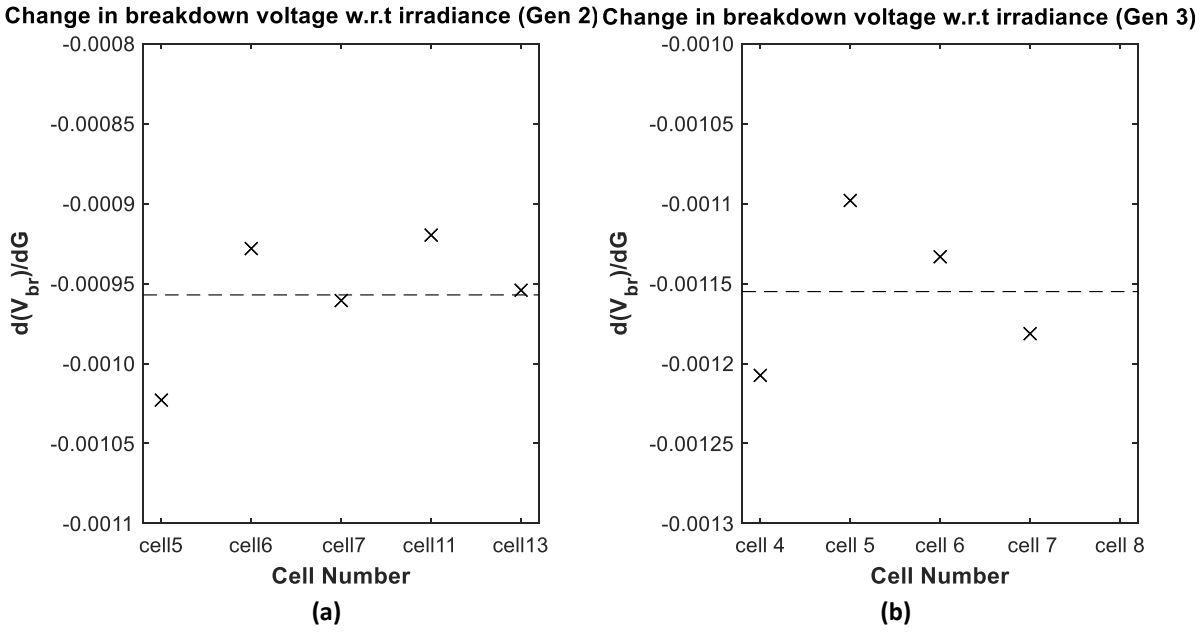

Figure 4.12: Rate of change of breakdown voltage w.r.t irradiance for (a) gen 2 and (b) gen 3 cells

5

ACCURATE SIMULATIONS OF LOW BDV CELLS & YIELD COMPARISONS OF ROOFTOP SOLAR MODULE

In the previous chapter, solar cell model of the two available solar cells: Sunpower Maxeon gen2 and gen3 have been developed. This model possess a high quality resemblance to the original solar cells. In this chapter, the solar cell model is used to predict the behaviour in an urban environment.

5.1. INTERPOLATION TOOL FOR YIELD AND IV CURVES CALCULATIONS

To calculate the yield of solar modules for different scenarios an interpolation tool developed by the PVMD group has been used. Figure 5.1 represents the flow chart of the working methodology of this tool.

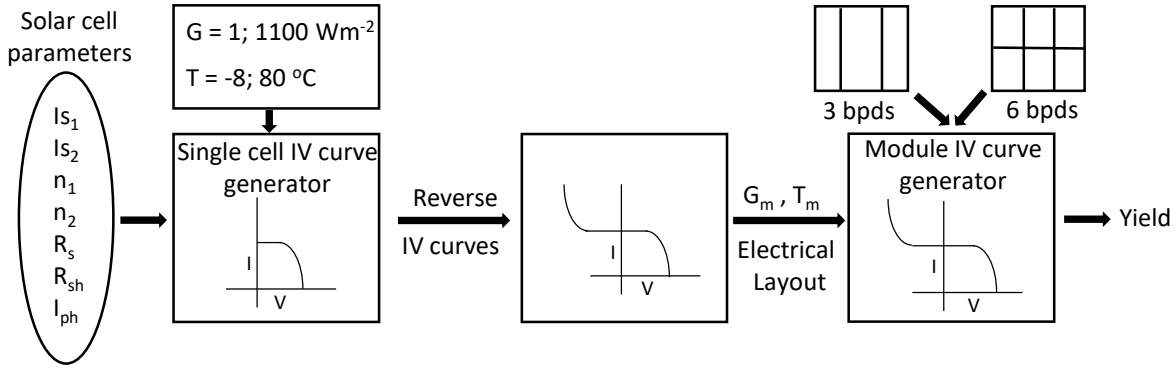

Figure 5.1: Flow chart of the interpolation tool

The first step is to generate IV curves for a single solar cell. The solar cell parameters obtained in the previous chapter are used as inputs along with irradiance and temperature. The irradiance (G) ranges from $1\,\mathrm{W\,m^{-2}}$ and increases with a step size of 1 until $1100\,\mathrm{W\,m^{-2}}$; similarly temperature (T) ranges from $-8\,^{\circ}\mathrm{C}$ until $80\,^{\circ}\mathrm{C}$ (which are the least and highest possible temperature values on the module) with a step size of 2 units. Therefore a total of 1100×45 forward IV curves have been generated for various irradiances and temperatures. As discussed in the previous chapter the dependency of reverse IV curves on temperature and irradiance has been neglected. Hence, measured reverse IV curves at $25\,^{\circ}\mathrm{C}$ have been added to the forward curves to obtain whole IV curves in both forward

and reverse bias.

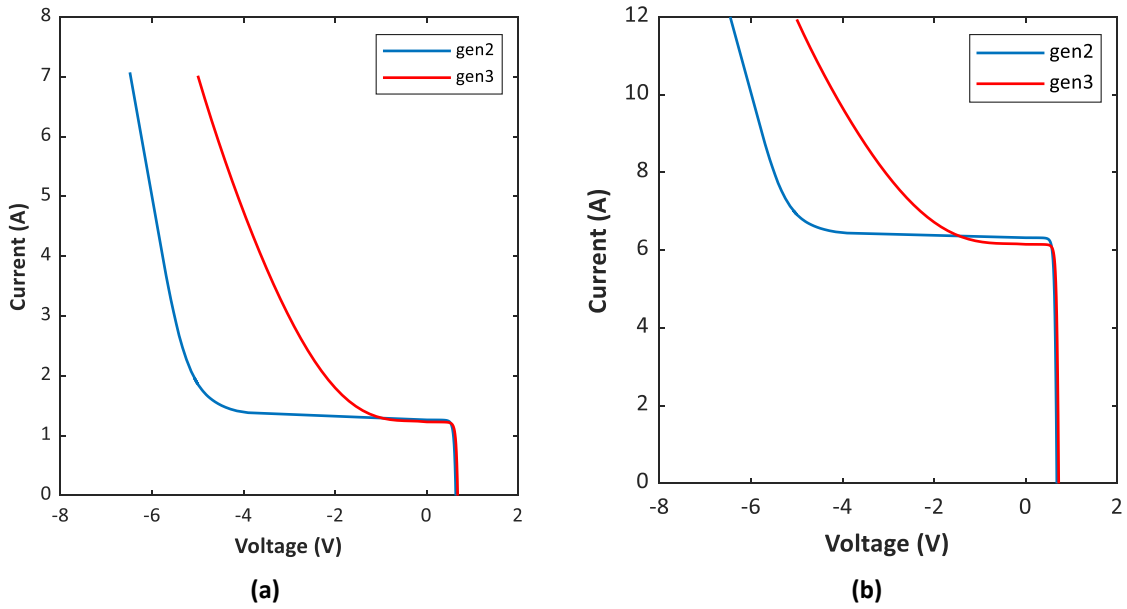

Figure 5.2: Fitted IV curves of gen 2 and gen 3 cells at 25 °C (a) 200 $\mathrm{W m^{-2}}$ and (b) 1000 $\mathrm{W m^{-2}}$

Figure 5.2 represents the comparison between IV curves of gen 2 and gen 3 solar cells at a temperature of 25 °C and irradiance of 200 $\mathrm{W m^{-2}}$ and 1000 $\mathrm{W m^{-2}}$. A total of 1100 × 45 IV curves have been generated as mentioned above. From this figure, it is clearly visible that the short circuit current of gen 2 cells is higher than gen 3 cells, while gen 3 cells have a softer breakdown compared to gen 2 cells

The next step is to obtain the IV curves for solar modules located at different places of a rooftop. The same rooftop which has been used for validation of the use of low BDV cells in chapter 3 has been used for this model. The irradiances, temperatures of the solar modules together with the electrical layouts are inputs for this step. The solar module irradiances are calculated using forward ray tracing and are measured every 10 minutes for a whole year (same as in chapter 3); while the module temperatures are calculated using the Faiman model [38] which considers that irradiance and temperature are coupled. Since the reverse characteristics are assumed to be independent of temperature the Faiman model has no effect in the reverse bias operation of solar cell. Moreover the Faiman model is reasonably accurate in the forward bias, which contributes to the yield. Hence, usage of Faiman model is justified.

The location of the solar modules on the rooftop, the solar module topologies are the same as discussed in 3.3 and . Apart from different locations of the rooftop and the two topologies (96 cell 3BPDs an 6BPDs), two types of solar cells gen 2 and gen 3 have been used. The diodes used are schottky diode which have a turn on voltage of around 0.4 V The operating temperatures of the diodes is assumed to be a constant value of 30 °C to avoid further complexities in the modeling. Using all this information the multiple solar module IV curves over a year have been generated. The maximum power points of the IV curves have been manually calculated resembling an ideal maximum power point tracker. These maximum power points are summed up to calculate yield.
Table 5.1 shows the value of irradiation and yield of various solar modules placed at different locations on the rooftop, with different electrical layouts. The yield of solar modules made of same type

Module	**Irradiation** ($kWhm^{-2}$)	**Cell Model**	**Yield - 3 BPDs** (kWh)	**Yield - 6 BPDs** (kWh)
A	909.81	gen 2	249.62	253.19
		gen 3	265.69	268.84
B	480.30	gen 2	55.41	77.50
		gen 3	61.09	84.93
C	648.66	gen 2	116.63	141.47
		gen 3	125.31	151.09

Table 5.1: Yield of solar module made of gen 2 and gen 3 solar cells for 3 BPDs and 6BPDs configuration at three different locations.

of solar cells but with higher number of bypass diodes is higher compared to modules with lower number of bypass diodes as shown.in figure 5.3(a). The module B receives 47.2 % less irradiation than module A, while module B produces 77.8 % less power than module A assuming both modules are made of gen 2 cells and have 3 bypass diode configuration. Similarly when module C and module A are compared, for a 28.7 % drop of irradiation, there is a decline of 53.28 % power output. This difference in irradiation drop and power output drop is due to the mismatch losses caused due to partial shading. The modules with higher number of bypass diodes minimise these losses and hence produce higher yield. From figure 5.3 it can be clearly seen that gen 2 cells with 6 bypass diodes outperforms gen 3 cells with 3 bypass diodes in both locations B and C where partial shading is significant.

As shown in figure 5.3(b) modules made of gen 3 solar cells have higher yield than those made of gen 2 cells and having same number of bypass diodes at all the locations . The higher yield of solar modules made up of gen 3 cells can be attributed to their higher rated efficiency and maximum power point. Due to this reason, the yield of gen 3 cells with 3 bypass diodes is greater than gen 2 cells with 6 bypass diodes at location A, where partial shading is not very dominant. However, the effect of low reverse breakdown voltage of gen 3 solar cells on the performance of the module can't be determined. To obtain more conclusive results of the comparison between modules made of gen 2 and gen 3 cells specific yield is calculated along with analysis of different loss mechanisms.

5.2. SPECIFIC YIELD OF SOLAR MODULES MADE WITH GEN 2 AND GEN 3 CELLS

Specific yield is one of the most commonly used performance metrics for numerous solar modules. The factors that majorly impact the specific yield are the location, choice of module and bypass diode configuration. Table 5.2 exhibits the values of specific yields for various solar module configurations. Coincidentally specific yield follows the same trend as the yield. The specific yield of a solar module made with gen 3 cells with 6 bypass diodes outperforms the rest of the solar modules. It can also be seen that modules with gen 3 cells perform better than gen 2 cells. Especially in the case of module B which experiences high amounts of partial shading compared to the other to modules, there is a spike of 5.3 % in specific yield when gen 2 cells are replaced by gen 3 cells. Whereas the gain for module A and module C are 1.6 % and 2.6 % respectively. The use of low reverse breakdown solar cells at location B plays a significant role in reduction of mismatch losses due to partial shading. Partial shading causes power dissipation in some solar cells leading to higher temperatures.

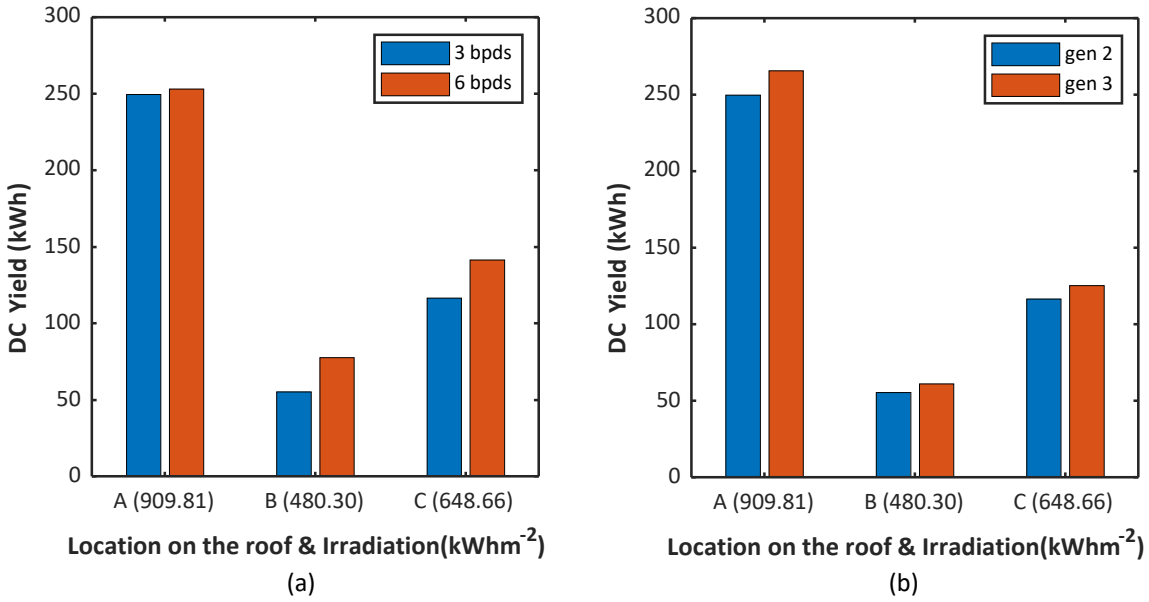

Figure 5.3: (a) Yield of solar module made of gen 2 solar cells and (b) solar module with 3 bypass diodes

Specific Yield (kWh/kWp)	No. of BPDs	A	B	C
Gen 2	3	754.50	167.49	352.53
	6	765.28	234.25	427.61
Gen 3	3	766.93	176.34	361.73
	6	776.03	245.16	436.15

Table 5.2: Specific yield of solar module made of gen 2 and gen 3 solar cells for 3 BPDs and 6BPDs configuration at three different locations.

5.3. DIFFERENT LOSS MECHANISMS

The STC efficiency of a solar cell is calculated at standard test conditions. The solar modules rarely operate at standard test conditions and have a different efficiency called operating efficiency. An analysis of various losses such as optical, thermal and partial shading losses which explain the difference between efficiency at STC and operating efficiency has been discussed in this section. Cell to module losses are neglected i.e size of module is equal to the product of number of cells per module and area of the cell.

5.3.1. OPERATIVE EFFICIENCY

The operative efficiency of a solar module is a parameter used to describe the efficiency of a solar module under real operating conditions and it is defined as the ratio of output energy yield of a module over a year to the maximum energy incident on the module :

$$\eta_{\mathrm{op}} = \frac{\int_{\mathrm{year}} \mathrm{MPP(t)} \cdot \mathrm{dt}}{\int_{\mathrm{year}} \mathrm{G_m}(t) \cdot \mathrm{A_m} \cdot \mathrm{dt}} \tag{5.1}$$

5.3.2. OPTICAL LOSSES

Optical losses could be reflection, refraction or absorption losses. The solar modules are assumed to have a glass sheet on top and a white back sheet. Only reflection losses at the air-glass junction

Operative efficiency(%)	No. of BPDs	A	B	C
Gen 2	3	18.68	7.85	12.24
	6	18.95	10.99	14.85
Gen 3	3	19.88	8.66	13.15
	6	20.12	12.04	15.86

Table 5.3: Operating efficiency of various solar modules.

are considered while refraction, absorption, and reflection at back contact are neglected.

Figure 5.4 shows a schematic of solar cell with its optical losses. The reflective losses for normally incident light can simply be written as :

$$R = \left(\frac{n_1 - n_2}{n_1 + n_2}\right)^2 \tag{5.2}$$

The optical gain due to texturing and white back sheet have been traded off by neglecting the parasitic absorption losses. Substituting the values of n_1 and n_2 (refractive indices of air and glass) from figure 5.4 in the equation 5.2 gives 4 %. This means that the efficiency at standard test conditions reduces by 4 % due to optical losses.

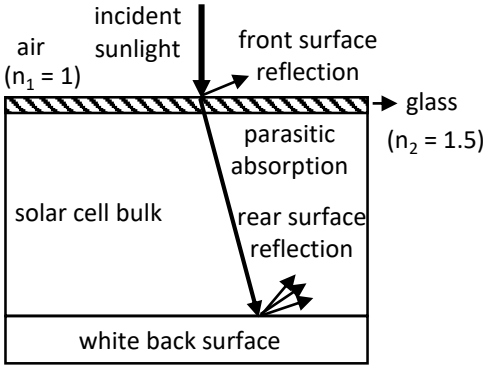

Figure 5.4: Optical losses schematic of solar cell

	Gen 2	Gen 3
STC efficiency (%)	22.52	23.59
Optical loss (%)	0.9008	0.9436

Table 5.4: Optical losses

5.3.3. THERMAL LOSSES

In reality when a substring is bypassed the temperature should increase but this increase in temperature is not accounted by the Faiman model. The temperature is calculated as a function of incident irradiance on the solar module. According to the results of the Faiman model, the annual average temperature at locations A, B, C are 24.03 °C, 18.99 °C, 20.97 °C respectively.

Module	Irradiance ($kWh\,m^{-2}$)	Cell Model	Yield - 3 BPDs (kWh)	Yield - 6 BPDs (kWh)
A	909.81	gen 2	262.77	266.50
		gen 3	277.34	280.58
B	480.30	gen 2	55.64	79.60
		gen 3	61.37	86.93
C	648.66	gen 2	118.38	145.84
		gen 3	127.10	155.13

Table 5.5: Yield calculation after ignoring thermal effects

To calculate the thermal power loss: a constant temperature input of 25 °C is given to the IV interpolation tool and yield is calculated as shown in 5.5. The difference in the yield of this model and the

model which varies with temperature gives the thermal losses. The change in yield due to thermal losses is calculated to be around 5 %, 0.5 % and 1.5 % for locations A, B and C.

5.3.4. MISMATCH LOSSES DUE TO PARTIAL SHADING

Mismatch losses due to partial shading are calculated by subtracting the operating efficiency, thermal and optical losses from the STC efficiency. Tables 5.6, 5.7, 5.8, 5.9 represent all the losses in different solar module topologies at different locations.

(%)	A	B	C
Operating efficiency	18.68	7.85	12.24
Optical losses	0.90		
Thermal losses	0.98	0.03	0.18
Mismatch losses	1.96	13.73	9.19
STC Efficiency	22.52		

Table 5.6: Loss distribution in gen 2 cells with 3BPDs

(%)	A	B	C
Operating efficiency	19.88	8.66	13.15
Optical losses	0.94		
Thermal losses	0.87	0.04	0.19
Mismatch losses	1.89	13.95	9.30
STC Efficiency	23.59		

Table 5.7: Loss distribution in gen 3 cells with 3BPDs

(%)	A	B	C
Operating efficiency	18.95	10.99	14.85
Optical losses	0.90		
Thermal losses	1.00	0.30	0.46
Mismatch losses	1.68	10.34	6.31
STC Efficiency	22.52		

Table 5.8: Loss distribution in gen 2 cells with 6BPDs

(%)	A	B	C
Operating efficiency	20.12	12.04	15.86
Optical losses	0.94		
Thermal losses	0.88	0.28	0.42
Mismatch losses	1.65	10.32	6.36
STC Efficiency	23.59		

Table 5.9: Loss distribution in gen 3 cells with 6BPDs

To have a better understanding, the losses are plotted as a percentage of STC efficiency. as shown in figures 5.5, 5.6. The optical losses are constant and equal to 4 %. A few of the common trends that can be observed from the plots are : Operating efficiency of module A in all the cases is very high compared to module B and module C. The reason being, high irradiation at the location A, due to which the solar module mostly operates in forward bias hence, increasing the operating efficiency.

The mismatch losses portray a behaviour exactly opposite to the operating efficiency. At location B, due to low irradiation levels, the solar modules operate in reverse bias dissipating energy hence, the locations B and C have relatively very higher mismatch losses.

As discussed earlier, the rise in temperature due to bypassing of substrings is ignored. The Faiman model calculates the module temperature based on incident irradiation. The reverse IV curves have already been assumed to be independent of temperature. The fraction of temperature losses. The steep rise of thermal losses at locations B and C when more bypass diodes are used can be attributed to the fact that, mismatch losses have reduced due to the use of more bypass diodes. This decrease in mismatch losses are compensated by increase in operating efficiency and increase in thermal losses. The percentage of thermal losses reduce, while using gen 3 cells, possible reason could be the better temperature coefficients for gen 3 cells. The increase in specific yield from gen2 to gen3 cannot only be attributed to the better temperature coefficients of gen3 and hence it can be concluded that the reverse characteristics are also responsible for the gain

Turning ON of one bypass diode could lead to a reduction of a whole arrays power generation. Due to a possible chance of bypassing of array during partial shading conditions, the mismatch loss in module B and module C is significant. Module A is the best illuminated solar module hence the

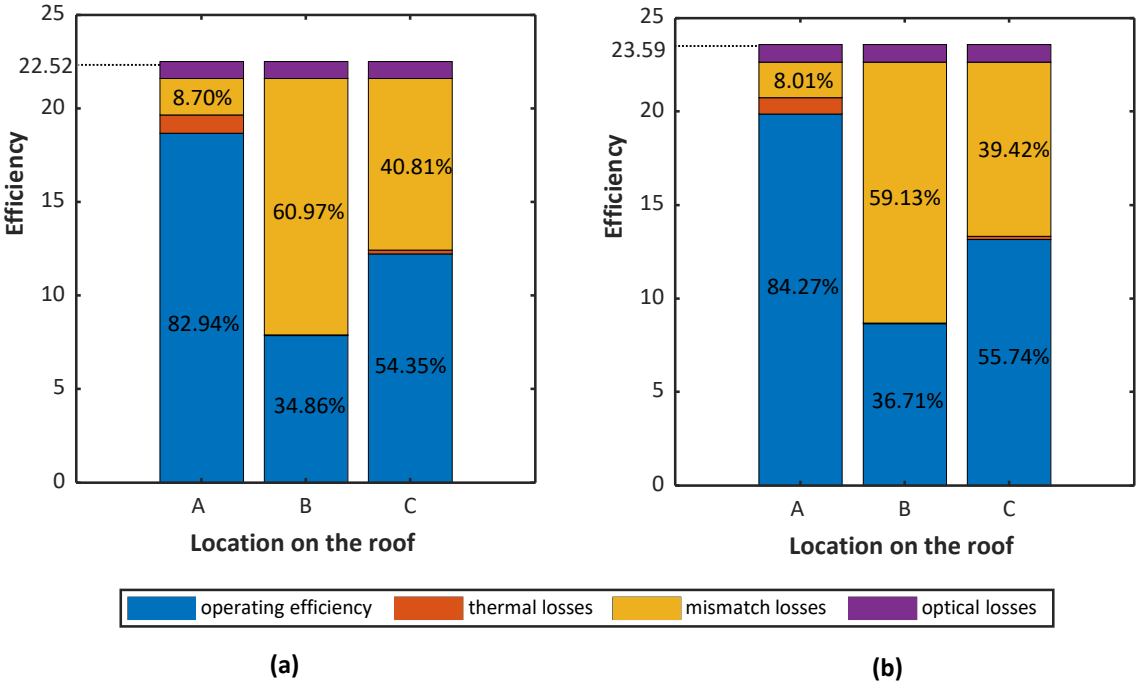

Figure 5.5: (a) Percentages of loss distribution in gen 2 cells with 3 BPDs and (b) gen 3 cells with 3 BPDs

mismatch losses are very low. Usage of gen 3 cells instead of gen 2 cells improves the mismatch error by a very small percentage. The turning on of the bypass diodes being the reason. The use of cells with an even lower BDV can improve the operating efficiency. Using higher number of bypass diodes reduces the size of the arrays hence, lesser number of non productive cells during partial irradiation which results in higher operating efficiency.

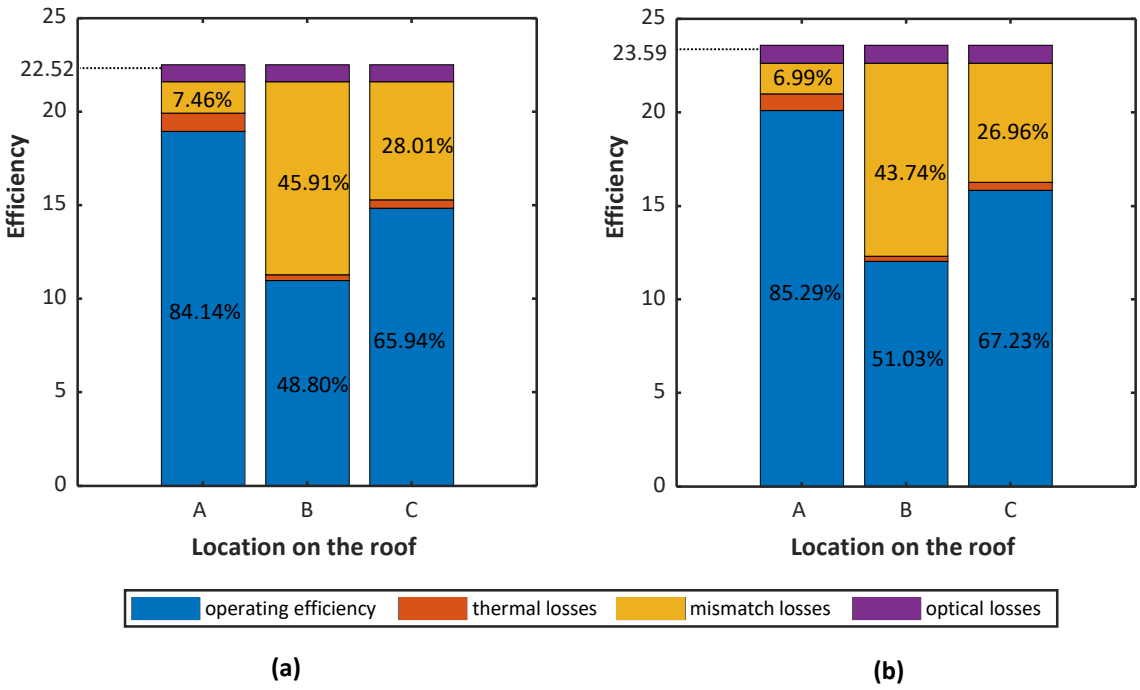

Figure 5.6: (a) Percentages of loss distribution in gen 2 cells with 6 BPDs and (b) gen 3 cells with 6 BPDs

6

CONCLUSIONS AND RECOMMENDATIONS

The aim of the research was to evaluate the potential and performance of solar modules made of low reverse breakdown solar cells in urban landscapes. The potential of these solar modules can be determined by estimating the maximum amount of solar radiation that a module can convert as a function of its electrical layout.

For a case study, a PV system is modelled on a rooftop facing south with a tilt of 36 degrees. The initial set of simulations are run for an eight parameter model of a solar cell which is built based on the one diode model. The module location for this study is chosen in such a way that it is neither the most shaded (to avoid very optimistic results) nor the least shaded (to avoid very optimistic results). The reverse characteristics of the module have been manipulated while keeping the forward characteristics unchanged. The breakdown voltage of solar cells have been varied in the range of $-0.12\,\mathrm{V}$ and $-14\,\mathrm{V}$. There is an almost 36.23 % increase in DC gain for cells with $-0.12\,\mathrm{V}$ when compared with $-14\,\mathrm{V}$ cells. Similarly, with a $-0.90\,\mathrm{V}$ solar cells there is a gain of almost 11 %. There is no solar cell with a reverse BDV of $-1\,\mathrm{V}$ but it might be a possibility in the future that these kind of cells are manufactured. There are several companies such as AE solar manufacturing schottky diodes with a forward voltage of 0.3 V. For a reverse BDV of $-0.25\,\mathrm{V}$ there is a DC gain of almost 27.49 %. From this it can be concluded that instead of having one bypass diode per cell which has a complex manufacturing process it's worth exploring how to manufacture very low reverse BDV cells. Also, the solar cells with BDV -5.45 V, -3.70 V and -1.94 V represent measured sunpower solar cells. The relative increase in yield for each of these solar cells with respect to a solar cell with ∞ BDV is 2.40 %, 4.58 % & 7.00 % respectively. This is a significant gain in yield and hence shows that it is already worth exploring the the yield of commercially available low BDV solar cells with a much more accurate model.

The two main assumptions in the previous solar cell model are measuring performance at a constant temperature of 25 °C and keeping the forward characteristics unchanged. Therefore a much more accurate double diode thermo-electric model has been built for the commercially available Sunpower Maxeon gen 2 and gen 3 solar cells. Although a double diode model needs greater computation power than the one diode model, due to higher number of parameter it has still been chosen, due to the higher accuracy of double diode model in partial shaded conditions which is very common in urban landscapes. For the solar cell fitting, measurements of 10 gen 2 cells and 10 gen 3 cells have been made in the dark for varying temperatures and also at various irradiance and temperatures. However, the measurements were limited due to the lack of equipment and hence, the IV curve measurements were only taken in the range of $-3\,\mathrm{A}$ to 3 A. Initially the forward characteristics have been fitted using the Hovinen model. The external parameters from the fitted model turned

out to have a deviation of less than 1 % from the original solar cell measurements. The Bishop's model was used to fit the reverse IV curves in the model. But managing a constant slope at the short circuit current point at different temperatures was difficult to model. Especially with the slope of gen 3 cells being greater than gen 2 cells did not help. Due to the limitations in measurements and in view of time the reverse IV curves have been left independent of irradiance and temperature. The measured reverse IV curves have been manually fitted to the existing forward IV curves. Due to the low irradiance and temperature coefficient, the accuracy of the model is not jeopardised. However, it is suggested to add the thermal model for reverse bias in the future.

Finally the potential and performance of solar modules in urban landscapes for a solar module made up of 96 solar cells has been analysed for three different locations on the same rooftop discussed above. The locations were chosen in such a way that the modules are highly illuminated, highly shaded and intermediately shaded at each locations. The solar module with 6 bypass diodes (BPDs) has a better performance than a similar module with 3 bypass diodes irrespective of the location and type of cell chosen. The higher number of diodes reduce the mismatch losses during partial shading condition thereby increasing the operational efficiency. Similarly, a solar module with 3 bypass diodes made of Sunpower Maxeon gen 3 solar cells has a better performance than module made of gen 2 cells. This not only accounts for better forward parameters of gen 3 cells but also its better temperature coefficients.

To sum up, the electrical potential increases by around 36.21 % when the reverse BDV is changed from infinite to 0.12 V and keeping the forward characteristics unchanged. Next, commercially available low reverse BDV solar cells are represented by a thermo-electric model based on the two diode solar cell model. However the reverse characteristics have not been modeled with varying irradiance and temperature partly owing to the limitations in measurement equipment. This is something which could be worked on in the future. Finally the commercially available low reverse BDV cells performance is compared with each other with the help of the developed model.

BIBLIOGRAPHY

[1] Muhammad A Alam et al. "Explanation of soft and hard breakdown and its consequences for area scaling". In: *International Electron Devices Meeting 1999. Technical Digest (Cat. No. 99CH36318)*. IEEE. 1999, pp. 449–452.

[2] MC Alonso-Garcia and JM Ruiz. "Analysis and modelling the reverse characteristic of photovoltaic cells". In: *Solar Energy Materials and Solar Cells* 90.7-8 (2006), pp. 1105–1120.

[3] EA Alsema. "Energy requirements and CO2 mitigation potential of PV systems". In: (1998).

[4] Ajith Amerasekera et al. "Self-heating effects in basic semiconductor structures". In: *IEEE transactions on Electron Devices* 40.10 (1993), pp. 1836–1844.

[5] Andres Calcabrini, Raoul Weegink, Olindo Isabella, Miro Zeman. *The ultimate potential of reconfigurable modules in partially shaded urban photovoltaic systems*. 2019.

[6] J Bauer et al. "Hot spots in multicrystalline silicon solar cells: avalanche breakdown due to etch pits". In: *physica status solidi (RRL)–Rapid Research Letters* 3.2-3 (2009), pp. 40–42.

[7] JW Bishop. "Computer simulation of the effects of electrical mismatches in photovoltaic cell interconnection circuits". In: *Solar cells* 25.1 (1988), pp. 73–89.

[8] JW Bishop. "Microplasma breakdown and hot-spots in silicon solar cells". In: *Solar Cells* 26.4 (1989), pp. 335–349.

[9] bp. *Statistical Review of World Energy*. URL: `https://www.bp.com/en/global/corporate/energy-economics/statistical-review-of-world-energy.html`.

[10] Kadra Branker, MJM Pathak, and Joshua M Pearce. "A review of solar photovoltaic levelized cost of electricity". In: *Renewable and sustainable energy reviews* 15.9 (2011), pp. 4470–4482.

[11] Otwin Breitenstein et al. "Understanding junction breakdown in multicrystalline solar cells". In: *Journal of Applied Physics* 109.7 (2011), p. 5.

[12] Santoshi Tejasri Buddha. *Topology reconfiguration to improve the photovoltaic (PV) array performance*. Arizona State University, 2011.

[13] CE Chamberlin et al. "Comparison of PV module performance before and after 11 and 20 years of field exposure". In: *2011 37th IEEE Photovoltaic Specialists Conference*. IEEE. 2011, pp. 000101–000105.

[14] Kuei-Hsiang Chao, Pei-Lun Lai, and Bo-Jyun Liao. "The optimal configuration of photovoltaic module arrays based on adaptive switching controls". In: *Energy Conversion and Management* 100 (2015), pp. 157–167.

[15] Jaeeock Cho et al. "Efficiency enhanced emitter wrap-through (EWT) screen-printed solar cells with non-uniform thickness of silicon nitride passivation layer in via-holes". In: *Solar energy* 90 (2013), pp. 188–194.

[16] Haifeng Chu et al. "Soft breakdown behavior of interdigitated-back-contact silicon solar cells". In: *Energy Procedia* 77 (2015), pp. 29–35.

[17] Ed Dlugokencky and Pieter Tans. "Trends in atmospheric carbon dioxide". In: *NOAA/ESRL. www. esrl. noaa. gov/gmd/ccgg/trends/global. html. Accessed* 5 (2016).

[18] Peng Dong et al. "Efficient low-cost IBC solar cells with a front floating emitter: Structure optimization and passivation layer study". In: *Energies* 11.4 (2018), p. 939.

[19] Fabian Fertig et al. "Illumination and temperature dependence of breakdown mechanisms in multicrystalline silicon solar cells". In: *Energy Procedia* 38 (2013), pp. 32–42.

[20] Fabian Fertig et al. "Impact of junction breakdown in multi-crystalline silicon solar cells on hot spot formation and module performance". In: *cell* 40.60 (2011), p. 80.

[21] ISE with support of PSE Projects GmbH Fraunhofer Institute for Solar Energy Systems. *Photovoltaics Report*. URL: https://www.ise.fraunhofer.de/content/dam/ise/de/documents/publications/studies/Photovoltaics-Report.pdf (visited on 06/23/2020).

[22] Martin A Green et al. "Solar cell efficiency tables (version 50)". In: *Progress in Photovoltaics: Research and Applications* 25.7 (2017), pp. 668–676.

[23] Shelly Hagerman, Paulina Jaramillo, and M Granger Morgan. "Is rooftop solar PV at socket parity without subsidies?" In: *Energy Policy* 89 (2016), pp. 84–94.

[24] Hamed Hanifi et al. "A novel electrical approach to protect PV modules under various partial shading situations". In: *Solar Energy* 193 (2019), pp. 814–819.

[25] W Herrmann, W Wiesner, and W Vaassen. "Hot spot investigations on PV modules-new concepts for a test standard and consequences for module design with respect to bypass diodes". In: *Conference Record of the Twenty Sixth IEEE Photovoltaic Specialists Conference-1997*. IEEE. 1997, pp. 1129–1132.

[26] Anssi Hovinen. "Fitting of the solar cell IV-curve to the two diode model". In: *Physica Scripta* 1994.T54 (1994), p. 175.

[27] Haider Ibrahim and Nader Anani. "Variations of PV module parameters with irradiance and temperature". In: *Energy Procedia* 134 (2017), pp. 276–285.

[28] IEA. *Trends in PV applications 2019*. URL: https://iea-pvps.org/trends_reports/2019-edition/ (visited on 05/15/2016).

[29] Texas Instruments. *Smart Bypass Diode: SM74611*. URL: http://www.ti.com/lit/ds/symlink/sm74611.pdf (visited on 05/10/2016).

[30] Wm. Robert Johnston. *Historical World Population Data*. URL: http://www.johnstonsarchive.net/other/worldpop.html (visited on 02/21/2015).

[31] Fabian Kiefer et al. "High efficiency n-type emitter-wrap-through silicon solar cells". In: *IEEE Journal of Photovoltaics* 1.1 (2011), pp. 49–53.

[32] Katherine Kim. "Hot spot detection and protection methods for photovoltaic systems". PhD thesis. University of Illinois at Urbana-Champaign, 2014.

[33] Katherine A Kim and Philip T Krein. "Hot spotting and second breakdown effects on reverse IV characteristics for mono-crystalline Si photovoltaics". In: *2013 IEEE Energy Conversion Congress and Exposition*. IEEE. 2013, pp. 1007–1014.

[34] Katherine A Kim and Philip T Krein. "Photovoltaic hot spot analysis for cells with various reverse-bias characteristics through electrical and thermal simulation". In: *2013 IEEE 14th Workshop on Control and Modeling for Power Electronics (COMPEL)*. IEEE. 2013, pp. 1–8.

[35] Katherine A Kim and Philip T Krein. "Reexamination of photovoltaic hot spotting to show inadequacy of the bypass diode". In: *IEEE Journal of Photovoltaics* 5.5 (2015), pp. 1435–1441.

[36] Karl Knapp and Theresa Jester. "An empirical perspective on the energy payback time for photovoltaic modules". In: *PROCEEDINGS OF THE SOLAR CONFERENCE*. AMERICAN SOLAR ENERGY SOCIETY; AMERICAN INSTITUTE OF ARCHITECTS. 2000, pp. 641–648.

[37] Damiano La Manna et al. "Reconfigurable electrical interconnection strategies for photovoltaic arrays: A review". In: *Renewable and Sustainable Energy Reviews* 33 (2014), pp. 412–426.

[38] Sandia National Laboratories. *Faiman Module Temperature model*. URL: https://pvpmc.sandia.gov/modeling-steps/2-dc-module-iv/module-temperature/faiman-module-temperature-model/.

[39] Global Monitoring Laboratory. *Trends in Atmospheric Carbon Dioxide*. URL: https://www.esrl.noaa.gov/gmd/ccgg/trends/data.html (visited on 06/11/2020).

[40] Sudha Mahadevan, SM Hardas, and G Suryan. "Electrical breakdown in semiconductors". In: *physica status solidi (a)* 8.2 (1971), pp. 335–374.

[41] Sander A Mann et al. "The energy payback time of advanced crystalline silicon PV modules in 2020: a prospective study". In: *Progress in Photovoltaics: Research and Applications* 22.11 (2014), pp. 1180–1194.

[42] Keith R McIntosh and Christiana B Honsberg. “The influence of edge recombination on a solar cell’s IV curve”. In: *Proc. 16th PVSEC, Glasgow*. 2000, pp. 1651–1654.

[43] EL Meyer. “Extraction of saturation current and ideality factor from measuring Voc and Isc of photovoltaic modules”. In: *International Journal of Photoenergy* 2017 (2017).

[44] M. E. Nell and A. M. Barnett. “The spectral p-n junction model for tandem solar-cell design”. In: *IEEE Transactions on Electron Devices* 34.2 (1987), pp. 257–266.

[45] Wolfgang Palz and Henri Zibetta. “Energy pay-back time of photovoltaic modules”. In: *International Journal of Solar Energy* 10.3-4 (1991), pp. 211–216.

[46] Boudewijn B Pannebakker, Arjen C de Waal, and Wilfried GJHM van Sark. “Photovoltaics in the shade: one bypass diode per solar cell revisited”. In: *Progress in photovoltaics: Research and Applications* 25.10 (2017), pp. 836–849.

[47] R Perez and M Perez. “A fundamental look at supply side energy reserves for the planet”. In: *Int. Energy Agency SHC Program. Sol. Updat* 62 (2015), pp. 4–6.

[48] R Ramaprabha and BL Mathur. “A comprehensive review and analysis of solar photovoltaic array configurations under partial shaded conditions”. In: *International Journal of Photoenergy* 2012 (2012).

[49] Carlos Andres Ramos-Paja et al. “Mathematical model of total cross-tied photovoltaic arrays in mismatching conditions”. In: *2012 IEEE 4th Colombian Workshop on Circuits and Systems (CWCAS)*. Ieee. 2012, pp. 1–6.

[50] F Reil et al. “Determination of arcing risks in PV modules with derivation of risk minimization measures”. In: *2013 IEEE 39th Photovoltaic Specialists Conference (PVSC)*. IEEE. 2013, pp. 3159–3164.

[51] Tatsuo Saga. “Advances in crystalline silicon solar cell technology for industrial mass production”. In: *NPG Asia Materials* 2.3 (2010), pp. 96–102.

[52] Paula Sánchez-Friera et al. “Analysis of degradation mechanisms of crystalline silicon PV modules after 12 years of operation in Southern Europe”. In: *Progress in photovoltaics: Research and Applications* 19.6 (2011), pp. 658–666.

[53] B Senitzky and PD Radin. “Effect of Internal Heating on the Breakdown Characteristics of Silicon p-n Junctions”. In: *Journal of Applied Physics* 30.12 (1959), pp. 1945–1950.

[54] Nahla Mohamed Abd Alrahim Shannan, Nor Zaihar Yahaya, and Balbir Singh. “Single-diode model and two-diode model of PV modules: A comparison”. In: *2013 IEEE International Conference on Control System, Computing and Engineering*. IEEE. 2013, pp. 210–214.

[55] Arno HM Smets et al. *Solar Energy: The physics and engineering of photovoltaic conversion, technologies and systems*. UIT Cambridge, 2015.

[56] Vaclav Smil. *Energy Transitions: Global and National Perspectives*. Praeger, 2016.

[57] Sunpower. *Sunpower Maxeon gen 2 cells*. URL: `https://us.sunpower.com/solar-resources/sunpower%5C%C2%5C%AE-maxeon%5C%E2%5C%84%5C%A2-gen-ii-solar-cells`.

[58] Sunpower. *Sunpower Maxeon gen 2 cells*. URL: `https://us.sunpower.com/solar-resources/sunpower%5C%C2%5C%AE-maxeon%5C%E2%5C%84%5C%A2-gen-iii-solar-cells`.

[59] Piotr Szaniawski et al. “Light-enhanced reverse breakdown in Cu (In, Ga) Se2 solar cells”. In: *Thin Solid Films* 535 (2013), pp. 326–330.

[60] Simon M Sze and Kwok K Ng. *Physics of semiconductor devices*. John wiley & sons, 2006.

[61] SM Sze and G Gibbons. “Effect of junction curvature on breakdown voltage in semiconductors”. In: *Solid-state electronics* 9.9 (1966), pp. 831–845.

[62] Benjamin Thaidigsmann et al. “Loss analysis and efficiency potential of p-type MWT–PERC solar cells”. In: *Solar energy materials and solar cells* 106 (2012), pp. 89–94.

[63] TOM Tiedje et al. “Limiting efficiency of silicon solar cells”. In: *IEEE Transactions on electron devices* 31.5 (1984), pp. 711–716.

[64] K Et-Torabi et al. “Parameters estimation of the single and double diode photovoltaic models using a Gauss–Seidel algorithm and analytical method: A comparative study”. In: *Energy Conversion and Management* 148 (2017), pp. 1041–1054.

[65] Yaw-Juen Wang and Po-Chun Hsu. “An investigation on partial shading of PV modules with different connection configurations of PV cells”. In: *Energy* 36.5 (2011), pp. 3069–3078.

[66] Stefan Wendlandt et al. “Hot spot risk analysis on silicon cell modules”. In: *25th European Photovoltaic Solar Energy Conference and Exhibition*. Valencia, Spain. 2010, pp. 4002–4006.

[67] Cort J Willmott and Kenji Matsuura. “Advantages of the mean absolute error (MAE) over the root mean square error (RMSE) in assessing average model performance”. In: *Climate research* 30.1 (2005), pp. 79–82.

[68] worldometer. *World Population by Year*. URL: `https://www.worldometers.info/world-population/world-population-by-year/` (visited on 06/11/2020).

[69] Abdallah Zegaoui et al. “Photovoltaic cell/panel/array characterizations and modeling considering both reverse and direct modes”. In: *Energy Procedia* 6 (2011), pp. 695–703.

[70] M Zeman et al. “Modelling of thin-film silicon solar cells”. In: *Solar Energy Materials and Solar Cells* 119 (2013), pp. 94–111.

[71] Qi Zhang and Qun Li. “Temperature and reverse voltage across a partially shaded Si PV cell under hot spot test condition”. In: *2012 38th IEEE Photovoltaic Specialists Conference*. IEEE. 2012, pp. 001344–001347.

[72] Teresa Zhang. *Solar Power World*. URL: `$https://www.solarpowerworldonline.com/2017/08/specific-yield-overview$` (visited on 08/14/2017).

[73] Tiantian Zhang, Meng Wang, and Hongxing Yang. “A review of the energy performance and life-cycle assessment of building-integrated photovoltaic (BIPV) systems”. In: *Energies* 11.11 (2018), p. 3157.

[74] Jianhua Zhao, Aihua Wang, and Martin A Green. “High-efficiency PERL and PERT silicon solar cells on FZ and MCZ substrates”. In: *Solar Energy Materials and Solar Cells* 65.1-4 (2001), pp. 429–435.